ISSN 0030-6096

OSAKA CITY MEDICAL JOURNAL

Vol. 64
No. 2

2018

PUBLISHED BY
OSAKA CITY MEDICAL ASSOCIATION
OSAKA JAPAN

Osaka City Medical Journal
Vol. 64, No. 2, December 2018

CONTENTS

Osaka City Med. J. Vol. 64, 75-86, 2018

Obsessions and Compulsions are Strongly Associated with Anxiety and Depressive Symptoms in Childhood and Adolescent Autism Spectrum Disorder

Yoshihiro Iwakura[1)], Dai Miyawaki[1)], Hiroto Kusaka[1)], Ayako Goto[2)], Nobuyoshi Asada[1)], Erika Yanagawa[1)], Naomi Asada[1)], Hiroki Terakawa[1)], Kaoru Hirai[1)], Yusuke Miki[1)], and Koki Inoue[1)]

Department of Neuropsychiatry[1)], Osaka City University Graduate School of Medicine; and Department of Psychiatry[2)], Hannan Hospital

Abstract

Background

Autism spectrum disorder (ASD) is highly comorbid with obsessive-compulsive disorder (OCD) in children. Although the association between obsessions and compulsions (OC) and anxiety and depressive symptoms has been acknowledged, some researchers maintain that in individuals with ASD, OC are less related to anxiety symptoms. The purpose of this study was to examine correlations between OC and other factors, including anxiety and depressive symptoms, in both ASD and non-ASD groups.

Methods

We assessed a referral sample of 138 children (aged 9-15 years, 41.3% male). Multiple regression analyses were performed separately for the ASD group and the non-ASD group to examine correlations between OC (as measured by the Leyton Obsessional Inventory-Child Version) and age, sex, socioeconomic status, OCD, attention deficit hyperactivity disorder (ADHD), chronic tic disorder (CTD), Tourette's syndrome (TS), scores on the State-Trait Anxiety Inventory for Children, and scores on the Birleson Depression Self-Rating Scale for Children.

Results

Multiple regression analyses revealed that anxiety, depression, and OCD were significantly related to OC in both the ASD and the non-ASD groups. ADHD, CTD, and TS were not related to OC.

Conclusions

Our findings suggest that OC are associated with anxiety and depressive symptoms, regardless of the presence of ASD.

Key Words: Autism Spectrum Disorder; Obsessive-compulsive Disorder; Anxiety; Depression

Received September 5, 2017; accepted November 28, 2017.

Correspondence to: Yoshihiro Iwakura, MD.
Department of Neuropsychiatry, Osaka City University Graduate School of Medicine,
1-4-3 Asahimachi, Abeno-ku, Osaka 545-8585, Japan
Tel: +81-6-6645-3821; Fax: +81-6-6636-0439
E-mail: m2019955@med.osaka-cu.ac.jp

Introduction

Autism spectrum disorder (ASD) is characterized by substantial impairment in social communication and social interactions across multiple contexts and by restricted, repetitive patterns of behavior, interests, or activities[1].

One research indicates that obsessions and compulsions (OC) are related to anxiety and depressive symptoms and can lead to isolation and hopelessness[2]. In one 3-year follow-up study of children and adolescents, anxiety and depressive symptoms predicted the severity of OC after follow-up[3]. Although ASD is highly comorbid with obsessive-compulsive disorder (OCD) in children[4,5], some researchers have suggested that, unlike typical OCD patients, patients with ASD appear to enjoy their OC and do not experience anxiety from them[6]. One review suggests that repetitive behavior in children with OCD is provoked by unwanted and bothersome thoughts that cause anxiety. In contrast, repetitive behavior in children with ASD may not cause distress[7]. It has been proposed that individuals with ASD tend not to subjectively evaluate OC as negative (as distressing, unwanted, senseless, and ego-dystonic) and that they might have little awareness about their OC, partially owing to autistic individuals' impaired ability to process and talk about their own internal state of mind[8]. Furthermore, some studies have identified different types of OC between individuals with ASD and those without ASD (non-ASD)[9-14]. OCD and neurodevelopmental disorders such as ASD, attention deficit hyperactivity disorder (ADHD), and tic disorder (TD) may share underlying genetic factors[15]. Therefore, OC in patients with ASD, ADHD, and TD could be attributed to underlying some genetic factors rather than to anxiety and depressive symptoms.

However, many researchers have reported that autistic children and adolescents have a higher prevalence of major depressive disorder and anxiety disorders, including OCD[16-21]. Moreover, as our clinical experience asserts, patients with OCD experience substantial anxiety and depressive symptoms, regardless of the presence of ASD.

As above, difference of association between OC and anxiety and depressive symptoms in ASD and non-ASD is controversial. Hence, we investigated the association between OC and anxiety and depressive symptoms, taking into account factors that has associated with OCD in previous research, such as ADHD, chronic TD (CTD), and Tourette's syndrome (TS). Our aims were 1) to ascertain that anxiety and depressive symptoms are positively correlated with OC regardless of the presence of ASD, 2) to investigate the relationship between OC and other factors such as anxiety, depression, ADHD, CTD, and TS.

Methods

Subjects

The study subjects were 164 elementary or junior high school students aged 9-15 years, who were consecutively referred to the children's psychiatry outpatient clinic of Osaka City University Hospital (Osaka, Japan) between January 2011 and December 2013. The subjects attended the clinic for at least 3 months to be assessed by a trained multidisciplinary team, which included experienced child psychiatrists, a psychologist, and a psychiatric social worker. Children with intellectual disability (n =17) (IQ <70; Wechsler Intelligence Scale for Children-Third Edition; WISC-Ⅲ[22]), children with acute psychotic states (n=5), and children with severe neurological impairments or intractable epilepsy (n=4) were excluded from this study. The WISC-Ⅲ was used to evaluate the intelligence of

all subjects with ASD. For the non-ASD group, we obtained information about academic achievement and daily living skills from parents and teachers. All children with suspected intellectual disability (full IQ <70) were assessed using the WISC-Ⅲ.

The remaining 138 children were divided into two groups, 73 ASD children and 65 non-ASD children. The diagnostic approach for ASD was based on the following three sources: 1) a comprehensive developmental history; 2) the clinician's interview with each child and their parents; and 3) direct observations of the children by two child psychiatrists. A diagnosis of ASD was made using the criteria in the American Psychiatric Association's Diagnostic and Statistical Manual of Mental Disorders, Fifth Edition (DSM 5)[1].

Procedure

We explained to participants the study purpose, procedures, potential risks, and alternatives to participation. We obtained written informed consent from all the children and their parents. The study protocol was reviewed and approved by the Human Subject Review Committee of Osaka City University. The approval number was 2382.

To diagnose comorbid psychiatric disorders, we used the Japanese version of the Schedule for Affective Disorders and Schizophrenia for School-Age Children-Present and Lifetime version (K-SADS-PL-J). This is a semi-structured interview designed to assess current and past episodes of psychopathology in children and adolescents according to DSM-Ⅳ-TR criteria and is administered through interviews with the child and a parent. This diagnostic tool is known for its scrupulousness and high inter-rater reliability[23]. Finally, a multidisciplinary team meeting was held to elucidate the best-estimate diagnosis for all participants once the interviews were completed.

Measures

Individuals who met the inclusion criteria were administered a series of clinical interview and self-report measures, which assessed OC, anxiety, and depressive symptoms. All measures were presented in Japanese and had been validated in that language.

1. Leyton Obsessional Inventory-Child Version (LOI-CV)

The LOI-CV is a self-report 20-item questionnaire that measures the presence or absence (using Yes/No responses) of several obsessive preoccupations and behaviors. Items with a positive response are rated in terms of interference with personal functioning (range 0-3, no interference-interferes a lot)[24]. Therefore, this instrument comprises two subscales: symptom presence (maximum score, 20) and interference (maximum score, 60). The LOI-CV has been shown to be a valid screening instrument for assessing OC in children and adolescents[25]. Internal reliability was high for the total scale (α=0.86)[26]. The LOI-CV showed acceptable internal consistency (α=0.79) in a study of 50 American children and adolescents with OCD[27]. We chose the LOI-CV from several published OC measures because it has been widely used in Japan with community samples and was therefore suitable for our subjects, almost all of whom had not been diagnosed with OCD.

2. The State-Trait Anxiety Inventory for Children (STAIC)

The STAIC is designed to assess state and trait anxiety in children and contains two 20-item scales. The child responds to each item by selecting one of several options. Each subscale score ranges from 20 to 60. The STAIC-State scale asks children how they feel at a particular moment in time; for example, "I feel very nervous, nervous, not nervous". The STAIC-Trait scale asks how they generally feel; for example, "I am shy hardly ever, sometimes, often[28]".

3. The Birleson Depression Self-Rating Scale for Children (DSRS)

The DSRS is a self-rating depression scale for children[29]. Unlike the Children's Depression Inventory (CDI), which was developed from the Beck Depression Inventory for adults, the DSRS was developed in clinical practice with children and makes fewer cognitive demands than the CDI[30,31]. It contains 18 statements. The young person is asked to match these statements to his/her own situation during the last week and to assign an intensity rating (applies "most of the time", "sometimes", or "never"). A score of 2, 1, or 0 is awarded depending on the direction of the statement. Its usefulness in child populations has been demonstrated[32,33].

Statistical analysis

All statistical analyses were performed using SPSS version 22.0 statistical software (SPSS Japan, Inc., Tokyo, Japan). Descriptive data were presented as means, standard deviations, medians, and ranges. Statistical significance was determined using the Mann-Whitney U test or Student's t-test, as appropriate. The chi-square test was used to compare categorical variables. Spearman correlation coefficients were used to test relationships between LOI-CV score, STAIC score, and DSRS score separately for the ASD and the non-ASD groups. To identify the factors associated with LOI-CV score, we conducted separate multiple regression analyses for the ASD group and non-ASD group using LOI-CV score as the dependent variable and age, sex, STAIC total score, DSRS total score, diagnosis of OCD, ADHD, CTD or TS, and parental absence as independent variables. P-values <0.05 (two-sided probability) were deemed to indicate statistical significance.

Results

Table 1 shows the comparison of demographic characteristics of the participants in the ASD and non-ASD groups. Of the 138 children (57 males and 81 females; mean age, 12.7 years), 73 were diagnosed with ASD. The ASD group had a mean age of 12.4 years and contained 40 males (54.8%). The non-ASD group had a mean age of 13.1 years and contained 17 males (26.2%). The ASD group contained a significantly higher proportion of males than the non-ASD group ($\chi^2=11.63$, df=1, p=0.001). There were no significant between-group differences in socioeconomic status (receiving public assistance or not and having a parent absent or not), comorbid rate (for all comorbidities but anorexia nervosa, enuresis, and ADHD), LOI-CV score, and DSRS score. The mean age (p=0.015), the comorbid rate of anorexia nervosa (p=0.011), and STAIC scores were significantly lower in the ASD group than in the non-ASD group. Proportion of males (p=0.001) and comorbid rates of enuresis (p=0.039) and ADHD (p=0.024) were significantly higher in the ASD group than in the non-ASD group.

Table 2 shows between-group comparisons of LOI-CV scores for several variables. LOI-CV total scores were significantly higher in females (p=0.044), the parent-absent group (p=0.004), and the OCD group (p=0.001).

Tables 3 shows correlations between continuous variables in the ASD group and non-ASD group (age, LOI-CV total score, STAIC total score, DSRS score). Both groups showed significant correlations for the same variables (and no significant correlations between age and other variables). LOI-CV score was significantly correlated with STAIC and DSRS scores. STAIC and DSRS scores were highly and significantly correlated (r=0.715 in both groups).

We had planned to use age, sex, STAIC score, DSRS score, diagnosis of OCD, ADHD, CTD or TS, and parental absence as independent variables in the multiple regression analyses. However, because of the high correlation between STAIC total scores and DSRS scores (r=0.715), we were unable to use both these variables as independent variables in the multiple regression analyses owing

Table 1. Participant characteristics

	All (n=138)		ASD group (n=73)		Non-ASD group (n=65)		χ^2/t/U	p
Demographic variables								
Age	12.7 (1.8)	13.2 (8.3-15.8)	12.4 (1.8)	12.7 (8.3-15.8)	13.1 (1.8)	13.3 (9.2-15.8)	2058 [b]	0.015*
Male gender, n (%)	57	(41.3)	40	(54.8)	17	(26.2)	11.634 [c]	0.001*
Socioeconomic status								
Receipt of public assistance, n (%)	7	(5.1)	3	(4.1)	4	(6.2)	0.298 [c]	0.707
Absence of a parent, n (%)	40	(29.0)	20	(27.4)	20	(30.8)	0.19 [c]	0.709
K-SADS-PL-J diagnoses								
Major depressive disorder	24	(17.4)	13	(17.8)	11	(16.9)	0.019 [c]	1.000
Dysthymia	9	(6.5)	3	(4.1)	6	(9.2)	1.479 [c]	0.192
Adjustment disorder	16	(11.6)	5	(6.8)	11	(16.9)	3.404 [c]	0.108
Bipolar disorder	4	(2.9)	2	(2.7)	2	(3.1)	0.014 [c]	0.645
Psychotic disorder not otherwise specified	1	(0.7)	0	(0.0)	1	(1.5)	1.131 [c]	0.471
Panic disorder	8	(5.8)	2	(2.7)	6	(9.2)	2.653 [c]	0.148
Separation anxiety disorder	7	(5.1)	5	(6.8)	2	(3.1)	1.016 [c]	0.447
Social phobia	31	(22.5)	17	(23.3)	14	(21.5)	0.06 [c]	0.841
Specific phobia	13	(9.4)	7	(9.6)	6	(9.2)	0.005 [c]	1.000
Generalized anxiety disorder	25	(18.1)	14	(19.2)	11	(16.9)	0.118 [c]	0.826
Obsessive-compulsive disorder	16	(11.6)	12	(16.4)	4	(6.2)	3.548 [c]	0.068
Posttraumatic stress disorder	1	(0.7)	0	(0.0)	1	(1.5)	1.131 [c]	0.471
Enuresis	5	(3.6)	5	(6.8)	0	(0.0)	4.619 [c]	0.039*
Encopresis	0	(0.0)	0	(0.0)	0	(0.0)		
Anorexia nervosa	29	(21.0)	9	(12.3)	20	(30.8)	7.044 [c]	0.011*
ADHD	24	(17.4)	18	(24.7)	6	(9.2)	5.696 [c]	0.024*
Oppositional defiant disorder	27	(19.6)	18	(24.7)	9	(13.8)	2.554 [c]	0.134
Conduct disorder	20	(14.5)	9	(12.3)	11	(16.9)	0.586 [c]	0.476
Chronic tic disorder or Tourette's syndrome	18	(13.0)	13	(17.8)	5	(7.7)	3.102 [c]	0.127
Chronic motor or vocal tic disorder	13	(9.4)	10	(13.7)	3	(4.6)	3.325 [c]	0.084
Tourette's syndrome	5	(3.6)	3	(4.1)	2	(3.1)	0.105 [c]	1.000
Self-report scores								
LOI-CV total scores	18.8 (13.6)	16 (0-64)	18.7 (12.6)	16 (0-50)	18.9 (14.7)	15 (0.0-64.0)	2315 [b]	0.808
STAIC								
Total scores	77.7 (17.8)	76 (45-67)	74.0 (16.6)	71 (45-112)	81.9 (18.2)	83 (50-111)	1799.5 [b]	0.014*
State scores	35.9 (11.5)	34 (20-40)	33.3 (10.7)	30 (20-56)	38.8 (11.7)	42 (20-60)	1736 [b]	0.006*
Trait scores	41.9 (9.1)	42 (22-38)	40.7 (8.9)	40 (22-60)	43.12 (11.7)	43 (24-57)	1985 [b]	0.098
DSRS total scores	15.4 (6.2)	15 (4-28)	14.6 (5.6)	14 (4-29)	16.4 (6.8)	17 (5-33)	1.782 [a]	0.077

Notes: Values are expressed as mean (SD) and median (range) or n (%). [a] t-test. [b] Mann-Whitney U-test. [c] Chi-square analysis. * $p<0.05$.

Abbreviations: K-SADS-PL-J, The Japanese version of the Schedule for Affective Disorders and Schizophrenia for School-Age Children-Present and Lifetime version; ASD, autism spectrum disorder; ADHD, attention deficit hyperactivity disorder; LOI-CV, Leyton Obsessional Inventory-Child Version; STAIC, State-Trait Anxiety Inventory for Children; and DSRS, Birleson Depression Self-Rating Scale for Children.

Table 2. Comparison of Leyton Obsessional Inventory-Child Version (LOI-CV) scores

		LOI-CV total scores		U	p
		Mean (SD)	Median (range)		
Sex					
Male	n=57	16.2 (12.7)	14 (0-50)	1844.000	0.044*
Female	n=81	20.6 (14.0)	17 (2-64)		
Public assistance					
(+)	n=7	21.0 (14.7)	15 (5-46)	408.500	0.636
(−)	n=131	18.7 (13.5)	16 (0-64)		
Absence of a parent					
(+)	n=40	24.0 (14.5)	17.5 (4-58)	1344.000	0.004*
(−)	n=91	16.6 (12.6)	14.5 (0-64)		
Obsessive-compulsive disorder					
(+)	n=16	30.0 (15.0)	26 (9-58)	483.000	0.001*
(−)	n=122	17.3 (12.7)	15 (0-64)		
ASD					
(+)	n=73	18.7 (12.6)	16 (0-50)	2315.000	0.808
(−)	n=65	18.9 (14.7)	15 (0-64)		
ADHD					
(+)	n=24	19.8 (13.2)	17 (3-46)	1271.000	0.589
(−)	n=114	18.6 (13.7)	15 (0-64)		
Chronic tic disorder/Tourette's syndrome					
(+)	n=18	17.6 (11.7)	16 (1-46)	1059.000	0.896
(−)	n=120	18.9 (13.8)	16 (0-64)		

Notes: Mann-Whitney U test was used because the LOI-CV scores were not normally distributed. Values are expressed as mean (SD), median (range) or n (%).

Abbreviations: ASD, autism spectrum disorder; ADHD, attention deficit hyperactivity disorder; and LOI-CV, Leyton Obsessional Inventory-Child Version.

Table 3. Spearman's correlations between age and LOI-CV, STAIC, and DSRS scores

		Age	LOI-CV total score	STAIC total score	DSRS-C total score
ASD group	Age				
	LOI-CV total score	−0.034			
	STAIC total score	0.214	0.589**		
	DSRS total score	0.137	0.557**	0.715**	
non-ASD group	Age				
	LOI-CV total score	−0.032			
	STAIC total score	0.201	0.562**		
	DSRS total score	0.125	0.594**	0.715**	

Notes: ** $p<0.01$.

Abbreviations: LOI-CV, Leyton Obsessional Inventory-Child Version; STAIC, State-Trait Anxiety Inventory for Children; DSRS, Birleson Depression Self-Rating Scale for Children; and ASD, Autism Spectrum Disorder.

to multicollinearity. Therefore, we performed (for both the ASD group and the non-ASD group) two multiple regression analyses with STAIC or DSRS score as an independent variable. Table 4 shows the results of multiple regression analyses For the ASD group. In the analysis 1 (including STAIC score as independent variable), the independent variables that predicted LOI-CV total score were

Table 4. Multiple regression results showing predictors of LOI-CV total scores in the autism spectrum disorder group

	Variable	B	SE	β	p-value	95% CI of B		VIF
analysis 1	Constant	4.326	11.684		0.712	−19.008	27.661	
	Sex	1.461	2.633	0.058	0.581	−3.797	6.719	1.203
	Age	−0.240	0.898	−0.033	0.790	−2.033	1.554	1.717
	Absence of a parent	1.289	2.852	0.046	0.653	−4.407	6.985	1.134
	OCD	8.788	3.778	0.261	0.023*	1.243	16.332	1.374
	ADHD	5.642	3.530	0.195	0.115	−1.408	12.692	1.622
	CTD or TS	−1.484	3.559	−0.045	0.678	−8.592	5.625	1.300
	STAIC	0.403	0.078	0.533	<0.001*	0.247	0.560	1.171
analysis 2	Constant	−2.476	11.775		0.834	−25.992	21.040	
	Sex	1.461	2.669	0.064	0.550	−3.727	6.934	1.202
	Age	0.107	0.894	0.015	0.905	−1.679	1.893	1.655
	Absence of a parent	0.218	2.900	0.008	0.940	−5.575	6.010	1.140
	OCD	10.287	3.782	0.305	0.008*	2.374	17.840	1.338
	ADHD	3.271	3.668	0.113	0.376	−4.054	10.596	1.702
	CTD or TS	−1.087	3.603	−0.033	0.764	−8.282	6.109	1.294
	DSRS	1.149	0.235	0.509	<0.001*	0.680	1.627	1.148

Notes: R^2=0.406; Durbin-Watson=2.071 in analysis 1; and R^2=0.389; Durbin-Watson=1.958 in analysis 2.

Abbreviations: B, unstandardized coefficient; SE, standard error; β, standardized partial regression coefficient; VIF, variance inflation factor; LOI-CV, Leyton Obsessional Inventory-Child Version; ASD, autism spectrum disorder; OCD, obsessive-compulsive disorder; ADHD, attention deficit hyperactivity disorder; CTD, chronic tic disorder; TS, Tourette's syndrome; STAIC State-Trait Anxiety Inventory for Children; and DSRS, Birleson Depression Self-Rating Scale for Children.

STAIC score (β=0.533; p<0.001) and OCD (β=0.261; p=0.023); in the analysis 2 (including DSRS score as independent variable), the predictors were DSRS score (β=0.509; p<0.001) and OCD (β=0.305; p=0.008). Table 5 shows the result of multiple regression analyses for the non-ASD group. In the analysis 3 (including STAIC as independent variable), the independent variables that predicted LOI-CV total score were STAIC score (β=0.435; p<0.001), OCD (β=0.259; p=0.019), and parental absence (β=0.274; p=0.014); in the analysis 4 (including DSRS score as independent variable), the predictors were DSRS score (β=0.519; p<0.001) and OCD (β=0.261; p=0.012).

Discussion

To the best of our knowledge, no studies have compared ASD and non-ASD groups on the association between OC and anxiety and depressive symptoms and simultaneously considered factors possibly related to OC, such as age, sex, the diagnosis of ADHD, CTD, TS, and parental absence. In the present study, we aimed to 1) ascertain whether anxiety and depressive symptoms were positively correlated with OC regardless of the presence of ASD, 2) to investigate the relationship between OC and other possibly related factors. The results suggested that OC is related to the presence of OCD and anxiety and depressive symptoms, regardless of the presence of ASD. We expected parental absence to be a confounding factor in the non-ASD group because of its correlation with DSRS scores. In fact, in the non-ASD sample, the DSRS score mean in the parental absence group (mean=19.9; SD =6.7) was significantly higher than in the other group (mean=14.9; SD=6.3) (p=0.005).

Taking into account the relationship between OC severity and anxiety and depressive symptoms,

Table 5. Multiple regression results showing predictors of LOI-CV total scores in the non-autism spectrum disorder group

	Variable	B	SE	β	p-value	95% CI of B		VIF
analysis 3	Constant	−0.963	12.166		0.937	−25.325	23.398	
	Sex	−1.660	3.969	−0.050	0.677	−9.608	6.288	1.412
	Age	0.222	0.908	0.027	0.808	−1.596	2.041	1.223
	Absence of a parent	8.637	3.415	0.274	0.014*	1.799	15.476	1.153
	OCD	15.698	6.530	0.259	0.019*	2.623	28.773	1.143
	ADHD	0.262	5.590	0.005	0.963	−10.931	11.455	1.215
	CTD or TS	−1.722	6.220	−0.032	0.783	−14.178	10.734	1.275
	STAIC	0.350	0.094	0.435	<0.001*	0.163	0.538	1.330
analysis 4	Constant	−2.212	11.493		0.848	−25.225	20.802	
	Sex	0.734	3.635	0.022	0.841	−6.544	8.013	1.328
	Age	−0.048	0.863	−0.006	0.956	−1.777	1.681	1.239
	Absence of a parent	6.193	3.338	0.196	0.069	−0.491	12.877	1.235
	OCD	15.807	6.091	0.261	0.012*	3.609	28.004	1.115
	ADHD	−3.104	5.318	−0.062	0.562	−13.753	7.544	1.233
	CTD or TS	1.074	5.949	0.020	0.857	−10.839	12.987	1.308
	DSRS	1.127	0.237	0.519	<0.001*	0.652	1.602	1.313

Notes: R^2=0.420; Durbin-Watson=2.122 in analysis 3; and R^2=0.483; Durbin-Watson=2.193 in analysis 4.

Abbreviations: B, unstandardized coefficient; SE, standard error; β, standardized partial regression coefficient; VIF, variance inflation factor; LOI-CV, Leyton Obsessional Inventory-Child Version; ASD, autism spectrum disorder; OCD, obsessive-compulsive disorder; ADHD, attention deficit hyperactivity disorder; CTD, chronic tic disorder; TS, Tourette's syndrome; STAIC State-Trait Anxiety Inventory for Children; and DSRS, Birleson Depression Self-Rating Scale for Children.

these results are in accord with findings from several previous studies[2,3]. Mack et al compared clinical characteristics and symptom severity of children with OCD plus ASD with those of children with OCD plus TS or OCD alone, using the Children's Yale-Brown Obsessive Compulsive Scale (CY-BOCS), which is considered the gold standard measure of OC severity in youth[34,35]. They found that children in all groups experienced similar levels of impairment[12]. Mito et al compared the severity and prevalence of OC, anxiety, and depression in an ASD group and a non-ASD group of OCD patients. They reported that elevated ASD scores had little impact on severity and prevalence of OC[36]. However, they defined ASD simply as high autism quotient scores, which is an insufficient measure. These previous studies are limited because they focused only on patients diagnosed with OCD. Substantial numbers of adolescents suffer from subclinical OCD, which is characterized by OC that are not severe enough to meet the full OCD criteria and has a prevalence ranging from 2.7% to 19%[37,38].

Our results are inconsistent with findings from one previous study. Ruta et al examined OC features and symptom severity in children and adolescents with Asperger's syndrome using the CY-BOCS. The Asperger's syndrome group showed greater OC severity than the control group[13]. However, this study used a univariate analysis and did not consider possible confounding factors such as anxiety and depressive symptoms.

Although many studies have examined the association between OC and ASD from various perspectives, they suffer from methodological problems. We included subjects regardless of OCD diagnosis and used a range of information to more accurately diagnose ASD. We also investigated the

association between OC and factors thought to be related to OCD.

Many researchers have pointed that ASD, ADHD, and TS are highly comorbid with OCD in children[4,5,39,40]. However, some researchers have suggested that individuals with ASD appear to enjoy their OC and do not experience anxiety from them[4,5]. Moreover, individuals with ASD and other neurodevelopmental disorders may show a particular type of OC.

The concept of obsessive-compulsive spectrum disorders (OCSD) was proposed in response to observations of disparate disorders marked by obsessive thinking and/or compulsive behavior, including ASD and TS[41,42]. Hollander et al subdivided OCSD into three clusters: 1) body image/body sensitization/body weight concern disorders; 2) impulse control disorders; and 3) neurological disorders with repetitive behaviors. ASD and TD were included in the last category. They suggested that, for disorders in the last cluster, OC are based on underlying neurological dysfunction rather than on the anxiety typically found in OCD[41].

Ortiz et al investigated comorbidities and clinical characteristics of children with OCD and defined two subtypes of OCD: one subtype is characterized by childhood onset, a predominance of males, high familial aggregation, and comorbid neurodevelopmental disorders such as ADHD, TS, and CTD; the second subtype is phenotypically more related to anxiety and depressive disorders, is more common in females, and has a later onset during adolescence[43]. Other researchers have suggested that neurodevelopmental disorders such as ASD, ADHD, and TD share underlying genetic factors that converge at the level of cortico-striatal-thalamocortical circuits[15].

These previous research findings suggest that OC may be related to neurodevelopmental disorders such as ASD, ADHD, CTD, and TS, regardless of anxiety and depressive symptoms, and may be less related to anxiety and depressive symptoms in ASD. However, we found that OC was significantly associated with anxiety and depressive symptoms in both the ASD and non-ASD groups. We found no relation between OC and ADHD, CTD, and TS.

Many studies have reported that OC are distressing, impair function, and are related to anxiety and depressive symptoms[2,3,44-49]. Therefore, to prevent exacerbation of OCD symptoms, potential treatment of patients with OCD should focus on treatment of anxiety and depressive symptoms[3,50]. Hence, although recent research has focused on OCD heterogeneity, we should consider comorbid anxiety and depressive symptoms regardless of comorbid ASD and other neurodevelopmental disorders when we meet patients who present with OC.

Limitations

As our study samples were children and adolescents, we cannot generalize the findings to adult populations. Because we focused on patients' subjective symptoms in this study, we only used self-report measures. However, because of the difficulties that individuals with ASD can experience in describing their internal states, it is not known whether self-report measures are effective in identifying OC, anxiety, and depression in this group. Mazefsky et al reported the poor performance of a self-report measure to identify OCD in children with ASD[51]. However, other studies have shown strong correlations between parent and child self-reports of anxiety and depression in ASD[52-54].

We did not consider whether the participants had been received pharmacotherapy or not in this study. Because pharmacotherapy possibly alleviate OC, further study considering the history of pharmacotherapy are needed.

In this study, we examined OC in terms of symptom severity rather than clinical diagnoses and therefore did not investigate comprehensive OCD psychopathology. However, as mentioned above,

previous studies indicate that many adolescents suffer from subclinical OCD[37,38]. In one 2-year follow-up study, adolescents with subclinical OCD and those scoring highly on the LOI-CV were more likely to fulfill clinical OCD criteria after follow-up[55]. Moreover, OC in all age groups, particularly younger sufferers, is under-recognized because individuals tend to be secretive about their symptoms[35,56]. These characteristics of OC lead to delays in detection, diagnosis, and treatment. It is therefore important to investigate OC in children and adolescents regardless of whether they have OCD to prevent pathogenesis or exacerbation of OCD.

Conflicts of interest

The authors declare that they have no conflicts of interest.

References

1. American Psychiatric Association. Diagnostic and Statistical Manual of Mental Disorders. 5th ed. Washington DC: APA; 2013. pp. 50-59.
2. Grados MA, Labuda MC, Riddle MA, Walkup JT. Obsessive-compulsive disorder in children and adolescents. International Review of Psychiatry 1997;9:83-98.
3. Voltas N, Hernández-Martínez C, Arija V, Aparicio E, Canals J. A prospective study of paediatric obsessive-compulsive symptomatology in a Spanish community sample. Child Psychiatry Hum Dev 2014;45:377-387.
4. Dekker MC, Koot HM. DSM-Ⅳ disorders in children with borderline to moderate intellectual disability. Ⅰ: prevalence and impact. J Am Acad Child Adolesc Psychiatry 2003;42:915-922.
5. Van Steensel FJ, Bögels SM, Perrin S. Anxiety disorders in children and adolescents with autistic spectrum disorders: a meta-analysis. Clin Child Fam Psychol Rev 2011;14:302-317.
6. Szatmari P. Differential diagnosis of Asperger disorder. In: Schopler E, Mesibov GB, Kunce LJ, editors. Asperger Syndrome or High-Functioning Autism? New York: Plenum Press, 1998. pp. 61-74.
7. Scahill L, Challa SA. Repetitive behavior in children with autism spectrum disorder: similarities and differences with obsessive-compulsive disorders. In: Mazzone L, Vitiello B, editors. Psychiatric Symptoms and Comorbidities in Autism Spectrum Disorder. Switzerland: Springer, 2016. pp. 39-50.
8. Baron-Cohen S. Do autistic children have obsessions and compulsions? Br J Clin Psychol 1989;28:193-200.
9. McDougle CJ, Kresch LE, Goodman WK, Naylor ST, Volkmar FR, Cohen DJ, et al. A case-controlled study of repetitive thoughts and behavior in adults with autistic disorder and obsessive-compulsive disorder. Am J Psychiatry 1995;152:772-777.
10. Russell AJ, Mataix-Cols D, Anson M, Murphy DG. Obsessions and compulsions in Asperger syndrome and high-functioning autism. Br J Psychiatry 2005;186:525-528.
11. Zandt F, Prior M, Kyrios M. Repetitive behaviour in children with high functioning autism and obsessive-compulsive disorder. J Autism Dev Disord 2007;37:251-259.
12. Mack H, Fullana MA, Russell AJ, Mataix-Cols D, Nakatani E, Heyman I. Obsessions and compulsions in children with Asperger's syndrome or high-functioning autism: a case-control study. Aust N Z J Psychiatry 2010;44:1082-1088.
13. Ruta L, Mugno D, D'Arrigo VG, Vitiello B, Mazzone L. Obsessive-compulsive traits in children and adolescents with Asperger syndrome. Eur Child Adolesc Psychiatry 2010;19:17-24.
14. Cadman T, Spain D, Johnston P, Russell A, Mataix-Cols D, Craig M, et al. Obsessive-compulsive disorder in adults with high-functioning autism spectrum disorder: what does self-report with the OCI-R tell us? Autism Res 2015;8:477-485.
15. Palumbo D, Maughan A, Kurlan R. Hypothesis Ⅲ. Tourette syndrome is only one of several causes of a developmental basal ganglia syndrome. Arch Neurol 1997;54:475-483.
16. Russell E, Sofronoff K. Anxiety and social worries in children with Asperger syndrome. Aust N Z J Psychiatry 2005;39:633-638.
17. Gillott A, Furniss F, Walter A. Anxiety in high-functioning children with autism. Autism 2001;5:277-286.
18. Strang JF, Kenworthy L, Daniolos P, Case L, Wills MC, Martin A, et al. Depression and anxiety symptoms in children and adolescents with autism spectrum disorders without intellectual disability. Res Autism Spectr Disord 2012;6:406-412.
19. White SW, Oswald D, Ollendick T, Scahill L. Anxiety in children and adolescents with autism spectrum disorders. Clin Psychol Rev 2009;29:216-229.
20. Leyfer OT, Folstein SE, Bacalman S, Davis NO, Dinh E, Morgan J, et al. Comorbid psychiatric disorders in

children with autism: interview development and rates of disorders. J Autism Dev Disord 2006;36:849-861.
21. Muris P, Steerneman P, Merckelbach H, Holdvinet I, Meesters C. Comorbid anxiety symptoms in children with pervasive developmental disorders. J Anxiety Disord 1998;12:387-393.
22. Wechsler D. Manual for the Wechsler Intelligence Scale for Children-Third Edition. San Antonio: Psychological Corporation, 1991.
23. Kaufman J, Birmaher B, Brent D, Rao U, Flynn C, Moreci P, et al. Schedule for Affective Disorders and Schizophrenia for School-Age Children-Present and Lifetime Version (K-SADS-PL): initial reliability and validity data. J Am Acad Child Adolesc Psychiatry 1997;36:980-988.
24. Berg CZ, Whitaker A, Davies M, Flament MF, Rapoport JL. The survey form of the Leyton Obsessional Inventory-Child Version: norms from an epidemiological study. J Am Acad Child Adolesc Psychiatry 1988;27: 759-763.
25. Canals JS, Hernandez-Martinez C, Cosi SM, Lazaro LG, Toro JT. The Leyton Obsessional Inventory-Child Version: validity and reliability in Spanish non-clinical population. International Journal of Clinical and Health Psychology 2011;12:81-96.
26. Bamber D, Tamplin A, Park RJ, Kyte ZA, Goodyer IM. Development of a short leyton obsessional inventory for children and adolescents. J Am Acad Child Adolesc Psychiatry 2002;41:1246-1252.
27. Storch EA, Park JM, Lewin AB, Morgan JR, Jones AM, Murphy TK. The Leyton Obsessional Inventory-Child Version Survey Form does not demonstrate adequate psychometric properties in American youth with pediatric obsessive-compulsive disorder. J Anxiety Disord 2011;25:574-578.
28. Spielberger CD, Edwards J, Monturi J, Lushene R. State-Trait Anxiety Inventory for Children. Palo Alto, CA: Consulting Psychologists Press, 1973.
29. Birleson P. The validity of depressive disorder in childhood and the development of a self-rating scale: a research report. J Child Psychol Psychiatry 1981;22:73-88.
30. Costello EJ, Angold A. Scales to assess child and adolescent depression: checklists, screens, and nets. J Am Acad Child Adolesc Psychiatry 1988;27:726-737.
31. Beck AT, Ward CH, Mendelson M, Mock J, Erbaugh J. An inventory for measuring depression. Arch Gen Psychiatry 1961;4:561-571.
32. Asaenow JR, Carlson GA. Depression Self-Rating Scale: utility with child psychiatric inpatients. J Consult Clin Psychol 1985;53:491-499.
33. Birleson P, Hudson I, Buchanan DG, Wolff S. Clinical evaluation of a self-rating scale for depressive disorder in childhood (Depression Self-Rating Scale). J Child Psychol Psychiatry 1987;28:43-60.
34. Goodman WK, Price LH, Rasmussen SA, Mazure C, Fleischmann RL, Hill CL, et al. The Yale-Brown Obsessive Compulsive Scale Ⅰ. Development, use, and reliability. Arch Gen Psychiatry 1989;46:1006-1011.
35. Scahill L, Riddle MA, McSwiggin-Hardin M, Ort SI, King RA, Goodman WK, et al. Children's Yale-Brown Obsessive Compulsive Scale: reliability and validity. J Am Acad Child Adolesc Psychiatry 1997;36:844-852.
36. Mito H, Matsuura N, Mukai K, Yanagisawa Y, Nakajima A, Motoyama M, et al. The impacts of elevated autism spectrum disorder traits on clinical and psychosocial features and long-term treatment outcome in adult patients with obsessive-compulsive disorder. Compr Psychiatry 2014;55:1526-1533.
37. Valleni-Basile LA, Garrison CZ, Jackson KL, Waller JL, McKeown RE, Addy CL, et al. Frequency of obsessive-compulsive disorder in a community sample of young adolescents. J Am Acad Child Adolesc Psychiatry 1994; 33:782-791.
38. Bryńska A, Wolańczyk T. Epidemiology and phenomenology of obsessive-compulsive disorder in non-referred young adolescents: a Polish perspective. Eur Child Adolesc Psychiatry 2005;14:319-327.
39. Abramovitch A, Dar R, Mittelman A, Wilhelm S. Comorbidity between attention deficit/hyperactivity disorder and obsessive-compulsive disorder across the lifespan: a systematic and critical review. Harv Rev Psychiatry 2015;23:245-262.
40. Pauls DL, Towbin KE, Leckman JF, Zahner GE, Cohen DJ. Gilles de la Tourette's syndrome and obsessive-compulsive disorder. Evidence supporting a genetic relationship. Arch Gen Psychiatry 1986;43:1180-1182.
41. Hollander E, Wong CM. Obsessive-compulsive spectrum disorders. J Clin Psychiatry 1995;56:3-6.
42. Bartz JA, Hollander E. Is obsessive-compulsive disorder an anxiety disorder? Prog Neuropsychophamacol Biol Psychiatry 2006;30:338-352.
43. Ortiz AE, Morer A, Moreno E, Plana MT, Cordovilla C, Lázaro L. Clinical significance of psychiatric comorbidity in children and adolescents with obsessive-compulsive disorder: subtyping a complex disorder. Eur Arch Psychiatry Clin Neurosci 2016;266:199-208.
44. LaSalle VH, Cromer KR, Nelson KN, Kazuba D, Justement L, Murphy DL. Diagnostic interview assessed neuropsychiatric disorder comorbidity in 334 individuals with obsessive-compulsive disorder. Depress Anxiety 2004;19:163-173.

45. Swedo SE, Rapoport JL, Leonard H, Lenane M, Cheslow D. Obsessive-compulsive disorder in children and adolescents. Clinical phenomenology of 70 consecutive cases. Arch Gen Psychiatry 1989;46:335-341.
46. Storch EA, Merlo LJ, Larson MJ, Geffken GR, Lehmkuhl HD, Jacob ML, et al. Impact of comorbidity on cognitive-behavioral therapy response in pediatric obsessive-compulsive disorder. J Am Acad Child Adolesc Psychiatry 2008;47:583-592.
47. Canavera KE, Ollendick TH, May JT, Pincus DB. Clinical correlates of comorbid obsessive-compulsive disorder and depression in youth. Child Psychiatry Hum Dev 2010;41:583-594.
48. Langley AK, Lewin AB, Bergman RL, Lee JC, Piacentini J. Correlates of comorbid anxiety and externalizing disorders in childhood obsessive compulsive disorder. Eur Child Adolesc Psychiatry 2010;19:637-645.
49. Peris TS, Bergman RL, Asarnow JR, Langley A, McCracken JT, Piacentini J. Clinical and cognitive correlates of depressive symptoms among youth with obsessive compulsive disorder. J Clin Child Adolesc Psychol 2010; 39:616-626.
50. Sun J, Li Z, Buys N, Storch EA. Correlates of comorbid depression, anxiety and helplessness with obsessive-compulsive disorder in Chinese adolescents. J Affect Disord 2015;174:31-37.
51. Mazefsky CA, Kao J, Oswald DP. Preliminary evidence suggesting caution in the use of psychiatric self-report measures with adolescents with high-functioning autism spectrum disorders. Res Autism Spectr Disord 2011; 5:164-174.
52. Blakeley-Smith A, Reaven J, Ridge K, Hepburn S. Parent-child agreement of anxiety symptoms in youth with autism spectrum disorders. Res Autism Spectr Disord 2012;6:707-716.
53. Ozsivadjian A, Hibberd C, Hollocks MJ. Brief report: the use of self-report measures in young people with autism spectrum disorder to access symptoms of anxiety, depression and negative thoughts. J Autism Dev Disord 2014;44:969-974.
54. Storch EA, Ehrenreich May J, Wood JJ, Jones AM, De Nadai AS, Lewin AB, et al. Multiple informant agreement on the anxiety disorders interview schedule in youth with autism spectrum disorders. J Child Adolesc Psychopharmacol 2012;22:292-299.
55. Roussos A, Francis K, Koumoula A, Richardson C, Kabakos C, Kiriakidou T, et al. The Leyton obsessional inventory-child version in Greek adolescents: standardization in a national school-based survey and two-year follow-up. Eur Child Adolesc Psychiatry 2003;12:58-66.
56. Junike MA. Obsessive-compulsive and related disorders: a hidden epidemic. N Engl J Med 1989;321:539-541.

Osaka City Med. J. Vol. 64, 87-97, 2018

Clinical Significance of Serum Duke Pancreatic Monoclonal Antigen Type 2 for Diagnosing Biliary Tract Cancer

Tokuji Ito, Shogo Tanaka, Shigekazu Takemura, Hiroji Shinkawa, Genya Hamano, Yukiko Kurashima, Takanori Aota, Masaki Koda, Toshihiko Shibata, and Shoji Kubo

Department of Hepato-Biliary-Pancreatic Surgery, Osaka City University Graduate School of Medicine

Abstract

Background

To evaluate the usefulness of serum Duke pancreatic monoclonal antigen type 2 (DUPAN-2) concentrations in patients with biliary tract cancer (BTC).

Methods

The serum concentrations of DUPAN-2, carbohydrate antigen 19-9 (CA19-9), and carcinoembryonic antigen (CEA) were prospectively measured in 90 patients with BTC and 47 patients with benign biliary tract disease before surgery and in 54 patients with BTC after surgery. The usefulness of each tumor marker was investigated.

Results

The receiver operating characteristic (ROC) curve for the serum concentration of DUPAN-2 in predicting BTC had the greatest area under the curve (AUC, 0.821; vs CA19-9, 0.788 and CEA, 0.698). The optimal cutoff value for DUPAN-2 was determined from the ROC curve (30 IU/mL). The sensitivity and specificity of DUPAN-2 were 74.4% and 83.0%, respectively. The diagnostic accuracy (positive predictive value + negative predictive value) of DUPAN-2 was 77.4% (CA19-9, 67.2%; CEA, 46.2%). Moreover, for patients with stage 0-I BTC, DUPAN-2 showed the highest sensitivity (60.9% vs CA19-9, 34.8% and CEA, 17.4%). Among the 36 patients with preoperative serum DUPAN-2 ≧30 IU/mL, the value decreased postoperatively in 34 patients (94%).

Conclusions

The measurement of the serum concentration of DUPAN-2 was useful for diagnosing BTC, even at an early stage.

Key Words: Duke pancreatic monoclonal antigen type 2; Biliary tract cancer; Sensitivity and specificity; Tumor

Received September 5, 2017; accepted November 28, 2017.

Correspondence to: Shoji Kubo, MD, PhD.
Department of Hepato-Biliary-Pancreatic Surgery, Osaka City University Graduate School of Medicine, 1-4-3 Asahimachi, Abeno-ku, Osaka 545-8585, Japan
Tel: +81-6-6645-3841; Fax: +81-6-6646-6057
E-mail: m7696493@msic.med.osaka-cu.ac.jp

Introduction

Biliary tract cancers (BTCs) represent the second most common type of hepatobiliary cancer[1] and are typically classified as intrahepatic cholangiocarcinoma (ICC), perihilar/hilar cholangiocarcinoma (CCs; pCC), distal CC (dCC), and gallbladder carcinoma (GBC)[2]. The clinical course of BTC is poor because of its silent clinical characteristics, the difficulties associated with diagnosing the disease at an early stage, and the limited available therapeutic options[3]. The incidence and mortality associated with BTC have continued to increase worldwide[4]. The clinical presentation and use of imaging techniques cannot completely distinguish BTC from benign biliary tract diseases (BBTD)[5-8]. Moreover, laboratory assessments for BTC are not sufficiently sensitive or specific. Currently, the serum carbohydrate antigen 19-9 (CA19-9) concentration is routinely determined in patients with biliary tract disease. However, the sensitivity and specificity of CA19-9 in diagnosing BTC vary widely[9-12], and elevated serum CA19-9 concentrations have been observed in some patients with BBTD[13,14]. Other serum markers, such as carcinoembryonic antigen (CEA), have been used to detect BTC, but the use of these markers in screening has been reported to be limited because of their low specificity and sensitivity[11,15,16]. The Japanese practice guidelines for managing BTC state that no tumor markers specific to BTC are available and that the diagnostic ability can be improved with a combination of tumor markers (e.g., CA19-9 and CEA)[17]. Unfortunately, new useful biomarkers for the diagnosis of BTC have yet to be developed[18]. Thus, the use of other serum tumor markers would be beneficial for diagnosing BTC.

Duke pancreatic monoclonal antigen type 2 (DUPAN-2) was discovered in 1982 as a high-molecular weight glycoprotein defined by a murine monoclonal antibody against a pancreatic ductal adenocarcinoma cell line[19]. DUPAN-2 has been established as an important serum tumor marker for pancreatic cancer[20] and has been reported to be a prognostic factor for pancreatic cancer after surgery[21,22]. Immunohistochemical studies have shown that DUPAN-2 is distributed in various adenocarcinomas[23]. Approximately 40% of BTC patients reportedly show serum DUPAN-2 concentrations of >400 IU/mL[20,24]. However, a cutoff value of >400 IU/mL was determined for diagnosing pancreatic cancer[20,24]. Thus, the optimal cutoff value and accuracy of serum DUPAN-2 as a tumor marker for diagnosing BTC has not been investigated.

In the present study, we collected clinical data, including the serum concentrations of DUPAN-2, CA19-9, and CEA, from patients with BTC and BBTD and investigated the clinical significance of DUPAN-2 as a tumor marker for BTC.

Methods

Patients

This study enrolled 90 patients with BTC (BTC group) and 49 with BBTD (control group) treated surgically at the Department of Hepato-Biliary-Pancreatic Surgery, Osaka City University Hospital, between January 2013 and April 2017. The laboratory test results, including serum concentrations of DUPAN-2, CA19-9, and CEA were measured for the diagnosis, were prospectively collected. Among the 90 patients, the DUPAN-2 concentrations of 54 were able to be measured routinely (3-6 months) after surgery, and the concentrations of the remaining 36 could not be measured due to the short time since surgery (<3 months) in 2 patients and the requirement for follow-up at referral hospitals for 34 patients (26 of whom died). In cases of preoperative biliary decompression, the laboratory test results including the tumor markers after decompression were used.

Clinical information was obtained by a thorough review of the patients' medical histories. The diagnosis of BTC was pathologically made for all 90 patients. BTC was classified as ICC (n=29), pCC (n=22), dCC (n=21), and GBC (n=18). The control group included patients with acute or chronic cholecystitis (n=33), gallbladder polyps (n=4), hepatolithiasis (n=5), choledocholithiasis (n=2), and congenital biliary disease (n=3).

This study was approved by the Institutional Review Board of our institution (approval number, 3166; Osaka City University) and was conducted in accordance with the mandates of the 2008 Declaration of Helsinki.

Clinical data

Baseline preoperative clinical data that were collected included age; sex; number and proportion of patients with jaundice when tumor marker concentrations were measured; number and proportion of patients who had undergone preoperative biliary decompression; serum concentrations of total bilirubin, aspartate aminotransferase (AST), alanine aminotransferase (ALT), γ-glutamyltranspeptidase (γ-GTP), and alkaline phosphatase (ALP); primary tumor stage according to the International Union Against Cancer (UICC)/American Joint Committee on Cancer staging system[25]; histological findings (number and proportion of patients with lymph node metastasis, vascular invasion, and perineural invasion); and serum concentrations of DUPAN-2, CA19-9, and CEA.

Measurement of DUPAN-2, CEA, and CA19-9 concentrations

DUPAN-2 concentrations were measured by using enzyme immunoassay. For comparison, CEA and CA19-9 concentrations were measured by electrochemiluminescence immunoassay. DUPAN-2 serum concentrations of >1600 IU/mL were recorded as 1600 IU/mL and concentrations of <25 IU/mL were recorded as 25 IU/mL. CA19-9 serum concentrations of <2 IU/mL were recorded as 2 IU/mL, and CEA serum concentrations of <0.5 ng/mL were recorded as 0.5 ng/mL.

Statistical analysis

Pearson's correlation coefficient was used to investigate the correlations between the concentrations of DUPAN-2 and the concentrations of CA19-9, CEA, biliary enzymes, and transferase and between the concentrations of CA19-9 and CEA; values of −0.4 to 0.4 were considered to reflect the absence of correlation. To compare the abilities of tumor markers to distinguish patients with BTC from those with BBTD, receiver operating characteristic (ROC) curves were constructed that correlated with the true- and false-positive rates [sensitivity and (1-specificity)]. In addition, the area under the ROC curve (AUC) and 95% confidence interval (CI) were calculated for each marker. The optimal cutoff values of serum DUPAN-2 were determined by Youden's index.

Continuous variables were expressed as the median (25th and 75th percentiles). Inter-group differences were assessed by performing the Mann-Whitney *U* test. Differences in categorical variables were assessed by performing the chi-squared test or Fisher's exact test. p-values of <0.05 were considered to indicate statistical significance. All statistical analyses were performed by using SPSS® v.22.0 (IBM-SPSS, Inc., Chicago, IL, USA).

Results

Tumor markers

Significant differences in the preoperative serum concentration of DUPAN-2 [median (interquartile range)] were observed between patients with BTC [105 IU/mL (27-485 IU/mL)] and those with benign biliary disease [25 IU/mL (25-26 IU/mL), p<0.001, Fig. 1]. The serum concentrations of CA19-9 and

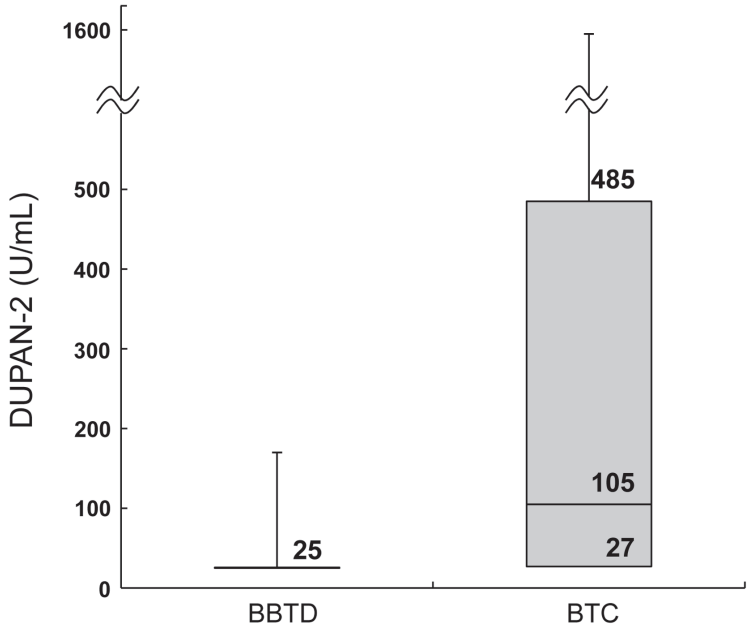

Figure. 1 The distribution of individual serum Duke pancreatic monoclonal antigen type 2 (DUPAN-2) concentrations in patients with biliary tract cancer (BTC) and benign biliary tract disease (BBTD). Data are presented as the upper and lower quartile and range (box) and the median value (horizontal line).

Table 1. Comparison of the clinicopathological characteristics between patients with biliary tract cancer and patients with benign biliary tract disease

	*BTC group (n=90)	Control group (n=47)	p value
Tumor markers			
DUPAN-2 (IU/mL)	105 (27, 485)	25 (25, 26)	<0.001
CA19-9 (IU/mL)	45 (11, 363)	6 (3, 11)	<0.001
CEA (ng/mL)	3.1 (2.1, 4.5)	2 (1.3, 2.9)	<0.001
Age (years old)	68 (63, 74)	62 (51, 70)	0.014
Sex (male/female)	53/37	15/32	0.004
Diagnosis of biliary tract cancer, n (%)			
Intrahepatic cholangiocarcinoma	29 (32)		
Perihilar/hilar cholangiocarcinoma	22 (25)		
Distal cholangiocarcinoma	21 (23)		
Gallbladder cancer	18 (20)		
Preoperative biliary decompression, n (%)	37 (41)	3 (6)	<0.001
Laboratory data			
Total bilirubin (mg/dL)	0.6 (0.5, 0.9)	0.5 (0.4, 0.7)	0.012
Aspartate aminotransferase (IU/L)	28 (22, 46))	22 (17, 27)	0.001
Alanine aminotransferase (IU/L)	27 (17, 54)	16 (14, 27)	0.002
g-glutamyltranspeptidase (IU/L)	125 (40, 276)	31 (19, 53)	<0.001
Alkaline phosphatase (IU/L)	351 (260, 706)	202 (177, 287)	<0.001
UICC stage [n (%)]			
0-Ⅰ	23 (26)		
Ⅱ	32 (36)		
Ⅲ	14 (16)		
Ⅳ	20 (22)		

Continuous values are expressed as the median (25th and 75th percentiles). *One patient who underwent exploratory laparotomy was excluded. BTC, biliary tract cancer; DUPAN-2, Duke pancreatic monoclonal antigen type 2; CA19-9, carbohydrate antigen 19-9; CEA, carcinoembryonic antigen; and UICC, International Union Against Cancer.

CEA in the patients in the BTC group were also significantly higher than those in the patients in the control group (Table 1).

No correlations were observed between the concentration of DUPAN-2 and those of CA19-9, CEA, AST, ALT, γ-GTP, or ALP (coefficients of correlation: CA19-9, 0.022; CEA, 0.039; total bilirubin, −0.013; AST, −0.055; ALT, −0.051; γ-GTP, −0.023; and ALP, −0.022). he coefficient of correlation between CA19-9 and CEA was 0.192.

Clinical characteristics of patients with BTC in comparison to patients with BBTD

An elderly male predominance was observed in patients in the BTC group (Table 1). Preoperative biliary decompression for obstructive jaundice had been performed in 37 (41%) of the 90 patients in the BTC group and 3 (6%) of the 47 patients in the control group ($p<0.001$). The serum concentrations of total bilirubin, AST, ALT, γ-GTP, and ALP in the patients in the BTC group were higher than those in the patients in the control group. The tumor stages of the patients in the BTC group (according to the UICC staging system) were stage 0 (n=1), stage Ⅰ (n=23), stage Ⅱ (n=32), stage Ⅲ (n=14), and stage Ⅳ (n=20).

ROC curve analysis

ROC curves were constructed to compare the ability of the 3 markers to differentiate between patients with BTC and those with BBTD. The curves that distinguished BTC from benign biliary disease are shown in Figure 2. The ROC curve for the prediction of BTC showed a greater AUC for the serum concentration of DUPAN-2 (0.821, 95% CI: 0.752-0.890) than for the serum concentrations of CA19-9 (0.788, 95% CI: 0.711-0.865) and CEA (0.698, 95% CI: 0.607-0.788). The optimal cutoff value of the serum DUPAN-2 concentration for distinguishing BTC from BBTD was 30 IU/mL.

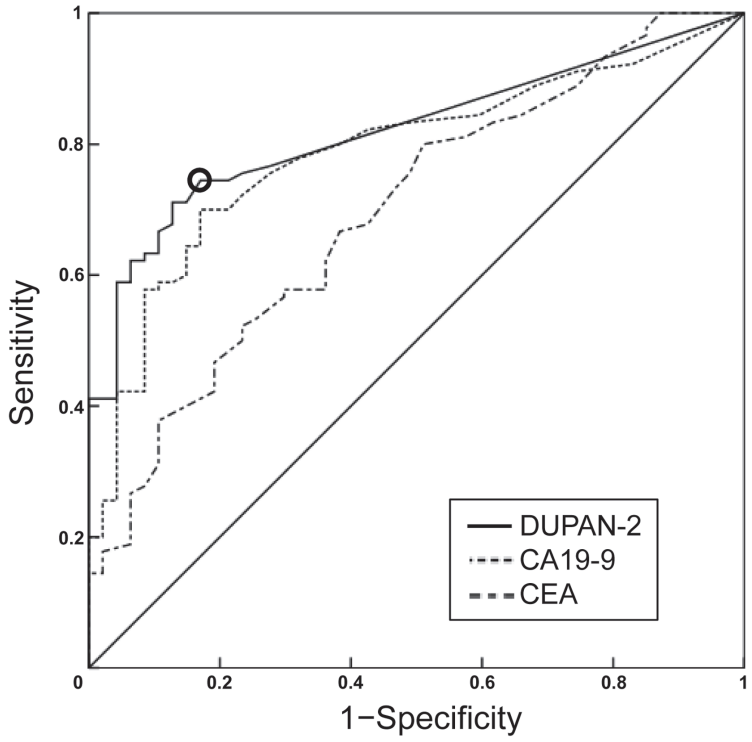

Figure. 2 The receiver operating characteristic (ROC) curves of Duke pancreatic monoclonal antigen type 2 (DUPAN-2), carbohydrate antigen 19-9 (CA19-9), and carcinoembryonic antigen (CEA) concentrations in patients with biliary tract cancer (BTC) were compared with those in patients with benign biliary tract disease (BBTD). Optimal cutoff values of serum DUPAN-2 were determined by Youden index (circle).

Table 2. Usefulness of DUPAN-2, CA19-9, and CEA for diagnosing biliary tract cancer

						Combination of tumor markers		
	DUPAN-2 (>400)	DUPAN-2 (≧30)	CA19-9	CEA	CA19-9+ CEA	DUPAN-2+ CA19-9	DUPAN-2+ CEA	DUPAN-2+ CA19-9+CEA
Sensitivity								
%	28.9	74.4	54.4	22.2	58.9	82.2	76.7	83.3
Number	26/90	67/90	49/90	20/90	53/90	74/90	69/90	75/90
Specificity								
%	100	83	91.5	93.6	87.2	76.6	78.7	72.3
Number	47/47	39/47	43/47	44/47	41/47	36/47	37/47	34/47
Positive predictive value								
%	100	89.3	92.5	87	89.8	87.1	87.3	85.2
Number	26/26	67/75	49/53	20/23	53/59	74/85	69/79	75/88
Negative predictive value								
%	42.3	62.9	51.2	38.6	52.6	69.2	63.8	69.4
Number	47/111	39/62	43/84	44/114	41/78	36/52	37/58	34/49
Diagnostic accuracy								
%	53.3	77.4	67.2	46.7	68.6	80.3	77.4	79.6
Number	73/137	106/137	92/137	64/137	94/137	110/137	106/137	109/137

DUPAN-2, Duke pancreatic monoclonal antigen type 2; CA19-9, carbohydrate antigen 19-9; and CEA carcinoembryonic antigen.

Accuracy of DUPAN-2, CA19-9, and CEA as tumor markers

The sensitivity, specificity, positive predictive value, negative predictive value, and accuracy of the various tumor makers in the diagnosis of BTC are listed in Table 2. The sensitivity, specificity, positive predictive value, negative predictive value, and accuracy of a DUPAN-2 cutoff value of >400 IU/mL for diagnosing BTC were 28.9% (26/90), 100% (47/47), 100% (26/26), 42.3% (47/111), and 53.3% (73/137), respectively. Among the 3 tumor markers, a DUPAN-2 cutoff value of ≧30 IU/mL showed the highest sensitivity (74.4%), negative predictive value (62.9%), and diagnostic accuracy (77.4%) for diagnosing BTC. The specificity and positive predictive values of all 3 markers exceeded 80% and 85%, respectively. Moreover, the sensitivity and diagnostic accuracy of DUPAN-2 alone were superior to those of CA19-9+CEA. The combination of DUPAN-2+CA19-9 and CA19-9+CEA increased the sensitivity but decreased the specificity and was not associated with a remarkable increase in accuracy relative to that of DUPAN-2 alone. In the BTC group, 22 (59.5%) of the 37 patients who were found to be negative for CA19-9+CEA were positive for DUPAN-2, whereas 8 (34.8%) of the 23 patients who were negative for DUPAN-2 were positive for CA19-9+CEA. The sensitivity, specificity, positive predictive value, negative predictive value, and accuracy of the various tumor markers in the patients with UICC stage 0-Ⅰ and stage Ⅱ-Ⅳ are listed in Table 3. In patients with stage 0-Ⅰ BTC, DUPAN-2 showed the highest sensitivity and diagnostic accuracy (60.9% and 75.7%, respectively) among the 3 markers (CA19-9, 34.8% and 72.9%; CEA, 17.4% and 68.6%; and CA19-9+CEA, 43.5% and 72.9%, respectively). Moreover, in patients with stage Ⅱ-Ⅳ BTC, DUPAN-2 showed the highest sensitivity (80.3%), negative predictive value (75.0%), and diagnostic accuracy (81.4%). Although the difference was not statistically significant, the serum concentration of DUPAN-2 tended to be higher in patients with Stage Ⅱ-Ⅳ BTC than in those with Stage 0-Ⅰ BTC (46 vs 110 IU/mL, p=0.095).

Table 3. Accuracy of DUPAN-2, CA19-9, and CEA according to the UICC stage

	Stage 0-Ⅰ				Stage Ⅱ-Ⅳ			
	DUPAN-2	CA19-9	CEA	CA19-9 +CEA	DUPAN-2	CA19-9	CEA	CA19-9 +CEA
Sensitivity								
%	60.9	34.8	17.4	43.5	80.3	62.1	24.2	65.2
Number	14/23	8/23	4/23	10/23	53/66	41/66	16/66	43/66
Specificity								
%	83	91.5	93.6	87.2				
Number	39/47	43/47	44/47	41/47				
Positive predictive value								
%	63.6	66.7	57.1	62.5	86.9	91.1	84.2	87.8
Number	14/22	8/12	4/7	10/16	53/61	41/45	16/19	43/49
Negative predictive value								
%	81.3	74.1	69.8	75.9	75	63.2	46.8	64.1
Number	39/48	43/58	44/63	41/54	39/52	43/68	44/94	41/64
Diagnostic accuracy								
%	75.7	72.9	68.6	72.9	81.4	74.3	53.1	74.3
Number	53/70	51/70	48/70	51/70	92/113	84/113	60/113	84/113

DUPAN-2, Duke pancreatic monoclonal antigen type 2; CA19-9, carbohydrate antigen 19-9; CEA, carcinoembryonic antigen; and UICC, International Union Against Cancer.

Postoperative transition of DUPAN-2

Of the 54 patients in whom the serum concentrations of DUPAN-2 were measured postoperatively, the preoperative serum DUPAN-2 concentration was ≧30 IU/mL in 42 patients (pre-positive group) and was <30 IU/mL in the remaining 12 patients (pre-negative group). In the pre-positive group, 36 had no recurrence, but 6 had recurrence within 3 to 6 months after surgery. Among the 36 patients without recurrence, serum DUPAN-2 concentration decreased in 34 patients (94%) and decreased to <30 IU/mL in 25 patients (69%) within 3 to 6 months after surgery. Of the 25 patients in whom the postoperative serum DUPAN-2 concentration decreased to <30 IU/mL in the pre-positive group, 5 had recurrence; in these 5 patients, the serum DUPAN-2 concentration was re-elevated to ≧30 IU/mL. On the other hand, among the 6 patients with recurrence within 3 to 6 months, the postoperative serum DUPAN-2 concentration decreased in 3 patients (50%, $p=0.015$ vs patients without recurrence) and decreased to <30 IU/mL in only 1 patient (17%, $p=0.023$ vs patients without recurrence). In the pre-negative group, serum DUPAN-2 concentration did not change postoperatively, even in 2 patients with postoperative recurrence.

Discussion

It is well known that the serum CA19-9 concentration increases in some patients with BTC; however, this manifestation is heterogeneous, with a sensitivity of 34.2%-90% and specificity of 54%-98%[9-12,26-29]. Moreover, the concentration of CA19-9 has been shown to increase in 13.8%-15.2% of patients with BBTD[10,30], 28% of patients with acute cholecystitis[31] and 35.6% of patients with cholelithiasis[32]. In the present study, the increase in the concentration of CA19-9 was low in the control group (8.5%), probably because the proportion of patients with biliary obstruction in whom increased levels of CA19-9 may be secreted or leak into the blood stream[31] was low. In addition, it

must be kept in mind that Lewis antigen-negative patients can show false-negative results[33]. Our results were in line with those of numerous studies suggesting that the serum CEA concentration is inferior to the serum CA19-9 concentration for diagnosing BTC[10,33,34]. The sensitivity and specificity of serum CEA for detection of BTC have been reported to be 13.7%-68.6% and 78.4%-86.7%, respectively[10,12,35,36]. Moreover, the serum CEA concentration has been shown to increase in only 20%-45% of patients with ICC[37-42]. Thus, the combination of CA19-9 and CEA (positivity for either marker) is most commonly used to detect BTC; however, the results of our study suggest a sensitivity of 58.9%, which is inadequate.

When we set the cutoff value to ≧30 IU/mL (as calculated from the ROC curve), DUPAN-2 showed a diagnostic value superior to that of the conventional markers (CA19-9, CEA, and CA19-9+CEA). Moreover, our study indicated serum DUPAN-2 concentration decreased (<30 IU/mL) postoperatively, and was re-elevated (≧30 IU/mL) in patients with recurrence. This evidence suggests that DUPAN-2 (≧30 IU/mL) is a useful tumor marker that can be used for diagnosing BTC. Moreover, whereas 59.5% of patients with BTC who were negative for CA19-9+CEA were positive for DUPAN-2, 34.8% of the patients who were negative for DUPAN-2 were positive for CA19-9+CEA (sensitivity of the 3 tumor markers, 83.3%). Thus, the combination of DUPAN-2 and CA19-9+CEA would also be useful for diagnosing BTC.

The serum concentrations of 4 of the 10 patients (40%) with BTC were >400 IU/mL in the previous study[20], whereas the serum concentrations of DUPAN-2 in 26 of 90 patients (28.9%) in this study were >400 IU/mL. Although it is difficult to compare the characteristics of subjects between the previous and present study, due to the unclear cancer stage and small population in the previous study[20], this difference may be related to the low proportion of patients with advanced BTC in this study, as all subjects in our study were operable. A study including patients with advanced disease (inoperable cases) may be able to emphasize the usefulness of the measurement of serum DUPAN-2, as the serum concentration of DUPAN-2 tended to be higher in patients with Stage Ⅱ-Ⅳ BTC than in those with Stage 0-Ⅰ BTC.

The cutoff value of the serum DUPAN-2 concentration was set as >400 IU/mL in previous studies[20,24] and is >150 IU/mL in Japan. To determine the cutoff value for pancreas cancer, the control group included patients with pancreatitis in whom the serum concentration of DUPAN-2 are often increased. In the present study, the serum concentrations of DUPAN-2 in most patients in the control group were low. Although the serum concentration of DUPAN-2 is reported to be influenced by hepatitis and cirrhosis[20], most patients in the control group in the present study did not have hepatitis or cirrhosis, and the laboratory test results were mostly within the normal reference ranges, as shown in Table 1. These patient characteristics in the control group in this study might have affected the establishment of the cutoff value (≧30 IU/mL) of DUPAN-2 and the high diagnostic accuracy in this study. Therefore, the evaluation of serum DUPAN-2 in patients with hepatitis and cirrhosis as a control group is necessary. An investigation of the relationship between the serum concentration of DUPAN-2 and the expression of DUPAN-2 in cancerous and noncancerous (hepatitis and cirrhosis) may clarify their association with liver disease.

An important feature of tumor markers is that they are useful for detecting early-stage diseases. Stage Ⅰ tumors are characterized by small and non-invasive growth without lymph node metastasis[25]. Such conditions are difficult to diagnose on the basis of imaging examinations[43,44] and/or conventional tumor markers[9,17,43,44]. The sensitivity of CA19-9, CEA, and CA19-9+CEA for patients with stage 0-Ⅰ

BTC was very low. On the other hand, the sensitivity (60.9%) and negative predictive value (81.3%) of DUPAN-2 for patients with stage Ⅰ BTC were higher. These findings suggest that DUPAN-2 would be useful for diagnosing patients with early-stage BTC. Among 36 patients with preoperative serum DUPAN-2 concentration ≧30 IU/mL, the postoperative serum DUPAN-2 concentration decreased in 34 patients (94%) and decreased to <30 IU/mL in 25 (69%) of 36 patients without recurrence from 3 to 6 months after surgery. In addition, postoperative recurrence reflected re-elevation of serum DUPAN-2 concentration. The finding that BTC caused elevated serum DUPAN-2 concentration before surgery suggested that the latter could be useful for diagnosis of postoperative cancer recurrence if the preoperative serum DUPAN-2 concentration is ≧30 IU/mL. However, for BTC patients with a preoperative serum DUPAN-2 concentration <30 IU/mL, diagnosis of recurrence might be ineffective.

This study had some limitations. Samples from healthy volunteers will be needed to further evaluate the accuracy of DUPAN-2 for diagnosing BTC. In the present study, however, these samples could not ethically be obtained. Moreover, we evaluated the decrease in the serum DUPAN-2 concentration after surgery in patients with high preoperative concentrations; however, we could not completely analyze the re-increase in the serum DUPAN-2 concentration in patients with postoperative recurrence because of the short follow-up period. Further studies with a large number of patients in a multicenter setting and a validation study will be necessary to obtain a definitive conclusion.

In conclusion, we investigated the usefulness of measuring the serum concentration of DUPAN-2 in patients with BTC in comparison with that of measuring the serum concentrations of CA19-9 and CEA, which are 2 conventional tumor markers. A serum DUPAN-2 concentration of ≧30 IU/mL or a combination of a DUPAN-2 concentration of ≧30 IU/mL with CA19-9 and CEA may be useful for diagnosing BTC, even at an early stage. Our results suggest that measurement of serum DUPAN-2 concentration would be useful for diagnosis of postoperative cancer recurrence.

References

1. Naghavi H, Wang H, Lozano R, Davis A. Global, regional, and national age-sex specific all-cause and cause-specific mortality for 240 causes of death, 1990-2013: a systematic analysis for the Global Burden of Disease Study 2013. Lancet 2015;385:117-171.
2. de Groen PC, Gores GJ, LaRusso NF, Gunderson LL, Nagorney DM. Biliary tract cancers. N Engl J Med 1999; 341:1368-1378.
3. Nakagohri T, Kinoshita T, Konishi M, Takahashi S, Gotohda N. Surgical outcome and prognostic factors in intrahepatic cholangiocarcinoma. World J Surg 2008;32:2675-2680.
4. Shaib Y, El-Serag HB. The epidemiology of cholangiocarcinoma. Semin Liver Dis 2004;24:115-125.
5. Deng FT, Li YX, Ye L, Tong L, Yang XP, Chai XQ. Hilar inflammatory pseudotumor mimicking hilar cholangiocarcinoma. Hepatobiliary Pancreat Dis Int 2010;9:219-221.
6. Van Beers BE. Diagnosis of cholangiocarcinoma. HPB (Oxford) 2008;10:87-93.
7. Singh VP, Rajesh S, Bihari C, Desai SN, Pargewar SS, Arora A. Xanthogranulomatous cholecystitis: what every radiologist should know. World J Radiol 2016;8:183-191.
8. Tanaka S, Kubota D, Lee SH, Oba K, Yamamoto T, Ikebe T, et al. Latent gallbladder carcinoma in a young adult patient with acute cholecystitis: report of a case. Surg Today 2007;37:713-715.
9. Patel AH, Harnois DM, Klee GG, LaRusso NF, Gores GJ. The utility of CA 19-9 in the diagnoses of cholangiocarcinoma in patients without primary sclerosing cholangitis. Am J Gastroenterol 2000;95:204-207.
10. Qin XL, Wang ZR, Shi JS, Lu M, Wang L, He QR. Utility of serum CA19-9 in diagnosis of cholangiocarcinoma: in comparison with CEA. World J Gastroenterol 2004;10:427-432.
11. Wang YF, Feng FL, Zhao XH, Ye ZX, Zeng HP, Li Z, et al. Combined detection tumor markers for diagnosis and prognosis of gallbladder cancer. World J Gastroenterol 2014;20:4085-4092.

12. Yu T, Yu H, Cai X. Preoperative prediction of survival in resectable gallbladder cancer by a combined utilization of CA 19-9 and carcinoembryonic antigen. Chin Med J (Engl) 2014;127:2299-2303.
13. Ong SL, Sachdeva A, Garcea G, Gravante G, Metcalfe MS, Lloyd DM, et al. Elevation of carbohydrate antigen 19.9 in benign hepatobiliary conditions and its correlation with serum bilirubin concentration. Dig Dis Sci 2008; 53:3213-3217.
14. Principe A, Del Gaudio M, Grazi GL, Paolucci U, Cavallari A. Mirizzi syndrome with cholecysto-choledocal fistula with a high CA19-9 level mimicking biliary malignancies: a case report. Hepatogastroenterology 2003; 50:1259-1262.
15. Nakeeb A, Lipsett PA, Lillemoe KD, Fox-Talbot MK, Coleman J, Cameron JL, et al. Biliary carcinoembryonic antigen levels are a marker for cholangiocarcinoma. Am J Surg 1996;171:147-152.
16. Chen CY, Shiesh SC, Tsao HC, Lin XZ. The assessment of biliary CA 125, CA 19-9 and CEA in diagnosing cholangiocarcinoma--the influence of sampling time and hepatolithiasis. Hepatogastroenterology 2002;49:616-620.
17. Miyazaki M, Yoshitomi H, Miyakawa S, Uesaka K, Unno M, Endo I, et al. Clinical practice guidelines for the management of biliary tract cancers 2015: the 2nd English edition. J Hepatobiliary Pancreat Sci 2015;22:249-273.
18. Macias RIR, Banales JM, Sangro B, Muntane J, Avila MA, Lozano E, et al. The search for novel diagnostic and prognostic biomarkers in cholangiocarcinoma. Biochim Biophys Acta 2018;1864:1468-1477.
19. Metzgar RS, Gaillard MT, Levine SJ, Tuck FL, Bossen EH, Borowitz MJ. Antigens of human pancreatic adenocarcinoma cells defined by murine monoclonal antibodies. Cancer Res 1982;42:601-608.
20. Sawabu N, Toya D, Takemori Y, Hattori N, Fukui M. Measurement of a pancreatic cancer-associated antigen (DU-PAN-2) detected by a monoclonal antibody in sera of patients with digestive cancers. Int J Cancer 1986; 37:693-696.
21. Yamamoto T, Yagi S, Kinoshita H, Sakamoto Y, Okada K, Uryuhara K, et al. Long-term survival after resection of pancreatic cancer: a single-center retrospective analysis. World J Gastroenterol 2015;21:262-268.
22. Okada K, Kawai M, Tani M, Hirono S, Miyazawa M, Shimizu A, et al. Predicting factors for unresectability in patients with pancreatic ductal adenocarcinoma. J Hepatobiliary Pancreat Sci 2014;21:648-653.
23. Borowitz MJ, Tuck FL, Sindelar WF, Fernsten PD, Metzgar RS. Monoclonal antibodies against human pancreatic adenocarcinoma: distribution of DU-PAN-2 antigen on glandular epithelia and adenocarcinomas. J Natl Cancer Inst 1984;72:999-1005.
24. Satake K, Takeuchi T. Comparison of CA19-9 with other tumor markers in the diagnosis of cancer of the pancreas. Pancreas 1994;9:720-724.
25. Edge S, Byrd D, Compton C, Fritz A, Greene F, Trotti A. In: AJCC Cancer Staging Manual (7th ed). New York: Springer-Verlag;2010.
26. Levy C, Lymp J, Angulo P, Gores GJ, Larusso N, Lindor KD. The value of serum CA 19-9 in predicting cholangiocarcinomas in patients with primary sclerosing cholangitis. Dig Dis Sci 2005;50:1734-1740.
27. Torzilli G, Makuuchi M, Ferrero A, Takayama T, Hui AM, Abe H, et al. Accuracy of the preoperative determination of tumor markers in the differentiation of liver mass lesions in surgical patients. Hepatogastroenterology 2002;49:740-745.
28. Hultcrantz R, Olsson R, Danielsson A, Järnerot G, Lööf L, Ryden BO, et al. A 3-year prospective study on serum tumor markers used for detecting cholangiocarcinoma in patients with primary sclerosing cholangitis. J Hepatol 1999;30:669-673.
29. Caturelli E, Bisceglia M, Villani MR, de Maio G, Siena DA. CA 19-9 production by a cystadenoma with mesenchymal stroma of the common hepatic duct: a case report. Liver 1998;18:221-224.
30. Ahrendt SA, Pitt HA, Nakeeb A, Klein AS, Lillemoe KD, Kalloo AN, et al. Diagnosis and management of cholangiocarcinoma in primary sclerosing cholangitis. J Gastrointest Surg 1999;3:357-367.
31. Ker CG, Chen JS, Lee KT, Sheen PC, Wu CC. Assessment of serum and bile levels of CA19-9 and CA125 in cholangitis and bile duct carcinoma. J Gastroenterol Hepatol 1991;6:505-508.
32. Shiozawa K, Ishii K, Mori T, Takamura N, Ikehara T, Shinohara M, et al. Heterochronous development of intrahepatic cholangiocellular carcinoma following hepatocellular carcinoma in a hepatitis B virus carrier. Intern Med 2001;40:624-630.
33. Blechacz B. Cholangiocarcinoma: current knowledge and new developments. Gut Liver 2017;11:13-26.
34. Janvilisri T, Leelawat K, Roytrakul S, Paemanee A, Tohtong R. Novel serum biomarkers to differentiate cholangiocarcinoma from benign biliary tract diseases using a proteomic approach. Dis Markers 2015;2015: 105358.
35. Ramage JK, Donaghy A, Farrant JM, Iorns R, Williams R. Serum tumor markers for the diagnosis of cholangiocarcinoma in primary sclerosing cholangitis. Gastroenterology 1995;108:865-869.

36. Li Y, Li DJ, Chen J, Liu W, Li JW, Jiang P, et al. Application of joint detection of AFP, CA19-9, CA125 and CEA in identification and diagnosis of cholangiocarcinoma. Asian Pac J Cancer Prev 2015;16:3451-3455.
37. Uenishi T, Hirohashi K, Kubo S, Yamamoto T, Yamazaki O, Kinoshita H. Clinicopathological factors predicting outcome after resection of mass-forming intrahepatic cholangiocarcinoma. Br J Surg 2001;88:969-974.
38. Yamanaka N, Okamoto E, Ando T, Oriyama T, Fujimoto J, Furukawa K, et al. Clinicopathologic spectrum of resected extraductal mass-forming intrahepatic cholangiocarcinoma. Cancer 1995;76:2449-2456.
39. Chu KM, Lai EC, Al-Hadeedi S, Arcilla CE Jr, Lo CM, Liu CL, et al. Intrahepatic cholangiocarcinoma. World J Surg 1997;21:301-305.
40. Harrison LE, Fong Y, Klimstra DS, Zee SY, Blumgart LH. Surgical treatment of 32 patients with peripheral intrahepatic cholangiocarcinoma. Br J Surg 1998;85:1068-1070.
41. Kashihara T, Ohki A, Kobayashi T, Sato T, Nishizawa H, Ogawa K, et al. Intrahepatic cholangiocarcinoma with increased serum CYFRA 21-1 level. J Gastroenterol 1998;33:447-453.
42. Kim HJ, Yun SS, Jung KH, Kwun WH, Choi JH. Intrahepatic cholangiocarcinoma in Korea. J Hepatobiliary Pancreat Surg 1999;6:142-148.
43. Khan SA, Davidson BR, Goldin R, Pereira SP, Rosenberg WM, Taylor-Robinson SD, et al. Guidelines for the diagnosis and treatment of cholangiocarcinoma: consensus document. Gut 2002;51 Suppl 6:Ⅵ 1-9.
44. Tsukada K, Takada T, Miyazaki M, Miyakawa S, Nagino M, Kondo S, et al. Diagnosis of biliary tract and ampullary carcinomas. J Hepatobiliary Pancreat Surg 2008;15:31-40.

Osaka City Med. J. Vol. 64, 99-111, 2018

Comparison of Long-term Outcomes between Thoracoscopic Esophagectomy and Open Esophagectomy by Using the Propensity Score Matching in 655 Patients with Esophageal Cancer

Shigeru Lee, Harushi Osugi, Satoru Kishida, Yushi Fujiwara,
Ryoya Hashiba, Ken Gyobu, Shoji Kubo, and Toshihiko Shibata

Department of Gastroenterological Surgery, Osaka City University Graduate School of Medicine

Abstract

Background

The recent development of minimally invasive surgery has been beneficial, therefore the number of patients underwent thoracoscopic esophagectomy (TSE) has been increasing worldwide. Nevertheless, a multicenter randomized controlled trial of long-term oncological outcomes of TSE for patients with esophageal cancer in comparison with open esophagectomy (OE) has not been yet in manuscript form.

Methods

We compared the data between 454 patients who underwent curative TSE and 201 patients who underwent curative OE from May 1995 to December 2014. In total, 174 paired cases of the 655 enrolled patients, 87 paired cases of 397 patients without metastatic mediastinal lymph node, and 66 paired cases of 258 patients with metastatic mediastinal lymph node−matched using the propensity score (PS) method−were selected for statistical analysis.

Results

After PS matching, the 5-year overall survival rate was 55.6% and 55.0% in the TSE and OE groups, respectively; no significant difference was observed in the survival curves. After PS matching among those without mediastinal lymph node metastasis, the 5-year overall survival rate was 76.3% and 62.5% in the TSE and OE groups, respectively, and after PS matching among those with mediastinal lymph node metastasis, the 5-year overall survival rate was 41.5% and 43.6% in the TSE and OE groups, respectively; no significant difference was observed in the survival curves.

Conclusions

Regardless of mediastinal lymph node metastasis, the oncological outcomes of TSE for patients with esophageal cancer do not significantly differ compared to those of OE. TSE should be considered as a standard procedure for resectable esophageal cancer.

Key Words: Thoracoscopic esophagectomy; Esophageal cancer; Propensity score matching; Long-term oncological outcome

Received September 5, 2017; accepted November 28, 2017.

Correspondence to: Shigeru Lee, MD.
Department of Gastroenterological Surgery, Osaka City University Graduate School of Medicine,
1-4-3 Asahimachi Abeno-ku, Osaka 545-8585, Japan
Tel: +81-6-6645-3880; Fax: +81-6-6646-6057
E-mail: sgr-lee@med.osaka-cu.ac.jp

Introduction

Esophageal resection is the mainstay of curative treatment in resectable esophageal cancer. However, surgeries for esophageal cancer are highly invasive and frequently result in complications. Since the first report on thoracoscopic surgery for esophageal cancer published by Cuschieri and colleagues in 1992[1], and as thoracoscopic surgery devices have evolved, the use of thoracoscopic surgery for esophageal cancer has been increasing worldwide, with the goal of reducing invasiveness and incidence of complications. The conditions in Japan are similar − a 2011 nationwide survey reported that, of 5354 annual cases of surgery for esophageal cancer, thoracoscopic esophagectomy (TSE) was performed in 1436 cases (26.8%)[2]. The first multicenter randomized controlled trial (RCT) of perioperative outcomes of TSE, in comparison with open esophagectomy (OE), for patients with esophageal cancer was recently reported[3]. Biere and colleagues concluded that, in the perioperative period, the amount of intraoperative bleeding, incidence of postoperative pneumonia, and duration of hospitalization are significantly lower with TSE than with OE. Moreover, the overall and disease-free survival duration after the operation is the most important oncological outcome parameter. However, no multicenter RCTs have investigated the long-term oncological outcomes of TSE.

The number of observational studies using the propensity score (PS) method has been increasing in recent years[4-6]. PS matching was proposed by Rosenbaum and Rubin in 1983[7] and is a method of assessment that adjusts the balance of patient characteristics between groups, thus making it a useful method of statistical analysis in cases where an RCT is difficult to perform. In the present study, we report our experience with TSE and compare its long-term oncological outcome to that of OE during the same period using PS matching method.

Methods

Patients

Since May 1995, we have routinely performed TSE with extensive mediastinal lymphadenectomy according to the same surgical principles as open surgery. From May 1995 to December 2014, 795 patients with thoracic esophageal cancer were candidates for radical esophagectomy without preoperative radiotherapy at our hospital. The contraindications for TSE are: (1) contiguous tumor spread, (2) preoperative radiotherapy due to contiguous tumor spread, (3) severely extensive pleural adhesions, and (4) pulmonary function that is incapable of sustaining single-lung ventilation. TSE was performed in 527 patients and planned OE was performed in 268 patients. TSE was converted to conventional OE in 56 patients due to pleural adhesions in 22 patients, contiguous tumor spread in 18 patients, suspected contiguous tumor spread in 10 patients, intrathoracic bleeding in 4 patients, and pulmonary function that is incapable of sustaining single-lung ventilation in 2 patients. Complete TSE was performed in 471 patients. In 17 patients, the tumor or metastatic lymph nodes had penetrated other vital structures, and therefore, palliative esophagectomy was performed thoracoscopically. Thus, curative TSE with extended lymph node dissection was completed in 454 patients (TSE group). In patients who had previously undergone gastrectomy for gastric cancer or peptic ulcer, we performed reconstruction using a jejunal pedicled graft via the posterior mediastinal route under open thoracotomy, due to the safety associated with a reconstructive conduit. From May 1995 to December 2014, in 268 patients were performed OE for esophageal cancer, but 67 patients received no curative operation. In total, 201 patients who had any of the above contraindications for TSE and hence underwent curative resection by open thoracotomy or conversion to open thoracotomy

were defined as the OE group.

Preoperative evaluations included physical examination, chest radiography, laboratory tests, respiratory function tests, electrocardiography, upper gastrointestinal endoscopy with biopsy, barium swallowing, computed tomography (CT) from the neck to the abdomen, and endoscopic ultrasonography. Positron-emission tomography (PET) was also performed from April 2006. Clinicopathological staging was performed according to the 2009 International Union Against Cancer TNM classification (7th edition)[7].

Surgery

The thoracoscopic procedure is performed with the patients in the left lateral position. The trachea was intubated with a double-lumen tube, and the right lung is deflated during the thoracic procedure. Four 11.5-mm trocars are inserted as follows: third intercostal space in the anterior axillary line, 5th intercostal space in the posterior axillary line, 7th intercostal space in the middle axillary line, and 7th intercostal space in the anterior axillary line. A 5-cm minithoracotomy is created in the 5th intercostal space in the middle axillary line, where the camera and a 3-cm wide retractor designed by us are inserted. In patients with lower esophageal cancer, abdominothoracic resection comprising radical lymphadenectomy (including the lymph nodes at the celiac trunk, left gastric artery, paracardial, periesophageal, bifurcational, the upper mediatinal, and the surrounding laryngeal recurrent nerve) was performed. In patients with upper or mid-esophageal cancer, cervicoabdominothoracic (three-field) resection comprising radical lymphadenectomy was performed. The magnifying effect of a video, according to the microanatomy by positioning the camera at close vicinity to the dissection, is essential to perform the higher quality of dissection than open surgery (Fig. 1). The conventional open surgery procedure is performed with the patients in the left lateral position and the right lung is deflated with a double-lumen tube in the same way as the thoracoscopic procedure. The conventional open surgery was performed using right posterolateral thoracotomy.

Propensity score analysis

We performed one-to-one matching between TSE group and OE group on the basis of estimated PS by using multivariate logistic regression analysis (stepwize method) for each patient. The usefulness and details of the PS approach in clinical studies have been discussed elsewhere[7,9,10]. The application of PS matching involves estimation of PS, followed by matching of patients according to the estimated PS and comparison of the outcomes in the matched patients. A one-to-one matched analysis using nearest-neighbor matching (Greedy matching) was performed on the basis of the estimated PS of the patients. A match occurred when a patient in the TSE group had an estimated score within 0.20 standard deviation of another in the OE group.

Statistical analysis

Descriptive statistics were presented for all patients and propensity score-matched patients. Patient characteristics, perioperative results, and surgical performance were analyzed. Continuous variables were compared by use of *t*-tests or Mann-Whitney's U-test, and categorical variables were compared by use of the chi-square test, Fisher's exact test. Univariate analyses were performed using Cox regression analysis with the forced entry method. We created Kaplan-Meier curves and used the log-rank test to assess prognosis after surgery. A value of $p<0.05$ was considered to be significant statistically each analysis. All statistical analysis were conducted with IBM SPSS version 22 (IBM, Armonk, NY, USA)

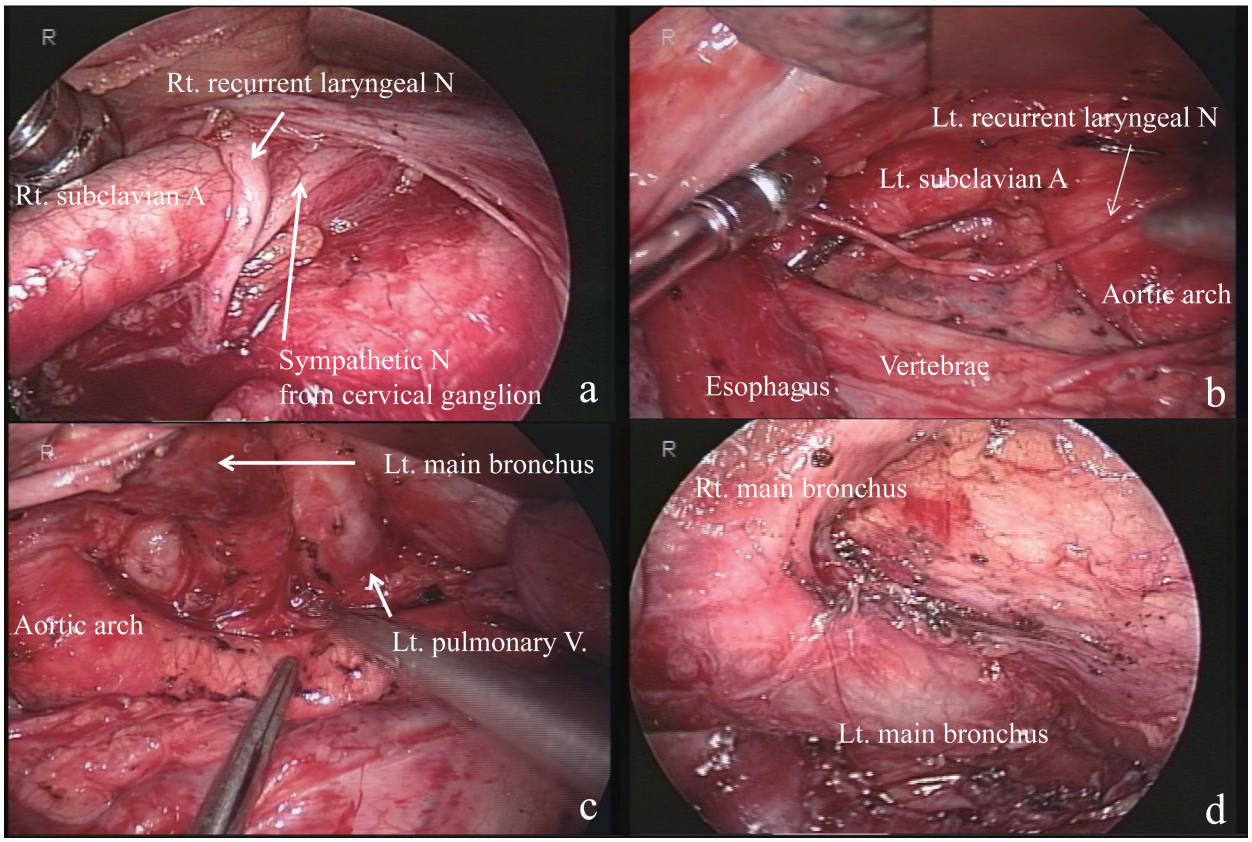

Figure. 1 Mediastinum after thoracoscopic radical esophagectomy. a, Right recurrent laryngeal nerve region. b, Left recurrent laryngeal nerve region. c, Infra-aortic arch region. d, Subcarinal region.

Results

The median and mean±standard deviation duration of follow-up among patients who survived in the TSE group before propensity matching were 4.07 years and 4.95±3.87 years, respectively, whereas those of patients in the OE group were 3.76 years and 4.89±4.06 years, respectively; no significant difference in these values is present between the two groups. Thirty-five patients (5.3%) who survived were not followed up more than 5 years after the operation, including 23 (5.0%) in the TSE group and 12 (6.0%) in the OE group; this number did not significantly differ between the two groups. No intraoperative mortalities were noted in either group. The 30-day and operative mortality rates of all patients in the present study were 0.8% (5/655) and 1.4% (9/655), respectively. The 30-day mortality rate was 0.7% (3/454) in the TSE group and 1.0% (2/201) in the OE group ($p=0.649$), whereas the operative mortality rate was 0.9% (4/454) in the TSE group and 2.5% (5/201) in the OE group ($p=0.103$). A trend toward improved operative mortality was noted in the TSE group, although this trend was not statistically significant.

The results of univariate analysis are summarized in Table 1. In univariate analysis, the following were all significant prognosticators: age; preoperative combined disease such as diabetes mellitus, cardiovascular disease; respiratory disease; history of premalignant condition; pT factor; pN factor; distant metastasis (M factor); permeation of the lymphatic vessels (ly); vascular invasion (v); pTNM stage; and number of metastatic lymph nodes. The characteristics of patients before PS matching are summarized in Table 2. Significant differences were observed between the two groups

Table 1. Univariate analysis of the prognostic influence of patient characteristics on overall survival in 655 patients performed curative resection

Variables	n	HR	95% CI	p value
Age (per year)	65.3±8.32*	1.027	1.011-1.043	**0.001**
Gender (Male/Female)	540/115	1.021	0.741-1.405	0.901
Combined disease	412	1.354	1.039-1.766	**0.025**
BMI	21.2±2.85*	0.926	0.886-0.969	**0.001**
Respiratory function				
%VC	111.2±16.6*	0.987	0.980-0.995	**0.001**
FEV1.0 (L)	2.54±0.62*	0.793	0.649-0.970	**0.024**
Preoperative another cancer				
Metachronous	67	1.661	1.150-2.400	**0.007**
Synchronous	65	1.161	0.778-1.734	0.464
Neoadjuvant chemotherapy	176	1.073	0.772-1.491	0.676
Adjuvant chemotherapy	258	1.488	1.160-1.909	**0.002**
Histology (Squamous cell carcinoma/ Others including adenocarcinoma)	613/42	1.521	0.973-2.379	0.066
Location				
Upper	63			0.259
Middle	343	1.261	0.844-1.885	0.257
Lower	199	0.913	0.698-1.193	0.504
Depth of tumor invasion				
pT0	8			<**0.001**
pT1	282	0.366	0.091-1.478	0.158
pT2	100	0.356	0.267-0.475	<**0.001**
pT3	265	0.602	0.421-0.862	**0.006**
Lymph node metastasis				
pN0	308			<**0.001**
pN1	170	0.177	0.123-0.253	<**0.001**
pN2	108	0.265	0.181-0.388	<**0.001**
pN3	69	0.593	0.408-0.862	**0.006**
Lymphatic vessel invasion	384	3.018	2.241-4.064	<**0.001**
Blood vessel invasion	107	2.336	1.755-3.107	<**0.001**
Distant metastasis	43	2.779	1.895-4.074	<**0.001**
Pathological stage				
pStage 0	4			<**0.001**
pStage 1	236	0.000	0.000-6.013	0.943
pStage 2	154	0.195	0.125-0.306	<**0.001**
pStage 3	218	0.301	0.190-0.475	<**0.001**
pStage 4	43	0.671	0.449-1.002	0.051

Significant differences are marked in bold. *Values depicted are expressed as mean±SD. BMI, body mass index; VC, vital capacity; FEV, forced expiratory volume; HR, hazard ratio; and CI, confidence intervals.

Table 2. Characteristics of all patients before and after propensity score matching

	Before propensity score matching (n=655)			After propensity score matching (n=348)			
	TSE group (n=454)	OE group (n=201)	p value	TSE group (n=174)	OE group (n=174)	p value	Standardized differences
Age (mean±SD)	64.5±8.23	66.9±8.28	**0.001**	66.7±8.19	66.2±8.41	0.010	0.041
Gender (Male/Female)	363 (80.0%)/ 91 (20.0%)	177 (88.1%)/ 24 (11.9%)	**0.012**	149 (85.6%)/ 25 (14.4%)	150 (86.2%)/ 24 (13.8%)	0.878	0.032
Combined disease	269 (59.3%)	143 (71.1%)	**0.004**	123 (70.7%)	120 (69.0%)	0.731	0.012
BMI (mean±SD)	20.9±2.88	21.1±2.81	0.102	21.0±2.57	20.9±2.92	0.744	0.037
Respiratory function							
%VC (mean±SD)	112.8±16.3	106.5±16.3	<**0.001**	107.1±14.9	107.3±16.4	0.670	0.013
FEV1.0 (L, mean±SD)	2.60±0.64	2.42±0.58	**0.001**	2.44±0.58	2.43±0.60	0.781	0.006
Preoperative another cancer							
Metachronous	30 (6.6%)	37 (18.4%)	<**0.001**	21 (12.1%)	25 (14.4%)	0.527	0.056
Synchronous	32 (7.1%)	33 (16.4%)	<**0.001**	21 (12.1%)	24 (13.6%)	0.632	0.031
Neoadjuvant chemotherapy	125 (27.5%)	51 (25.4%)	0.565	46 (26.4%)	39 (22.4%)	0.382	0.073
Adjuvant chemotherapy	180 (39.6%)	81 (40.3%)	0.821	70 (39.3%)	68 (38.2%)	0.450	0.023
Number of harvested mediastinal lymph node (mean±SD)	32.28±12.28	32.08±11.13	0.919	33.59±13.20	31.94±10.79	0.352	0.136
Number of metastatic mediastinal lymph node (mean±SD)	2.34±4.73	2.69±4.68	0.168	1.36±2.83	1.33±2.28	0.732	0.029
Total number of metastatic lymph node (mean±SD)	2.34±4.73	2.69±4.68	0.168	2.74±4.64	2.69±4.62	0.988	0.009
Histology			0.969			0.499	0.051
Squamous cell carcinoma	425 (93.6%)	188 (93.5%)		162 (93.1%)	165 (94.8%)		
Others included adenocarcinoma	29 (6.4%)	13 (6.5%)		12 (6.9%)	9 (5.2%)		
Depth of tumor invasion							
pT0/1-3	8 (1.8%)/ 446 (98.2%)	0 (0%)/ 201 (100%)	0.058	0 (0%)/ 174 (100%)	0 (0%)/ 174 (100%)	1.000	0.000
pT0-1/2-3	233 (51.3%)/ 221 (48.7%)	57 (28.4%)/ 144 (71.6%)	<**0.001**	56 (32.2%)/ 118 (67.8%)	56 (32.2%)/ 118 (67.8%)	1.000	0.000
pT0-2/3	302 (66.5%)/ 152 (33.5%)	88 (43.8%)/ 113 (56.2%)	<**0.001**	81 (46.6%)/ 93 (53.2%)	82 (47.1%)/ 92 (52.9%)	0.914	0.034
Lymph node metastasis							
pN0/1-3	219 (48.2%)/ 235 (51.8%)	89 (44.3%)/ 112 (55.7%)	0.349	78 (44.8%)/ 96 (55.2%)	77 (44.3%)/ 97 (55.7%)	0.914	0.023
pN0-1/2-3	335 (73.8%)/ 119 (26.2%)	143 (71.1%)/ 58 (28.9%)	0.482	120 (69.0%)/ 54 (31.0%)	123 (70.7%)/ 51 (29.3%)	0.726	0.029
pN0-2/3	411 (90.5%)/ 43 (9.5%)	175 (87.1%)/ 26 (12.9%)	0.183	153 (87.9%)/ 21 (12.1%)	152 (87.4%)/ 22 (12.6%)	0.871	0.034
Lymphatic vessel invasion	255 (56.2%)	129 (64.2%)	0.055	103 (59.2%)	111 (63.8%)	0.378	0.067
Blood vessel invasion	65 (14.3%)	42 (20.9%)	0.036	32 (18.7%)	33 (19.0%)	0.892	0.014
Distant metastasis	27 (5.9%)	17 (8.5%)	0.228	16 (9.0%)	16 (9.0%)	1.000	0.000
Pathological stage							
pStage 0/1-4	4 (0.9%)/ 450 (99.1%)	0 (0.0%)/ 201 (100%)	0.182	0 (0%)	0 (0%)	1.000	0.000
pStage 0-1/2-4	189 (41.6%)/ 265 (58.4%)	51 (25.4%)/ 150 (74.6%)	<**0.001**	53 (30.5%)/ 121 (69.5%)	47 (27.0%)/ 127 (73.0%)	0.477	0.134
pStage 0-2/3-4	287 (63.2%)/ 167 (36.8%)	107 (53.2%)/ 94 (46.8%)	0.016	91 (52.3%)/ 83 (47.7%)	95 (54.6%)/ 79 (45.4%)	0.667	0.072
pStage 0-3/4	428 (94.3%)/ 26 (5.7%)	184 (91.5%)/ 17 (8.5%)	0.193	163 (93.7%)/ 11 (6.3%)	159 (91.4%)/ 15 (8.6%)	0.415	0.091

Significant differences are marked in bold. TSE, thoracoscopic esophagectomy; OE, open esophagectomy; and BMI, body mass index.

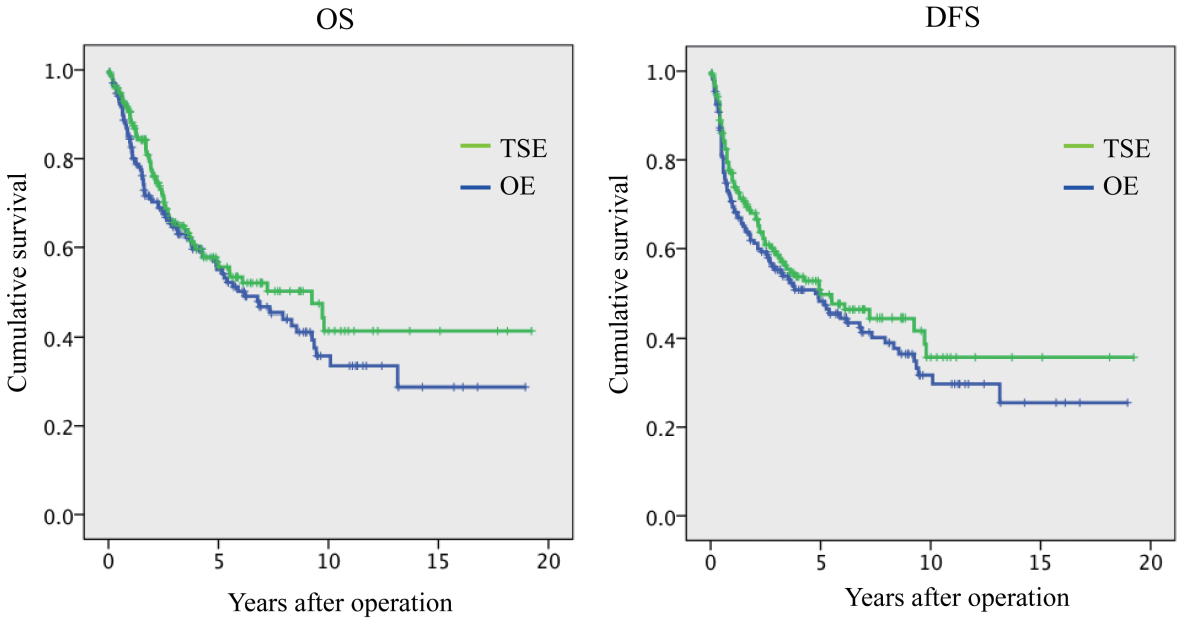

	2-year survival	5-year survival	Median (year)	95% CI (year)	p value
TSE	70.2%	55.0%	2.92	4.91-13.58	0.263
OE	76.7%	55.6%	2.90	3.98-8.38	

	2-year survival	5-year survival	Median (year)	95% CI (year)	p value
TSE	68.0%	49.7%	2.38	2.09-7.90	0.284
OE	61.2%	48.1%	2.61	2.58-6.96	

Figure. 2 The cumulative overall survival (OS) and disease-free survival (DFS) of all patients after propensity score matching. TSE, thoracoscopic esophagectomy; OE, open esophagectomy; and 95% CI, 95% confidence intervals.

in each of the following: age; gender; preoperative combined diseases; %VC; FEV1.0%; pT factor; and pTNM stage. The variables that were significantly different between the two groups and all significant prognosticators on univariate analysis were then used to perform PS matching.

As a result, 174 matched groups were created for each characteristic (*c* statistic=0.732). The patient characteristics after PS matching are summarized in Table 2. The standardized differences in all the meaningful characteristics between the matched groups were ≦0.1. The Kaplan-Meier survival curves were created for the TSE group and the OE group and were then assessed with a log-rank test. Before PS matching, the 5-year overall survival rate was 63.5% in the TSE group and 54.2% in the OE group; thus, the TSE group demonstrated a significantly favorable prognosis in its survival curve (p=0.030, not presented). After PS matching, however, the 5-year overall survival rate was 55.6% in the TSE group and 55.0% in the OE group; thus, there was no significant difference in the survival curves (p=0.263) (Fig. 2). After PS matching, the 5-year disease-free survival rate was 49.7% in the TSE group and 48.1% in the OE group; thus, no significant difference was noted in the survival curves (p=0.284) (Fig. 2).

Among the 397 patients without mediastinal lymph node metastasis, PS matching was similarly performed using the previously mentioned characteristics, resulting in the creation of 87 matched groups for each characteristic (*c* statistic=0.759). The patient characteristics before and after PS matching are summarized in Table 3. The standardized differences in all the characteristics between matched groups were ≦0.1. After PS matching, the 5-year overall survival rate was 76.3% in the

Table 3. Characteristics of patients without metastatic mediastinal lymph node before and after propensity score matching

	Before propensity score matching (n=397)			After propensity score matching (n=174)			
	TSE group (n=287)	OE group (n=110)	p value	TSE group (n=87)	OE group (n=87)	p value	Standardized differences
Age (mean±SD)	64.5±8.22	68.0±8.22	<**0.001**	66.2±7.49	67.0±8.32	0.910	0.072
Gender (Male/Female)	234 (81.5%)/ 53 (18.5%)	97 (90.0%)/ 11 (10.0%)	**0.040**	78 (89.7%)/ 9 (10.3%)	76 (87.4%)/ 11 (12.6%)	0.635	0.097
Combined disease	176 (61.3%)	79 (71.8%)	0.051	60 (69.0%)	63 (72.4%)	0.617	0.076
BMI (mean±SD)	21.5±2.90	21.1±2.81	0.116	21.1±2.80	21.3±2.92	0.744	0.080
Respiratory function							
%VC (mean±SD)	112.5±16.0	105.1±16.3	<**0.001**	108.4±15.4	107.7±15.9	0.670	0.013
FEV1.0 (L, mean±SD)	2.57±0.61	2.37±0.55	**0.001**	2.45±0.57	2.42±0.56	0.781	0.006
Preoperative another cancer							
Metachronous	20 (7.0%)	22 (20.0%)	<**0.001**	11 (12.6%)	11 (12.6%)	1.000	0.000
Synchronous	23 (8.0%)	14 (12.7%)	0.148	8 (9.2%)	10 (11.5%)	0.619	0.076
Neoadjuvant chemotherapy	78 (27.2%)	25 (22.7%)	0.365	22 (25.3%)	20 (23.0%)	0.723	0.054
Adjuvant chemotherapy	59 (20.6%)	24 (21.8%)	0.782	21 (24.1%)	18 (21.8%)	0.719	0.055
Number of harvested mediastinal lymph node (mean±SD)	32.04±11.94	30.96±11.48	0.319	33.59±13.20	31.94±10.79	0.352	0.146
Total number of metastatic lymph node (mean±SD)	0.63±2.33	0.61±2.05	0.381	0.78±2.61	0.86±3.09	0.482	0.036
Histology			0.129			0.650	0.069
Squamous cell carcinoma	268 (93.4%)	107 (97.3%)		84 (96.6%)	85 (97.7%)		
Others included adenocarcinoma	19 (6.6%)	3 (2.7%)		3 (3.4%)	2 (3.4%)		
Depth of tumor invasion							
pT0/1-3	6 (2.1%)/ 281 (97.9%)	0 (0%)/ 110 (100%)	0.126	0/ 0 (0%)	0/ 0 (0%)	1.000	0.000
pT0-1/2-3	187 (65.2%)/ 100 (34.8%)	43 (39.1%)/ 67 (60.9%)	<**0.001**	43 (47.8%)/ 47 (52.2%)	41 (45.6%)/ 49 (54.4%)	0.497	0.045
pT0-2/3	228 (79.4%)/ 59 (20.6%)	59 (53.6%)/ 51 (46.4%)	<**0.001**	55 (61.1%)/ 35 (38.9%)	54 (60.0%)/ 36 (40.0%)	0.749	0.023
Lymph node metastasis							
pN0/1-3	219 (76.3%)/ 68 (23.7%)	89 (80.9%)/ 21 (19.1%)	0.325	65 (74.7%)/ 22 (25.1%)	68 (78.2.%)/ 19 (21.8%)	0.721	0.081
pN0-1/2-3	268 (93.4%)/ 19 (6.6%)	104 (94.5%)/ 6 (5.5%)	0.669	81 (93.1%)/ 6 (6.9%)	83(95.4%)/ 4 (4.6%)	0.747	0.099
pN0-2/3	284 (98.7%)/ 3 (1.3%)	108 (98.2%)/ 2 (1.8%)	0.537	85 (97.7%)/ 2 (2.3%)	85 (97.7%)/ 2 (2.3%)	1.000	0.000
Lymphatic vessel invasion	116 (40.4%)	52 (47.3%)	0.216	41 (47.1%)	42 (48.3%)	0.879	0.239
Blood vessel invasion	30 (10.5%)	14 (12.7%)	0.518	10 (11.5%)	10 (11.5%)	1.000	0.000
Distant metastasis	5 (1.7%)	3 (2.7%)	0.532	3 (3.4%)	3 (3.4%)	1.000	0.000
Pathological stage							
pStage 0/1-4	4 (1.4%)/ 283 (98.6%)	0 (0.0%)/ 110 (100%)	0.213	0 (0%)/ 87 (100%)	0 (0%)/ 87 (100%)	1.000	0.000
pStage 0-1/2-4	189 (65.9%)/ 98 (34.1%)	51 (46.4%)/ 59 (53.6%)	<**0.001**	42 (48.3%)/ 45 (51.7%)	45 (51.7%)/ 42 (48.3%)	0.649	0.034
pStage 0-2/3-4	250 (87.1%)/ 37 (12.9%)	95 (86.4%)/ 15 (13.6%)	0.844	74 (85.1%)/ 13 (14.9%)	74 (85.1%)/ 13 (14.9%)	1.000	0.000
pStage 0-3/4	282 (98.0%)/ 5 (1.7%)	107 (97.3%)/ 3 (2.7%)	0.532	84 (96.6%)/ 3 (3.4%)	84 (96.6%)/ 3 (3.4%)	1.000	0.000

Significant differences are marked in bold. TSE, thoracoscopic esophagectomy; OE, open esophagectomy; and BMI, body mass index.

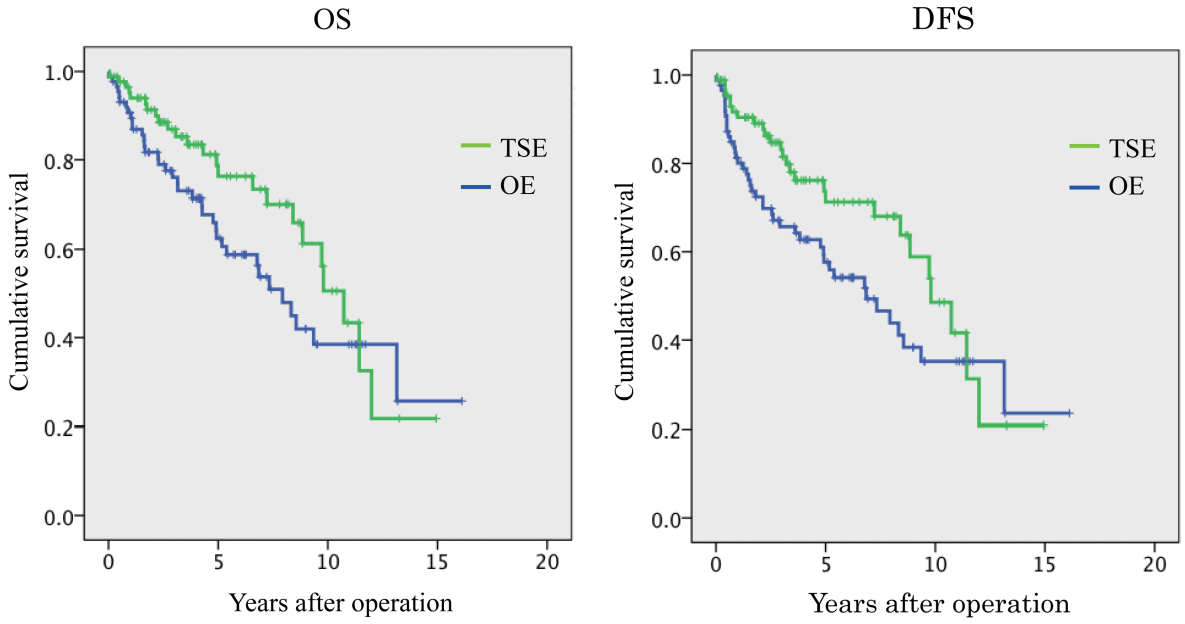

	2-year survival	5-year survival	Median (year)	95% CI (year)	p value
TSE	91.3%	76.3%	3.69	9.09-12.37	0.080
OE	81.7%	62.5%	4.02	6.06-9.80	

	2-year survival	5-year survival	Median (year)	95% CI (year)	p value
TSE	89.1%	71.3%	3.40	7.76-11.83	0.061
OE	72.4%	57.6%	3.66	4.03-9.67	

Figure. 3 The cumulative overall survival (OS) and disease-free survival (DFS) of patients without metastatic mediastinal lymph node after propensity score matching. TSE, thoracoscopic esophagectomy; OE, open esophagectomy; and 95% CI, 95% confidence intervals.

TSE group and 62.5% in the OE group (p=0.080). The 5-year disease-free survival rate was 69.2% in the TSE group and 57.3% in the OE group (p=0.061) (Fig. 3). There was no significant difference in the survival curves between the two groups, however, a trend toward improved survival curve after operation was noted in the TSE group.

Among the 258 patients with mediastinal lymph node metastasis, PS matching was similarly performed using the previously mentioned characteristics, resulting in the creation of 66 matched groups for each characteristic (*c* statistic=0.703). The patient characteristics before and after PS matching are summarized in Table 4. The standardized differences in all the characteristics between matched groups were ≦0.1. After PS matching, the 5-year overall survival rate was 41.5% in the TSE group and 43.6% in the OE group; thus, there was no significant difference in the survival curves (p= 0.671) (Fig. 4). After PS matching, the 5-year disease-free survival rate was 29.3% in the TSE group and 33.2% in the OE group; thus, there was similarly no significant difference in the survival curves (p =0.878) (Fig. 4).

Discussion

More than two decades have passed since the first report of TSE for patients with esophageal cancer by Cuschieri and colleagues in 1992[1]. However, TSE is not technically easy, and the operator needs to be sufficiently experienced to achieve satisfactory outcomes[11-13]. The recent development of

Table 4. Characteristics of patients with metastatic mediastinal lymph node before and after propensity score matching

	Before propensity score matching (n=258)			After propensity score matching (n=132)			
	TSE group (n=167)	OE group (n=91)	p value	TSE group (n=66)	OE group (n=66)	p value	Standardized differences
Age (mean±SD)	64.6±8.29	65.6±8.16	0.362	65.0±9.17	65.2±8.08	0.936	0.014
Gender (Male/Female)	129 (77.2%)/ 38 (22.8%)	78 (85.7%)/ 13 (14.3%)	0.105	53 (80.3%)/ 13 (19.7%)	54 (81.8%)/ 12 (18.2%)	0.826	0.039
Combined disease	93 (55.7%)	64 (70.3%)	**0.021**	38 (57.6%)	41 (62.1%)	0.723	0.000
BMI (mean±SD)	21.1±17.0	20.7±17.0	0.347	20.8±17.0	20.9±17.0	0.885	0.025
Respiratory function							
%VC (mean±SD)	113.5±17.0	109.2±16.6	**0.049**	110.6±17.5	109.1±16.6	0.825	0.039
FEV1.0 (L, mean±SD)	2.64±0.68	2.50±0.58	0.104	2.53±0.73	2.53±0.60	0.663	0.076
Preoperative another cancer							
Metachronous	10 (6.0%)	15 (16.5%)	**0.008**	9 (13.6%)	7 (10.6%)	0.791	0.000
Synchronous	9 (5.4%)	19 (20.9%)	<**0.001**	9 (13.6%)	9 (13.6%)	1.000	0.000
Neoadjuvant chemotherapy	47 (28.1%)	26 (28.6%)	0.886	17 (25.8%)	16 (24.2%)	0.841	0.035
Adjuvant chemotherapy	119 (71.3%)	56 (61.5%)	0.126	44 (66.7%)	43 (65.2%)	0.865	0.032
Number of harvested mediastinal lymph node (mean±SD)	32.71±10.73	33.30±10.73	0.494	33.29±12.19	33.21±11.53	0.764	0.098
Number of metastatic mediastinal lymph node (mean±SD)	2.92±3.32	3.29±3.54	0.245	2.98±3.69	3.27±3.26	0.245	0.083
Total number of metastatic lymph node (mean±SD)	5.27±6.29	5.19±5.51	0.780	5.68±7.61	5.30±5.61	0.860	0.057
Histology			0.151			0.729	0.068
Squamous cell carcinoma	157 (94.0%)	81 (89.0%)		63 (95.5%)	62 (93.9%)		
Others included adenocarcinoma	10 (6.0%)	10 (11.0%)		3 (4.5%)	4 (6.1%)		
Depth of tumor invasion							
pT0/1-3	2 (1.2%)/ 165 (98.8%)	0 (0%)/ 91 (100%)	0.542	0/ 0 (0%)	0/ 0 (0%)	1.000	0.000
pT0-1/2-3	46 (27.5%)/ 121 (72.5%)	14 (15.4%)/ 77 (84.6%)	**0.031**	17 (23.0%)/ 57 (77.0%)	14 (18.1%)/ 48 (81.9%)	0.497	0.099
pT0-2/3	74 (44.3%)/ 9 (55.7%)	29 (31.9%)/ 62 (68.1%)	0.062	23 (34.8%)/ 43 (65.2%)	23 (34.8%)/ 43 (65.2%)	1.000	0.000
Lymph node metastasis							
pN0/1-3	0 (0%)/ 167 (100%)	0 (0%)/ 91 (100%)	1.000	0/ 0 (0%)	0/ 0 (0%)	1.000	0.000
pN0-1/2-3	67 (40.1%)/ 100 (59.9%)	39 (42.9%)/ 52 (57.1%)	0.693	24 (36.4%)/ 42 (63.6%)	27 (40.9%)/ 39 (59.1%)	0.789	0.093
pN0-2/3	127 (76.0%)/ 40 (24.0%)	67 (73.6%)/ 24 (26.4%)	0.763	51 (77.3%)/ 15 (22.7%)	49 (74.2%)/ 17 (25.8%)	0.747	0.071
Lymphatic vessel invasion	139 (83.2%)	77 (84.6%)	0.861	60 (90.9%)	59 (89.4%)	0.770	0.051
Blood vessel invasion	35 (21.0%)	28 (30.8%)	0.095	18 (27.3%)	17 (25.8%)	0.892	0.034
Distant metastasis	21 (12.4%)	14 (15.4%)	0.569	9 (13.6%)	10 (15.2%)	0.804	0.043
Pathological stage							
pStage 0/1-4	0 (0%)/ 167 (100%)	0 (0%)/ 91 (100%)	1.000	0 (0%)/ 66 (100%)	0 (0%)/ 66 (100%)	1.000	0.000
pStage 0-1/2-4	0 (0%)/ 167 (100%)	0 (0%)/ 91 (100%)	1.000	0 (0%)/ 66 (100%)	0 (0%)/ 66 (100%)	1.000	0.000
pStage 0-2/3-4	37 (22.2%)/ 130 (77.8%)	12 (13.2%)/ 79 (86.8%)	0.098	10 (15.2%)/ 56 (84.8%)	11 (16.7%)/ 55 (83.3%)	0.812	0.041
pStage 0-3/4	146 (86.4%)/ 21 (13.6%)	77 (84.6%)/ 14 (15.4%)	0.569	57 (86.4%)/ 9 (13.6%)	56 (84.8%)/ 10 (15.2%)	0.804	0.043

Significant differences are marked in bold. TSE, thoracoscopic esophagectomy; OE, open esophagectomy; and BMI, body mass index.

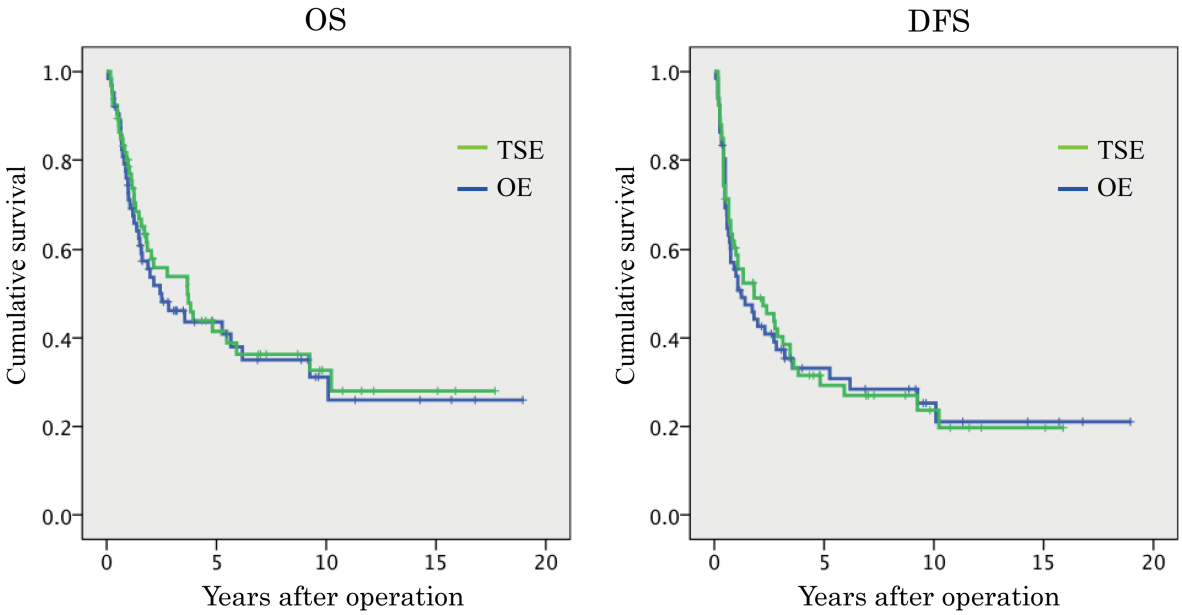

	2-year survival	5-year survival	Median (year)	95% CI (year)	p value
TSE	59.8%	41.5%	1.85	1.73-5.63	0.671
OE	53.8%	43.6%	1.97	0.73-4.30	

	2-year survival	5-year survival	Median (year)	95% CI (year)	p value
TSE	49.0%	29.3%	1.75	0.11-3.52	0.878
OE	42.6%	33.2%	1.07	0.26-2.21	

Figure. 4 The cumulative overall survival (OS) and disease-free survival (DFS) of patients with metastatic mediastinal lymph node after propensity score matching. TSE, thoracoscopic esophagectomy; OE, open esophagectomy; and 95% CI, 95% confidence intervals.

minimally invasive surgery has yielded many benefits, therefore the number of patients undergoing TSE has been increasing worldwide. In recent times, TSE in the prone or semi prone position is being increasingly performed in many countries[3,14], however; we continue to perform TSE in the left lateral position, because this approach is very safety, and educational for OE. As TSE in the left lateral position can be immediately converted to open surgery, we did not experience any intraoperative life threatening complication.

Biere and colleagues concluded that the short-term benefits were better with TSE than with OE in the first report of multicenter RCT of perioperative outcomes of TSE[3]. However, in a Japanese nationwide web-based database report, Takeuchi and colleagues reported that the overall morbidity was significantly higher in the minimally invasive esophagectomy group than in the OE group[2]. Moreover, the 30-day mortality rate and operative mortality rate after esophagectomy for cancer were 1.2% and 3.4%, respectively, in this report. Furthermore, in a review of over 1000 patients performed TSE, Luketich and colleagues reported that the combined 30-day mortality rate, including in-house mortality, after minimally invasive esophagectomy was 2.8%[14]. Hence, the 30-day mortality rate and operative mortality rate after esophagectomy for cancer in the present study of 0.8% and 1.4%, respectively, it appears acceptable; in particular, those after TSE were 0.7% and 0.9%, respectively, and those after OE were 1.0% and 2.5%, respectively, and there was no significant difference between the two groups. Specifically, the total 30-day mortality rate after TSE (0.7%) was acceptable.

Although a low mortality rate after esophagectomy was recently achieved, it remains high as compared with that after gastrectomy or colectomy[2,15-18]. Several reports state that the mortality rate after esophagectomy is correlated with the hospital volume and surgeon volume[11-13]. Esophagectomy requires experienced surgeons and a well-trained perioperative care team. Fujita and colleagues reported that the 30-day mortality rate and hospital mortality rate of a low-volume hospital and high-volume hospital were 2.0% and 6.0% and 0.6% and 2.1%, respectively[11]. The 5-year average of annual radical esophagectomies performed at our hospital is approximately 80. In the 2011 Japanese nationwide web-based database report, 5354 patients underwent esophagectomy for cancer across 713 hospitals[2]. The average number of patients who underwent esophagectomy in one hospital is 7.5, which means that many patients underwent esophagectomy in low volume hospitals in Japan. This situation may be attributable to the difference between hospital death or morbidity after esophagectomy in rest of Japan and our hospital. TSE requires a good expertise of the operating surgeons and of all assisting team, we have previously reported the learning curve of TSE for esophageal cancer[22]. In our team, TSE could be performed with beneficial outcomes after experience in treating 34 cases. Hence, the perioperative benefits of TSE in hospitals other than high-volume centers may remain controversial.

A multicenter RCT of the long-term oncologic outcomes of TSE for patients with esophageal cancer, in comparison with OE, has not been conducted. Hence, the long-term oncologic feasibility of thoracoscopic surgery for esophageal cancer is not established. To confirm the oncological benefits of TSE, an RCT is needed. However, we previously reported that the reduction of %VC on 3 months after operation was significantly lower in TSE than OE[19] and the amount of bleeding in thoracic procedure was significantly lesser in TSE than OE[20-22]. Thus, an RCT of TSE in comparison with OE among patients with esophageal cancer is difficult to perform because most of the patients with resectable esophageal cancer would prefer TSE.

In recent years, reports of the use of a PS method in observational studies have been increasing[4-6]. The advantage of using the PS method is that it balances the patient characteristics between groups, thus enabling the elimination of almost all selection bias[7,9,10]. By using this method to compare strictly and examine long-term survival following TSE and OE for thoracic esophageal cancer, a trend toward improved survival curve after operation for esophageal cancer without mediastinal lymph node metastasis was noted in the TSE group, however, we observed that TSE and OE demonstrate no significant differences in terms of overall survival and disease-free survival. Moreover, patients with mediastinal lymph node metastasis demonstrated no significant difference in, and nearly identical outcomes for, overall survival and disease-free survival between TSE and OE. The other advantages of TSE include favorable esthetic outcomes, reduction in bleeding, and preservation of postoperative respiratory function. When these advantages are taken into account, TSE can be considered superior to OE as a treatment procedure for resectable thoracic esophageal cancers, regardless of the presence of mediastinal lymph node metastasis. Thus far, a few systematic literature reviews of the oncological outcomes comparing minimum invasive esophagectomy to open esophagectomy have been published. Dantoc M and colleagues concluded that meta-analytic evidence found equivalent oncologic outcomes to conventional open esophagectomy[23]. The long-term oncological outcomes of our study matched using the PS method are similar to the results of meta-analysis that did not mention the existence of mediastinal lymph node metastasis.

References

1. Cuschieri A, Shimi S, Banting S. Endoscopic oesophagectomy through a right thoracoscopic approach. J R Coll Surg Edinb 1992;37:7-11.
2. Takeuchi H, Miyata H, Gotoh M, Kitagawa Y, Baba H, Kimura W, et al. A risk model for esophagectomy using data of 5354 patients included in a Japanese nationwide web-based database. Ann Surg 2014;260:259-266.
3. Biere SS, van Berge Henegouwen MI, Maas KW, Bonavina L, Rosman C, Garcia JR, et al. Minimally invasive versus open oesophagectomy for patients with oesophageal cancer; a multicenter, open-label, randomized controlled trial. Lancet 2012;379:1887-1892.
4. Gum PA, Thamilarasan M, Watanabe J, Blackstone EH, Lauer MS. Aspirin use and all-caouse mortakity among patients being evaluated for known or suspected coronary artery desease. JAMA 2001;286:1187-1194.
5. Stukel TA, Fisher ES, Wennberg DE, Alter DA, Gottlieb DJ, Vermeulen MJ. Analysis of observational studies in the presence of treatment selection bias; effects of invasivecardiac management on AMI survival score and instrumental variablw methods. JAMA 2007;297:278-285.
6. Griswold ME, Lacalio AR, Mulrow C. Propensity score adjustment with multilevel data: setting your site on decreasing selectin bias. Ann Intern Med 2010;152:393-395.
7. Rosenbaum PR, Rubin DB. The central role of the propensity score in observational studies for causal effects. Biometrika 1983;70:41-55.
8. Sobin LH, Gospodarowwicz MK, Wittekind C. UICC TNM Classification of Malignant Tumours, 7th edn. Oxford, wiley-Blackwell 2009. pp63-72.
9. D'Agostino RB Jr. Propensity score methods for bias reduction in the comparison of a treatment to a non-randomized control group. Stat Med 1998;17:2265-2281.
10. Austin PC, Mamdani MM. A comparison of propensity score methods: a case study estimating the effectiveness of post-AMI statin use. Stat Med 2006;25:2084-2106.
11. Fujita H, Ozawa S, Kuwano H, Ueda Y, Hattori S, Yanagawa T, et al. Esophagectomy for cancer: clinical concerns support centralizing operations within the larager hospitals. Dis Esophagus 2010;23:145-152.
12. Migliore M, Choong CK, Lim E, Goldsmith KA, Ritchie A, Wells Fc. A surgeon's case volume of esophagectomy for cancer strongly influences the operative mortality rate. Eur J Cardiothorac Surg 2007;32:375-380.
13. Rodgers M, Jobe BA, O'Rourke RW, Sheppard B, Diggs B, Hunter JG. Case volume as a predictor of inpatient mortality after esophagectomy. Arch Surg 2007;142:829-839.
14. Luketich JD, Pennathur A, Awais O, Levy RM, Keeley S, Shende M, et al. Outcomes after minimally invasive esophagectomy; review of over 1000 patients. Ann Surg 2012;256:95-103.
15. Moriwaki Y, Kobayashi S, Kunisaki C, Harada H, Imai S, Kido Y, et al. Is D2 lymphadenectomy in gastrectomy safe with regard to the skill of the operation? Dig Surg 2001;18:111-117.
16. Watanabe M, Miyata H, Gotoh M, Baba H, Kimura W, Tomita N, et al. Total gastrectomy risk model: data from 20,011 Japanese patients in a nationwide internet-based database. Ann Surg. 2014;260:1034-1039.
17. Kobayashi H, Miyata H, Gotoh M, Baba H, Kimura W, Kitagawa Y, et al. Risk model for right hemicolectomy based on 19,070 Japanese patients in the National Clinical Database. J Gastroenterol 2014;49:1047-1055.
18. Birkmeyer JD, Siewers AE, Finlayson EV, Stukel TA, Lucas FL, Batista I, et al. Hospital volume and surgical mortality in the United States. N Engl J Med 2002;346:1128-1137.
19. Taguchi S, Osugi H, Higashino M, Tokuhara T, Takada N, Takemura M, et al. Comparison of three-fields esophagectomy for esophageal cancer incorporating open or thoracoscopic thoracotomy. Surg Endosc 2003;17: 1445-1450.
20. Osugi H, Takemura M, Higashino M, Takada N, Lee S, Kinoshita H. A coparison of video-assisted thoracoscopic oesophageactomy and radical lymph node dissection for squamous cell cancer of the oesophagus with open operation. Br J Surg 2003;90:108-113.
21. Osugi H, Takemura M, Lee S, Nisihikaawa T, Fukuhara K, Iwasaki H, et al. Thoracocscopic esophagectomy for intrathoracic esophageal cancer. Ann Thorac Cardiovasc Surg 2005;11:221-227.
22. Osugi H, Takemura M, Higashino M, Takada N, Lee S, Ueno M, et al. Learning curve of viedo-assited thoracoscopic esophageactomy and extensive lymphadecetomy for squamous cell cencer of the thoracic esophagus and results. Surg Endosc 2002;17:515-519.
23. Dantoc M, Cox MR, Eslick GD. Evidence to support the use of minimally invasive esophagectomy for esophageal cancer: a meta-analysis. Arch Surg 2012;147:768-776.

Osaka City Med. J. Vol. 64, 113-119, 2018

Molecular Characterization of Familial Platelet Disorder with Propensity to Develop Acute Myeloid Leukemia during the course of Leukemogenesis

Masaharu Nakaya, Sadao Tokimasa, Takashi Hamazaki, and Haruo Shintaku

Department of Pediatrics, Osaka City University Graduate School of Medicine

Abstract

Background

Familial platelet disorder with propensity to develop acute myeloid leukemia (FPD/AML) is an autosomal dominant disorder characterized by congenital thrombocytopenia and a predisposition for AML. This disease is caused by germline mutations in *RUNX1*, a gene encoding a hematopoietic transcription factor located at chromosome 21q22. To explore the mechanisms of leukemogenesis in FPD/AML, we focused on and characterized the molecular genetics of an FPD/AML patient with early onset of AML.

Methods

Conventionally used and very accurate G-banding chromosome analysis, micro-array-based comparative genomic hybridization, and fluorescence *in situ* hybridization were used during the remission and relapse phases. RNA sequencing and real-time polymerase chain reaction were performed during the relapse phase.

Results

In the patient investigated in this study, we found a congenital complicated structural anomaly only on chromosome 21, which caused separation of the *RUNX1* gene. Upon leukemogenesis, the 5' region of *RUNX1* was amplified several folds with the breakpoint of *RUNX1* being located between exons 3 and 4. Neither additional fusion gene products nor previously reported mutations were observed.

Conclusions

These data suggest amplification of an aberrant *RUNX1* gene promotes the development of leukemia in patients with FPD/AML.

Key Words: FPD/AML; *RUNX1*; Leukemogenesis

Introduction

Familial platelet disorder with propensity to develop acute myeloid leukemia (FPD/AML)

Received September 13, 2017; accepted November 28, 2017.
Correspondence to: Sadao Tokimasa MD, PhD
Department of Pediatrics, Osaka City University Graduate School of Medicine,
1-4-3 Asahimachi, Abeno-ku, Osaka 545-8585, Japan
Tel: +81-6-6645-3816; Fax: +81-6-6636-8737
E-mail: tokimasa@med.osaka-cu.ac.jp

is an autosomal dominant disorder characterized by thrombocytopenia and a predisposition for myelodysplastic syndrome (MDS)/acute myeloid leukemia (AML). It is caused by germline aberrations in the hematopoietic transcription factor *RUNX1*, which is located at chromosome 21q22. Most cases of FPD/AML are a result of germline point mutations in the *RUNX1* gene, but there are rare cases with large deletions at 21q22[1]. *RUNX1* encodes a transcription factor, which contains an amino-terminal DNA-binding "RUNT" homology domain (RHD) and a carboxyl-terminal transactivation domain, essential for definitive hematopoiesis[2]. The predisposition of myeloid leukemia varies between individual patients. Although the average age of onset of leukemia in FPD/AML patients is 34 years, the youngest recorded patient was 6 years old[3].

The mechanisms of leukemogenesis are complex and largely uncharacterized. Several additional genetic events involved at this stage have been identified, including mutations in *CBL*[4], *CDC25C*[1], and *TET2*[5]. Various parts of *RUNX1* can combine with other genes to create fusion genes, such as *RUNX1/ETO*[6]. Therefore, haploinsufficiency of the *RUNX1* gene alone in FPD/AML patients is not sufficient for leukemogenesis and a certain "second hit" may be required[3].

To explore the mechanisms of leukemogenesis in FPD/AML patients, we extensively characterized the molecular genetics of *RUNX1* in a FPD/AML patient with early onset of AML. Unique chromosomal anomalies were discovered in the *RUNX1* locus, including amplification of a specific region of this gene over the course of leukemogenesis.

Methods

Case

The patient investigated in this study was male and the second child of healthy unrelated parents. His family history was unremarkable. He had a funnel chest, flexible ankle and mild mental retardation. Mild thrombocytopenia was noted soon after birth and no serious bleeding episodes were documented by the age of 7 years. At the age of 7 years, he developed AML (The French-American-British [FAB] classification M4). Several courses of chemotherapy were administered and resulted in complete remission. However, the patient showed relapse one year later and received a transplant of unrelated umbilical cord blood. He has been disease-free for more than 3 years.

Sample isolation and characterization

This present study was approved by the ethics committee of the Osaka City University (No. 2476) and the informed written consent was obtained from the parents of the patient.

Peripheral blood lymphocytes (PBLs) were isolated using a Ficoll gradient. *RUNX1* mutation analysis was performed on the patient's PBLs during complete remission.

Cytogenetic analysis

Karyotype analysis was performed using highly accurate G-banding at a resolution of 400-550 bands (LSI Medience Corporation, Tokyo, Japan). The definition of a cytogenetic clone and descriptions of karyotypes were according to the International System for Human Cytogenetic Nomenclature.

Micro-array-based comparative genomic hybridization (array-CGH)

Genomic copy numbers were measured using the Human Genome CGH Microarray 60k (Agilent Technologies, Santa Clara, CA) as previously described[7].

Fluorescence in situ hybridization

Fluorescence *in situ* hybridization (FISH) was performed using *RUNX1*-specific probes (LSI Medience Corporation, Tokyo, Japan) according to the manufacturer's instructions.

Table 1. Primer sequences

	Forward Primer	Reverse Primer
SOX1	ATTATTTTGCCCGTTTTCCC	TCAAGGAAACACAATCGCTG
SETD4	CATGCCGACTTTCGTTAGGT	AGGGCAGAAATGAGCAAGAG
intergenic region	TAGCACCCCAGTGAAAAAGG	CTGGGGTAGGCAAATTACCA
RUNX1		
exon 1	TCGCTCCGAAGGTAAAAGAA	TATGCTGTCTGAAGCCATCG
introns 1-2	GATGTGAGGGGCCTGAATAA	GGCTCTTTCTCCCTCCATCT
exon 2	CAGCGTTTACCATAGGTGCAT	GGAAGCCAAGCTCTGTTTTG
exon 3	TAAAGGCCCCTGAACGTGTA	GTTAGGACCCTGCAAACAGC
exon 4	GGCTGGCAATGATGAAAACT	CCGACAAACCTGAGGTCATT
exon 5	GGGCAGCATGAAACTAAGGA	CCTGGCCAATCTTCCATTTA
exon 6	CCAACAATTAATGCGCCTCT	ACTTCCAATGGGCACAACTC
introns 6-7.1	GTTCATTGGGACCAAGTGCT	CTCAAAGTGAGGCACGCATA
introns 6-7.2	TTCTAGCCTGCTCCTCCAAA	GGTACCAAGATGTGGGGTTG
introns 7-8	GAGCTGCACCAAACTGTGAA	ATCCCAAGAGCTGAAAAGCA
exon 8	CACGCGCTACCACACCTAC	GAGGCGCCGTAGTACAGGT
CLIC6	TGTTCTAAGCCTCCCAGCAT	GCACCAAGAGAAACACAGCA

Quantification of gene copy numbers

Copy numbers of specific genomic regions were quantified using real-time PCR. Genomic DNA was extracted from bone marrow cells. The copy number of a target region was expressed relative to a reference gene, *SOX1*. PCR was performed with the SYBR Green qPCR premix (Invitrogen) and analyzed using the 7300 real-time PCR system (Applied Biosystems). Primer sequences are presented in Table 1.

RNA sequencing

To prepare the library, the SureSelect Strand-Specific RNA library kit (Agilent Technologies, CA) was used according to the manufacturer's instructions. Briefly, total mRNA obtained from the PBLs was poly-A purified, fragmented, and reverse transcribed into first-strand cDNA using random primers. Following second-strand cDNA synthesis, end repair, addition of a single A base, adaptor ligation, and 13 cycles of PCR amplification, the enriched cDNA libraries were sequenced using an Illumina HiSeq 1500 system (Kazusa DNA Research Institute in Chiba, Japan) with 100 bp single-end RNA-sequence reads. Sequence files were generated in FASTQ format. Reads were then processed and aligned to the *Homo sapiens* reference genome (NCBI build 37.2) using TopHat. The unit of measurement was fragments per kilobase of exon per million fragments mapped. Obtained FASTQ files were analyzed for mapping and detection of fused genes using Strand NGS software 2.5 (Agilent Technologies, CA).

Results

Point mutations in the *RUNX1* gene were not detected by direct sequencing (data not shown). Screening for chimeric genes, such as *RUNX1-ETO*, in the bone marrow at the onset of leukemia, revealed no such genes. Conventional chromosomal analysis in the remission marrow identified inv (21) (p11.2q21) (data not shown). Chromosome analysis by the highly accurate technique revealed that one homologous chromosome 21 might be normal and the other had a complicated structure (Fig. 1 A and B). The short arm of the rearranged chromosome 21 was deleted without inducing

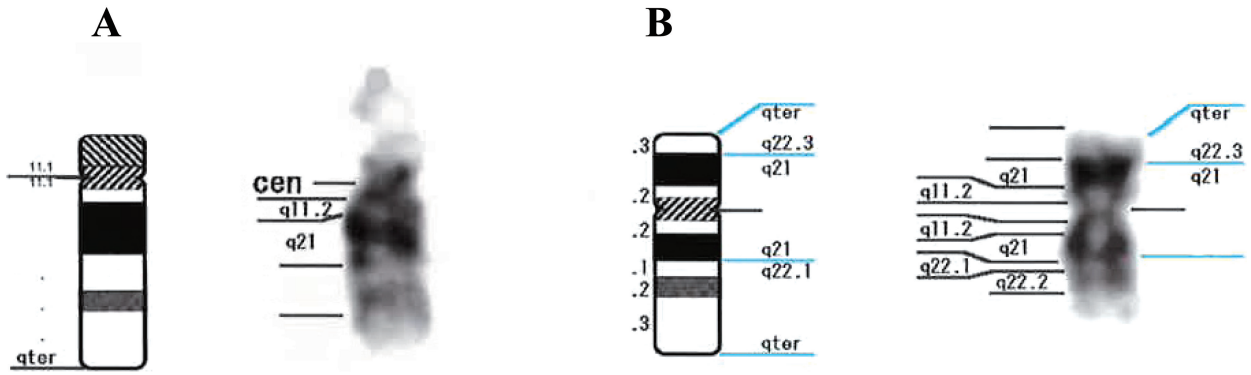

Figure 1. Chromosomal analysis by high-resolution G-banding. G-Banding image of normal chromosome 21 (A) and of the rearranged chromosome 21 (B).

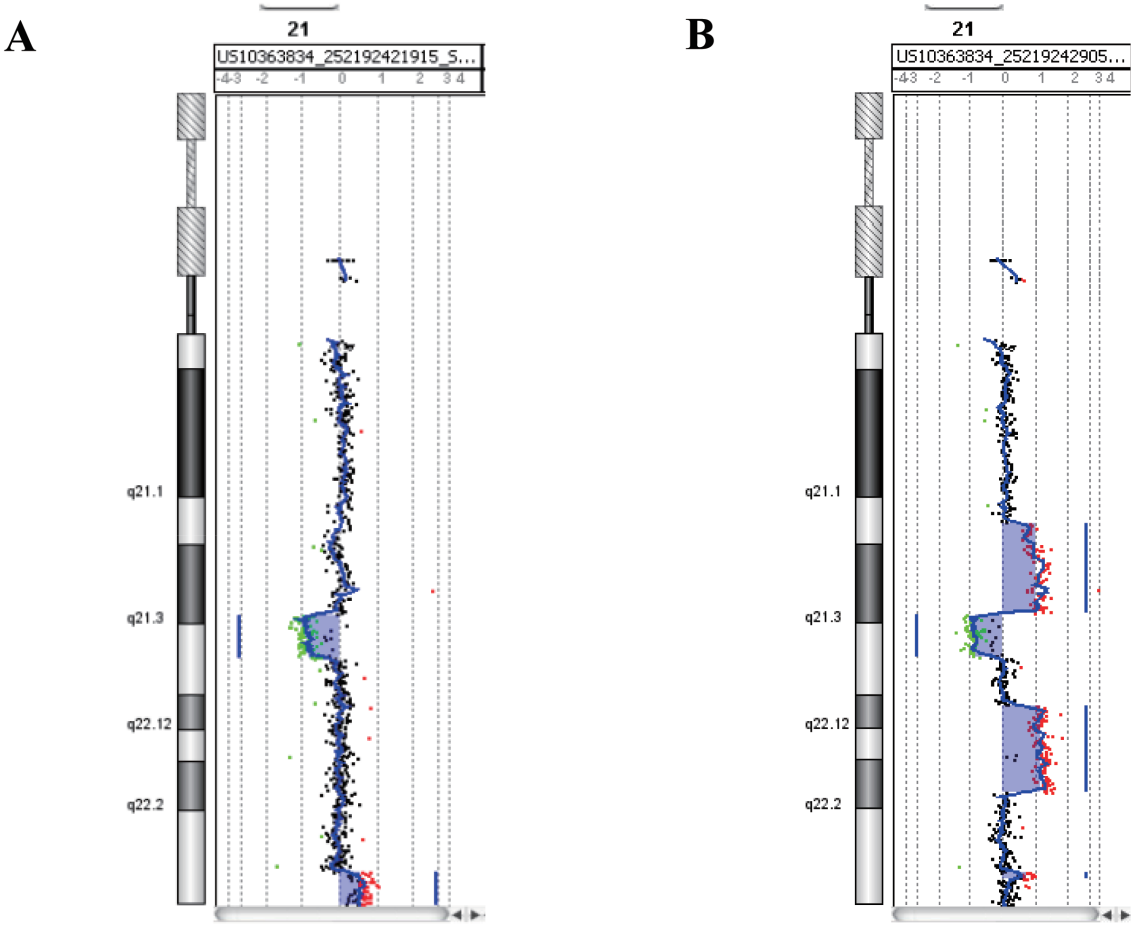

Figure 2. Array-CGH. The copy number of *RUNX1* in the genome was normal during remission (A) and increased during relapse (B).

any specific phenotype. The bands from q10 to q21 and from q22.3 to the telomere were duplicated, while the bands from q21 to q22.1 was deleted. Array-CGH analysis determined the copy number of *RUNX1* was normal in the remission bone marrow and amplified in the relapse bone marrow (Fig. 2). Moreover, examination of *RUNX1* by FISH revealed *RUNX1* had split signals during remission and amplified signals during relapse (Fig. 3).

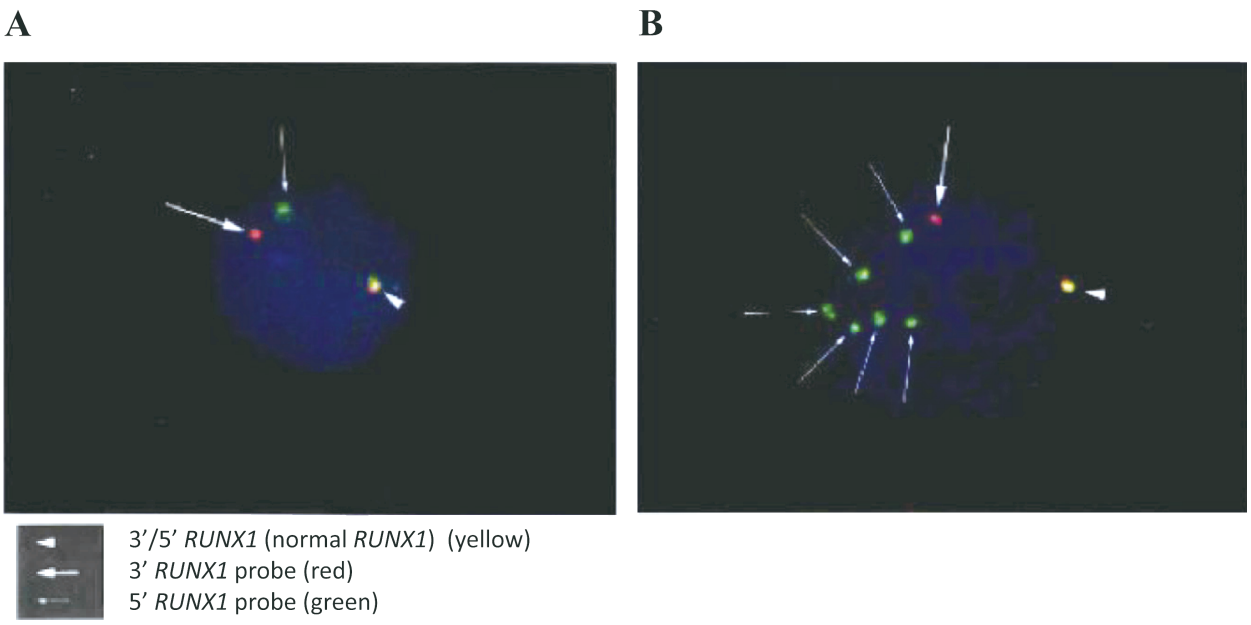

Figure 3. Dual color FISH using *RUNX1* 5' and 3' probes. The split red and green signals indicate translocation of *RUNX1* and the yellow signal indicates *RUNX1* with the absence of translocation during remission (A). The increased number of green signals indicates the amplification of the 5' side *RUNX1* gene during relapse (B). FISH, Fluorescence *in situ* hybridization.

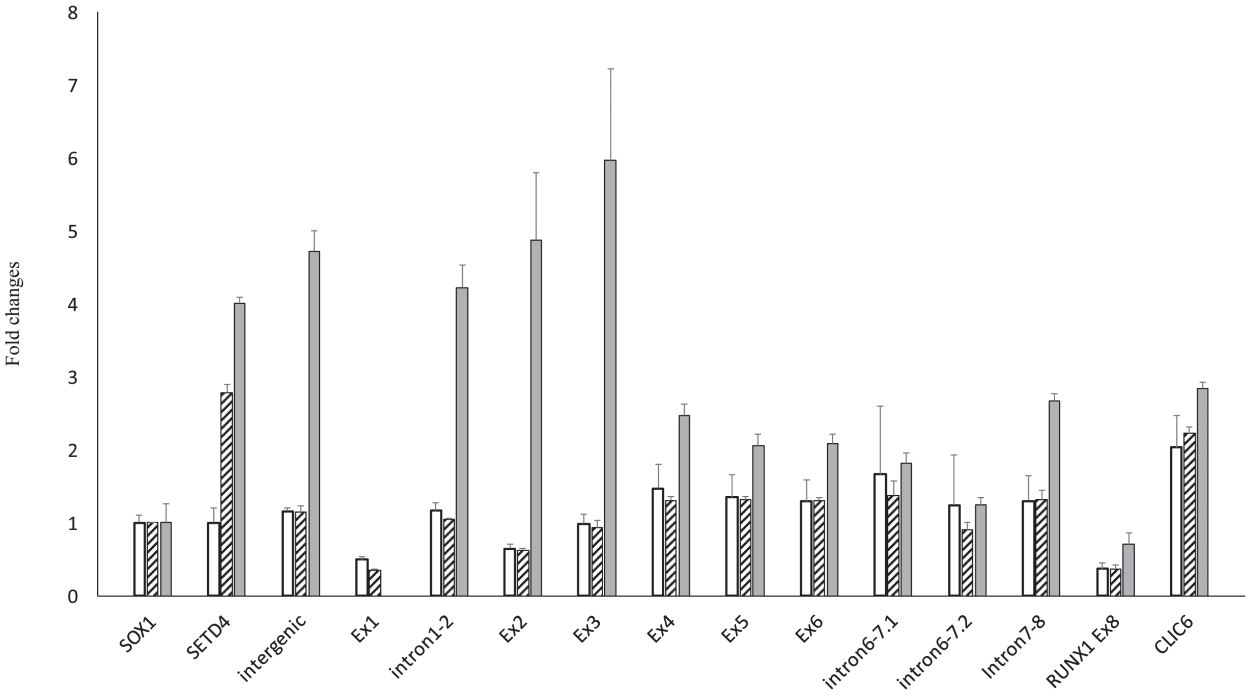

Figure 4. Copy number changes in the *RUNX1* genomic region and neighboring genes. Genomic DNA was extracted from bone marrow cells. Copy numbers of indicated regions were calculated relative to the reference region (*SOX1*) based on real-time PCR. White bar, normal control; hatched bar, patient during remission; and gray bar, leukemic cells.

To determine which regions of *RUNX1* were amplified during leukemogenesis, we measured the copy numbers of the genomic region of *RUNX1* and neighboring genes. The copy numbers were

expressed relative to a reference gene, *SOX1*, located on a different chromosome from *RUNX1*. Based on array-CGH and FISH analysis, we expected increases of several fold in copy number of the 5' regions of *RUNX1* when comparing remission to relapse. As shown in Figure 4, an increase of several fold in copy number was observed in the 5' neighboring gene (*SETD4*), 5' intergenic region, and exons 2 and 3 of *RUNX1*. However, significant changes were not observed in exon 4 of *RUNX1* and any 3' regions further downstream in the genome of leukemic cells. These data suggest the break point of the chromosomal abnormality resided between exons 3 and 4 of *RUNX1*. Amplification of the exon 2 and 3 region may be involved in leukemogenesis.

To explore the mechanisms of leukemogenesis in FPD/AML, we extracted RNA from patient bone marrow cells during relapse and analyzed it using RNA sequencing. Although RNA sequencing is an efficient tool for detecting fusion genes in cancer[8], neither additional fusion gene products nor previously reported additional mutations, such as *CDC25C*[1] were observed in this patient.

Discussion

In this study, we explored the molecular genetic changes that occur over the course of leukemogenesis with FPD/AML. Heterozygous disruption of the *RUNX1* gene is known to cause FPD, but is not sufficient to induce the development of AML. Therefore, we exhaustively searched for the "second hit" in an FPD/AML patient who developed AML earlier than in previously reported FPD cases. We found the followings in this patient: 1) a congenital complicated structural anomaly in chromosome 21; 2) the *RUNX1* gene was separated due to the chromosomal anomaly, which could explain the clinical presentation of FPD; 3) upon leukemogenesis, the 5' region of *RUNX1* was amplified several fold; 4) the breakpoint of *RUNX1* was located between exons 3 and 4; and 5) neither additional fusion gene products nor previously reported additional mutations were observed based on RNA sequencing. These data suggest amplification of aberrant *RUNX1* genes promotes leukemogenesis in patients with FPD/AML.

Only about half of individuals with FPD/AML develop hematological malignancies over the course of their life with long latency, suggesting additional genetic events are required for progression to the overt malignant phase[3]. Yoshimi et al recently found somatic *CDC25C* mutations in more than half of patients with FPD/AML in Japan, where the mutated *CDC25C* disrupted the G2/M checkpoint and promoted the cell cycle[1]. A French group reported a high frequency of *RUNX1* biallelic mutations in patients with FPD/AML. Although a variety of mutations have been identified at the AML stage, *CDC25C* mutations were not reported in their study[9]. *CDC25C* mutations were also not detected in a study on 13 individuals from FPD/AML families from the United States[10] suggesting environmental factors and/or ethnicity may play important roles in leukemic transformation.

Somatic aberrations of *RUNX1*, including point mutations and chromosomal translocations, often occur in MDS, AML, and acute lymphocytic leukemia[11]. Moreover, reverse engineering analysis of *TLX1*- and *TLX3*-mediated T-cell acute lymphocytic leukemia revealed wild-type *RUNX1* may serve as a tumor suppressor and abolish the oncogenic effects of *TXL1* and *TLX3*. The loss of function of *RUNX1* promotes oncogenesis[12]. On the other hand, Yanagida et al experimentally demonstrated an increased dose of *RUNX1* acts as a positive modulator of myeloid leukemogenesis. These authors speculated that an extra-copy of *RUNX1* through trisomy 21 may be related to Down's syndrome-related acute megakaryoblastic leukemia[13]. Antony-Debré et al reported that of the nine patients with FPD/AML who developed acute leukemia, three have a duplication of the *RUNX1*-mutated or

-deleted chromosome[14]. In our study, we observed a breakage in *RUNX1* between exons 3 and 4, which disrupted the RHD. The truncated RHD abrogates DNA-binding and transactivation capacity, while interfering with the wild-type protein during heterodimerization with CBFβ in a dominant-negative manner[15]. Collectively, we speculate the patient in our study manifested FPD due to haploinsufficiency of *RUNX1* and amplification of the truncated *RUNX1* may have led to early onset of AML.

To better manage and treat FPD/AML patients, further understanding of the pathogenesis and disease progression to hematopoietic malignancies in FPD/AML is required.

References

1. Yoshimi A, Toya T, Nannya Y, Takaoka K, Kirito K, Ito E, et al. Spectrum of clinical and genetic features of patients with inherited platelet disorder with suspected predisposition to hematological malignancies: a nationwide survey in Japan. Ann Oncol 2016;27:887-895.
2. Sood R, Kamikubo Y, Liu P. Role of RUNX1 in hematological malignancies. Blood 2017;129:2070-2082.
3. Hayashi Y, Harada Y, Huang G, Harada H. Myeloid neoplasms with germ line RUNX1 mutation. Int J Hematol 2017;106:183-188.
4. Shiba N, Hasegawa D, Park MJ, Murata C, Sato-Otsubo A, Ogawa C, et al. CBL mutation in chronic myelomonocytic leukemia secondary to familial platelet disorder with propensity to develop acute myeloid leukemia (FPD/AML). Blood 2012;119:2612-2614.
5. Manchev VT, Bouzid H, Antony-Debre I, Leite B, Meurice G, Droin N, et al. Acquired TET2 mutation in one patient with familial platelet disorder with predisposition to AML led to the development of pre-leukaemic clone resulting in T2-ALL and AML-M0. J Cell Mol Med 2017;21:1237-1242.
6. Mangan JK, Speck NA. RUNX1 mutations in clonal myeloid disorders: from conventional cytogenetics to next generation sequencing, a story 40 years in the making. Crit Rev Oncog 2011;16:77-91.
7. Shimojima K, Komoike Y, Tohyama J, Takahashi S, Paez MT, Nakagawa E, et al. TULIP1 (RALGAPA1) haploinsufficiency with brain development delay. Genomics 2009;94:414-422.
8. Maher CA, Kumar-Sinha C, Cao X, Kalyana-Sundaram S, Han B, Jing X, et al. Transcriptome sequencing to detect gene fusions in cancer. Nature 2009;458:97-101.
9. Preudhomme C, Renneville A, Bourdon V, Philippe N, Roche-Lestienne C, Boissel N, et al. High frequency of RUNX1 biallelic alteration in acute myeloid leukemia secondary to familial platelet disorder. Blood 2009;113:5583-5587.
10. Churpek JE, Pyrtel K, Kanchi KL, Shao J, Koboldt D, Miller CA, et al. Genomic analysis of germ line and somatic variants in familial myelodysplasia/acute myeloid leukemia. Blood 2015;126:2484-2490.
11. De Braekeleer E, Douet-Guilbert N, Morel F, Le Bris MJ, Ferec C, De Braekeleer M. RUNX1 translocations and fusion genes in malignant hemopathies. Future Oncol 2011;7:77-91.
12. Della Gatta G, Palomero T, Perez-Garcia A, Ambesi-Impiombato A, Bansal M, Carpenter ZW, et al. Reverse engineering of TLX oncogenic transcriptional networks identifies RUNX1 as tumor suppressor in T-ALL. Nat Med 2012;18:436-440.
13. Yanagida M, Osato M, Yamashita N, Liqun H, Jacob B, Wu F, et al. Increased dosage of Runx1/AML1 acts as a positive modulator of myeloid leukemogenesis in BXH2 mice. Oncogene 2005;24:4477-4485.
14. Antony-Debré I, Duployez N, Bucci M, Geffroy S, Micol JB, Renneville A, et al. Somatic mutations associated with leukemic progression of familial platelet disorder with predisposition to acute myeloid leukemia. Leukemia 2016;30:999-1002.
15. Michaud J, Wu F, Osato M, Cottles GM, Yanagida M, Asou N, et al. In vitro analyses of known and novel RUNX1/AML1 mutations in dominant familial platelet disorder with predisposition to acute myelogenous leukemia: implications for mechanisms of pathogenesis. Blood 2002;99:1364-1372.

Osaka City Med. J. Vol. 64, 121-130, 2018

Association between the Left Atrial Emptying Fraction and Silent Brain Infarction in Patients with Paroxysmal Atrial Fibrillation

Yu Kawai[1)], Kenichi Sugioka[1)], Shinichi Iwata[1)], Shinichi Sakamoto[2)], Sera Ishikawa[1)], Masahiko Takagi[1)], Yukio Miki[2)], and Minoru Yoshiyama[1)]

Departments of Cardiovascular Medicine[1)] and Diagnostic and Interventional Radiology[2)], Osaka City University Graduate School of Medicine

Abstract

Background

Patients with atrial fibrillation (AF) often show a high prevalence of silent brain infarction (SBI), which is an independent risk factor for the development of symptomatic stroke. The left atrial emptying fraction (LAEF) is also known to be associated with an increased risk of symptomatic stroke in patients with AF; however, little is known regarding the association between SBI and LAEF in patients with paroxysmal AF.

Methods

We investigated 77 neurologically asymptomatic patients with paroxysmal AF (56 men, median age 66 years) who were scheduled to undergo transcatheter pulmonary vein isolation or electrical cardioversion. All patients underwent brain magnetic resonance imaging to screen for SBI prior to the scheduled ablation or cardioversion. Comprehensive transthoracic echocardiography was performed to calculate the LAEF.

Results

SBI was observed in 21 patients (27%). Univariate analysis showed a negative association between LAEF and SBI [odds ratio (OR) 0.92, 95% confidence interval (CI) 0.87-0.98, p=0.005]. Receiver operating characteristic curve analysis indicated that the optimal cut-off value for SBI (area under the curve 0.70) was 45.5% with a sensitivity of 62% and a specificity of 79%. Multivariate logistic regression analysis indicated that LAEF <45.5% remained independently associated with SBI (OR 6.35, 95% CI 1.82-22.1, p=0.004) after adjusting for the CHA_2DS_2-VASc score and the estimated glomerular filtration rate.

Conclusions

An impaired LAEF is associated with SBI in patients with paroxysmal AF and might be a useful parameter for risk stratification. Intensive intervention in high-risk patients may avoid SBI and reduce the subsequent stroke risk.

Received June 20, 2017; accepted April 17, 2018.

Correspondence to: Yu Kawai, MD.
Department of Cardiovascular Medicine, Osaka City University Graduate School of Medicine,
1-4-3 Asahimachi, Abeno-ku, Osaka 545-8585, Japan
Tel: +81-6-6645-3801; Fax: +81-6-6646-6808
E-mail: yuukawai1122@gmail.com

Key Words: Paroxysmal atrial fibrillation; Silent brain infarction; Echocardiography; Left atrial emptying fraction

Introduction

Recent studies have focused on silent brain infarction (SBI) that is incidentally detected on brain magnetic resonance imaging (MRI) in patients with atrial fibrillation (AF)[1]. In patients presenting with SBI, most infarcts (80%-90%) are subcortical in location, and this condition is, therefore, classified as small-vessel occlusive disease or lacunar infarction caused by lipohyalinosis, microatheromas, or emboli[2]. The remaining (10%-20%) infarcts are cortical or large infarcts that are more likely to be secondary to cardiac embolism[2]. Because AF is associated with both micro- and macro-embolism[3,4], the American Heart Association/American Stroke Association statement recommends screening for AF in patients presenting with SBI[2]. Moreover, SBI is detected in approximately 25% of patients with AF who report no history of stroke[5] and is associated with occurrence of a stroke in future[6] or cognitive decline[7] in patients with AF. Therefore, identification of high-risk patients who may benefit from more intensive interventions is important to provide customized treatment for each patient, which is aimed at prevention of SBI.

Assessment of left atrial (LA) function could be an alternative strategy to facilitate risk stratification beyond traditional risk factors among AF patients with SBI. Impaired LA function is associated with an increased risk of an LA thrombus or thromboembolism[8-12]. However, the association between LA function (i.e., LA emptying function; LAEF) and the presence of SBI has not been addressed by clinical studies.

We aimed to assess the relationship between LAEF and the presence of SBI in patients with paroxysmal AF.

Methods

This cross-sectional single center study included 213 consecutive, neurologically asymptomatic patients with nonvalvular AF who underwent percutaneous pulmonary vein isolation or electrical cardioversion between 2011 and 2015 at the Osaka City University Hospital. We excluded patients who had undergone prior pulmonary vein isolation or any valve replacement procedure, those diagnosed with mitral stenosis, and those without MRI findings because of contraindications or patient's refusal. We selected 77 patients diagnosed with paroxysmal AF from among the remaining 157 patients. Paroxysmal AF was diagnosed in patients with a history of AF in whom an electrocardiogram indicated sinus rhythm when transthoracic echocardiography (TTE) was performed. The study protocol conformed to the guidelines of the Declaration of Helsinki (Second Revision, 1983) and was approved by the Ethics Committee of the hospital (approval number: 3214). Written informed consent was obtained from each patient prior to inclusion in the study.

Clinical variables such as age, body mass index, hypertension, diabetes mellitus, dyslipidemia, congestive heart failure, vascular disease, smoking status, chronic kidney disease, and information regarding prior treatment were obtained for each patient. Hypertension was defined as patient-reported history of hypertension, a systolic blood pressure ≧140 mm Hg or a diastolic blood pressure ≧90 mm Hg upon admission, or treatment with an oral antihypertensive drug[13]. Diabetes mellitus was defined as a fasting blood glucose level ≧126 mg/dL, a hemoglobin A1c (HbA1c) level ≧6.5%, existing diagnosis of diabetes mellitus or the reported use of an oral hypoglycemic drug[14].

Dyslipidemia was defined as a serum cholesterol level ≧220 mg/dL or a low-density lipoprotein cholesterol level ≧140 mg/dL upon admission or the reported use of a cholesterol-lowering drug[15]. A history of vascular disease was defined as the presence of myocardial infarction or peripheral artery disease. Patients were classified as non-smokers if they had never smoked or if they had stopped smoking for ≧10 years prior to inclusion in this study. Chronic kidney disease was defined as an estimated glomerular filtration rate <60 mL/min/1.73 m^2 (category ≧G3)[16,17]. We calculated the CHA_2DS_2-VASc score using the above information[18]. Duration of paroxysmal AF and anticoagulation therapy was determined from the patients' reports or medical records and were categorized into 2 groups: duration <6 months or ≧6 months.

All enrolled patients underwent 2-dimensional TTE that was performed using commercially available systems with patients placed in the left lateral decubitus position. Echocardiographic quantification was performed based on the American Society of Echocardiography guidelines[19]. End-diastolic left ventricular (LV) diameter, end-systolic LV diameter, end-diastolic interventricular septal thickness, end-diastolic LV posterior wall thickness, and LV ejection fraction were measured. The LV mass was calculated based on the LV linear dimensions using the following formula: {0.8×1.04×[(end-diastolic LV diameter+end-diastolic LV posterior wall thickness+end-diastolic interventricular septal thickness)^3−(end-diastolic LV diameter)^3]+0.6} g and was indexed to the body surface area. Maximal and minimal LA volumes were measured using the biplane modified Simpson's method using apical 4- and 2-chamber views. The maximal LA volume was obtained just prior to the opening of the mitral valve, and the minimal LA volume was obtained at the moment of mitral valve closure. Indexed LA volumes (LAVI) were calculated based on the patient's body surface area. These data were used to calculate the LAEF using the formula: LAEF=[(maximal LAVI−minimal LAVI)/maximal LAVI]×100[20] (Fig. 1). Early E and late A transmitral velocities were measured using a pulsed-wave Doppler based on the apical 3-chamber view with the sample volume positioned at the tip of the mitral leaflets[21].

All MRI examinations were performed using a 3.0-Tesla (T) unit (Achieva Quasar Dual; Philips Medical Systems, Best, The Netherlands) or a 1.5-T unit (Achieva Nova Dual; Philips Medical Systems, Best, The Netherlands) with a standard head coil. Axial T1-weighted images (3.0-T unit: repetition time 400 ms, echo time 15 ms, field of view 220 mm^2, imaging matrix 256×181, 5 mm thickness and 1 mm gap; 1.5-T unit: repetition time 737 ms, echo time 15 ms, field of view 220 mm^2, imaging matrix 256×180, 5 mm thickness and 1 mm gap) and axial T2-weighted images (3.0-T unit: repetition time 4000 ms, echo time 90 ms, field of view 220 mm^2, imaging matrix 448×300, 5 mm thickness and 1 mm gap; 1.5-T unit: repetition time 4560 ms, echo time 90 ms, field of view 220 mm^2, imaging matrix 352×272, 5 mm thickness and 1 mm gap) were obtained to evaluate SBI. SBI was defined as an area of low intensity observed on T1-weighted images and an area of high intensity observed on T2-weighted images with a diameter ≧3 mm[22] (Fig. 2). Lesions that demonstrated a high intensity on diffusion images were excluded from the analysis. The presence of SBI was confirmed by an experienced neuroradiologist (S.S.) who had been blinded to the clinical information of the patients enrolled in this study.

Statistical methods

Continuous variables were expressed as median values (interquartile ranges), and categorical variables as numbers and percentages. The distribution of clinical or echocardiographic variables was evaluated among patients with SBI versus those without SBI. We compared the groups using

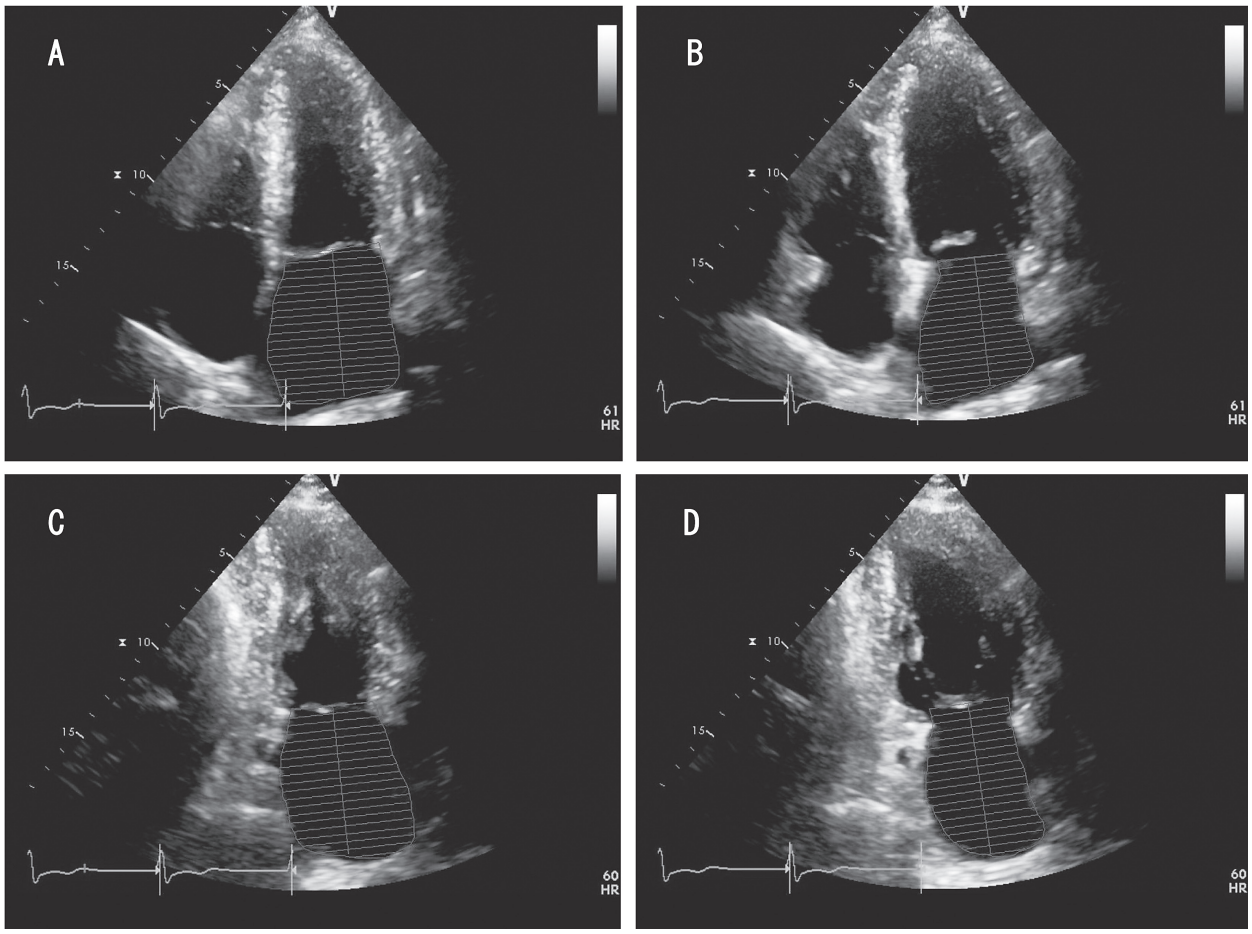

Figure 1. Echocardiographic assessment of left atrial volume using the biplane modified Simpson's method.
A=maximal left atrial volume using apical 4-chamber view.
B=minimal left atrial volume using apical 4-chamber view.
C=maximal left atrial volume using apical 2-chamber view.
D=minimal left atrial volume using apical 2-chamber view.

the unpaired *t* test for continuous variables with a normal distribution and the Mann-Whitney U test for continuous variables with a non-normal distribution. Categorical variables were compared using a chi-square test or the Fisher exact test (N ≧20). Univariate logistic regression analysis was performed to identify clinical and echocardiographic variables that were associated with the presence of SBI. A p value of <0.05 (except with regard to age and diabetes mellitus, which were included in the CHA_2DS_2-VASc score) was used to select variables that would be subjected to multiple logistic regression analysis. Moreover, we performed multivariate logistic regression analysis using propensity score as a covariate to minimize the potential selection bias. Because the cut-off value is useful for risk stratification in clinical settings, we used LAEF as a binary variable (LAEF <45.5% or ≧45.5%), which is the optimal cut-off value for predicting the presence of SBI (area under the curve 0.70) with a sensitivity of 62% and a specificity of 79% derived from receiver operating characteristic curve analysis. The covariates in Model 1 included the LAEF and the propensity score derived from the general risk factors for SBI (age, HbA1c, low-density lipoprotein cholesterol, systolic blood pressure, diastolic blood pressure, smoking, and estimated glomerular filtration rate) which had a concordance index of 0.70. The covariates in Model 2 included the LAEF and the propensity score derived from

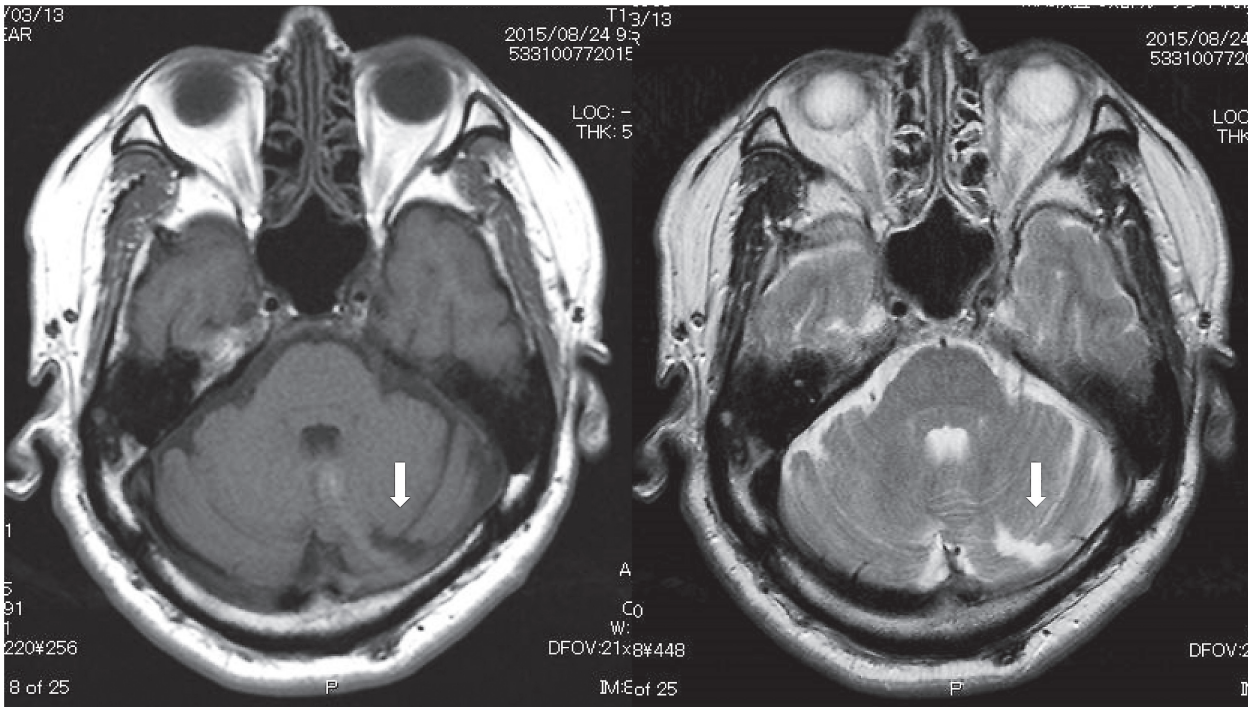

Figure 2. A representative case of silent brain infarction (SBI). This patient shows SBI in the left cerebellar hemisphere (arrow) concomitant with paroxysmal atrial fibrillation and a decreased left atrial emptying fraction (43%).

the variables associated with the presence of SBI noted using univariate analysis (age, congestive heart failure, hemoglobin, estimated glomerular filtration rate, antiplatelet drug usage, and angiotensin-converting enzyme inhibitor/angiotensin Ⅱ receptor blocker usage) which had a concordance index of 0.72. We also used inverse probability of treatment weighting method in these 2 models to confirm our results. We used dummy variables for analyses as following; 1=male, 0=female; 1=smoker, 0=non-smoker; 1=duration of atrial fibrillation ≧6 months, 0=duration of atrial fibrillation <6 months; 1=duration of anticoagulant usage <6 months, 0=duration of anticoagulant usage ≧6 months; 1=LAEF <45.5%, 0=LAEF ≧45.5%; other clinical variables and usage of medications: 1=presence, 0=absence. p values <0.05 were considered statistically significant. All statistical analyses were carried out using SPSS version 24 (IBM Corp., Armonk, NY, USA).

Results

Among the 77 patients diagnosed with paroxysmal AF, SBI was observed in 21 (27%). Among these 21 patients, subcortical and small (3-15 mm) infarcts were detected in 15, cortical or large infarcts in 14, and both varieties in 8. Baseline clinical characteristics of patients with and without SBI are shown in Table 1. All patients had been administered anticoagulants. Age, diabetes mellitus, congestive heart failure, chronic kidney disease, the CHA_2DS_2-VASc score, and use of antiplatelet agents and angiotensin-converting enzyme inhibitor/angiotensin Ⅱ receptor blockers were variables that were observed to be positively associated with the presence of SBI. Hemoglobin and estimated glomerular filtration rate were variables that were negatively associated with the presence of SBI. Echocardiographic characteristics of patients with and without SBI are shown in Table 2. LAEF was negatively associated with the presence of SBI, whereas the other variables including the LV ejection fraction, LV mass index, maximal LAVI, and mitral E velocity were not associated with the presence

Table 1. Baseline clinical characteristics of patients with and without silent brain infarction

	SBI (+) (N=21)	SBI (−) (N=56)	p
Age, years	68 (66-74)	65 (54-70)	0.01
Males, n (%)	16 (76)	40 (71)	0.68
Body mass index, kg/m^2	25 (23-27)	24 (22-27)	0.18
Hypertension, n (%)	16 (76)	31 (55)	0.10
Systolic blood pressure, mm Hg	126 (120-136)	130 (113-135)	0.97
Diastolic blood pressure, mm Hg	71 (69-78)	76 (69-80)	0.24
Diabetes mellitus, n (%)	8 (38)	9 (16)	0.04
Smoker, n (%)	7 (33)	20 (36)	0.85
Dyslipidemia, n (%)	6 (29)	22 (39)	0.38
Congestive heart failure, n (%)	6 (29)	1 (2)	0.001
Duration of atrial fibrillation (≧6 months), n (%)	11 (52)	41 (73)	0.08
Duration of anticoagulant usage (<6 months), n (%)	8 (30)	28 (50)	0.35
Hemoglobin A1c, %	5.8 (5.7-6.2)	5.7 (5.5-6.0)	0.05
Total cholesterol, mg/dL	167 (157-197)	176 (159-188)	0.90
High-density lipoprotein cholesterol, mg/dL	41 (37-46)	43 (39-53)	0.14
Low-density lipoprotein cholesterol, mg/dL	101 (85-122)	102 (89-118)	0.98
Triglycerides, mg/dL	135 (106-176)	117 (85-153)	0.23
Albumin, g/dL	4.2 (4.2-4.3)	4.3 (4.1-4.5)	0.22
Hemoglobin, g/dL	13.6 (12.9-14.9)	14.5 (13.7-15.1)	0.04
C-reactive protein, mg/dL	0.09 (0.05-0.11)	0.08 (0.02-0.14)	0.31
eGFR, mL/min/1.73m^2	60 (48-73)	70 (62-82)	0.004
Chronic kidney disease, n (%)	10 (48)	12 (21)	0.02
CHA_2DS_2-VASc score	3.0 (2.0-4.0)	1.5 (1.0-2.3)	0.003
Medications			
Antiplatelet agents, n (%)	3 (14)	0 (0)	0.02
Anticoagulants, n (%)	21 (100)	56 (100)	-
Vitamin K antagonists, n (%)	7 (33)	11 (20)	0.17
Direct oral anticoagulants, n (%)	14 (67)	45 (80)	0.17
Antiarrhythmic agents, n (%)	13 (62)	34 (61)	0.92
Statins, n (%)	6 (29)	15 (27)	0.88
ACEI/ARB, n (%)	29 (38)	12 (16)	0.001
Calcium channel blockers, n (%)	8 (38)	15 (27)	0.33
β-blocker, n (%)	9 (43)	15 (27)	0.18
Antidiabetic medication, n (%)	6 (29)	6 (11)	0.06

Continuous variables were expressed as median values (interquartile ranges), and categorical variables as numbers and percentages. SBI, silent brain infarction; eGFR, estimated glomerular filtration rate; ACEI, angiotensin-converting enzyme inhibitor; and ARB, angiotensin Ⅱ receptor blocker.

of SBI. Table 3 shows the clinical and echocardiographic variables associated with the presence of SBI and their OR obtained using univariate and multivariate analysis. LAEF (as a continuous variable) was inversely associated with the presence of SBI after adjusting for the CHA_2DS_2-VASc score and the estimated glomerular filtration rate (OR 0.92, 95% CI 0.86-0.98, p=0.007). Moreover, the CHA_2DS_2-VASc score (OR 1.94, 95% CI 1.11-3.40, p=0.02) and the LAEF <45.5% (OR 6.35, 95% CI 1.82-22.13, p=0.004), which is the optimal cut-off value for predicting the presence of SBI (area under the curve 0.70) with a sensitivity of 62% and a specificity of 79% derived from receiver operating characteristic curve analysis, remained independently associated with the presence of SBI after adjusting for the estimated glomerular filtration rate. Furthermore, LAEF <45.5% (a binary

Table 2. Echocardiographic findings in patients with and without silent brain infarction

	SBI (+) (N=21)	SBI (−) (N=56)	p
End-diastolic left ventricular diameter, mm	49 (43-55)	47 (44-49)	0.37
End-systolic left ventricular diameter, mm	30 (26-35)	28 (26-31)	0.21
Interventricular septal thickness, mm	9 (9-10)	9 (8-10)	0.09
Posterior wall thickness, mm	9 (8-10)	9 (8-10)	0.45
Left atrial diameter, mm	41 (38-46)	39 (34-43)	0.07
Left ventricular ejection fraction, %	60 (55-60)	60 (60-60)	0.08
Mitral E velocity, cm/s	65 (48-77)	60 (55-66)	0.63
Mitral A velocity, cm/s	63 (44-75)	63 (48-80)	0.87
Mitral E deceleration time, ms	246 (229-275)	225 (190-255)	0.63
Left ventricular mass index, g/m^2	103 (93-125)	98 (89-115)	0.10
Maximal left atrial volume index, mL/m^2	36 (29-45)	35 (27-41)	0.15
Left atrial emptying fraction, %	43 (36-56)	53 (47-60)	0.002

Continuous variables were expressed as median values (interquartile ranges), and categorical variables as numbers and percentages. SBI, silent brain infarct.

Table 3. Clinical and echocardiographic variables associated with silent brain infarction

	Univariate analysis		Multivariate analysis	
	OR (95% CI)	p	OR (95% CI)	p
Age, per 1year	1.08 (1.01-1.15)	0.08		
Male sex	1.28 (0.40-4.08)	0.68		
Diabetes mellitus	3.21 (1.04-9.98)	0.04		
Hypertension	2.58 (0.83-8.02)	0.10		
Dyslipidemia	0.62 (0.21-1.83)	0.38		
Smoking	0.90 (0.31-2.60)	0.85		
Estimated glomerular filtration rate, per 1 mL/min/1.73m^2	0.95 (0.92-0.99)	0.01	0.98 (0.94-1.02)	0.23
Chronic kidney disease	3.33 (1.15-9.70)	0.03		
Duration of anticoagulant use <6 months	0.62 (0.22-1.72)	0.35		
Duration of atrial fibrillation ≧6 months	0.40 (0.14-1.14)	0.09		
CHA_2DS_2-VASc score, per 1point	2.02 (1.27-3.20)	0.003	1.94 (1.11-3.40)	0.02
Left ventricular mass index, per 1 g/m^2	1.02 (1.00-1.05)	0.10		
Maximal left atrial volume index, per 1 mL/m^2	1.03 (0.99-1.06)	0.15		
Left atrial emptying fraction, per 1%	0.92 (0.87-0.98)	0.005		
Left atrial emptying fraction <45.5%	5.96 (2.01-17.68)	0.001	6.35 (1.82-22.13)	0.004

OR, odds ratio; and CI, confidence interval.

variable) remained independently associated with the presence of SBI using propensity scores (Table 4). Finally, we confirmed the significant association between LAEF <45.5% and the presence of SBI using inverse probability of treatment weighting method (model 1; OR 5.26, 95% CI 1.64-16.91, p=0.005, model 2; OR 3.75, 95% CI 1.15-12.21, p=0.03).

Discussion

In the present study, we observed that an impaired LAEF was significantly associated with the presence of SBI in patients with paroxysmal AF after adjusting for accepted risk factors or the CHA_2DS_2-VASc score and the estimated glomerular filtration rate. These results suggest that an

Table 4. Multivariate logistic regression analysis for silent brain infarction: Propensity score adjustment

	Model 1		Model 2	
	OR (95% CI)	p	OR (95% CI)	p
LAEF <45.5%	6.08 (1.89-19.60)	0.003	3.88 (1.20-12.61)	0.024

Model 1 adjusts for the propensity score derived from the general risk factors of silent brain infarction (age, hemoglobin A1c, low-density lipoprotein cholesterol, systolic blood pressure, diastolic blood pressure, smoking, and estimated glomerular filtration rate). Model 2 adjusts for the propensity score derived from variables associated with silent brain infarction noted using univariate analysis (age, congestive heart failure, hemoglobin, estimated glomerular filtration rate, antiplatelet drug usage, and angiotensin-converting enzyme inhibitor/angiotensin Ⅱ receptor blocker usage). OR, odds ratio; CI, confidence interval; and LAEF, left atrial emptying fraction.

impaired LAEF may be associated with microthrombus formation, which is a risk factor for the presence of SBI in patients with paroxysmal AF. To our knowledge, this is the first study to demonstrate that LAEF (calculated using TTE) is associated with the presence of SBI in patients with paroxysmal AF.

Our study showed that LAEF was statistically significantly associated with the presence of SBI — a finding that is in agreement with that of previous studies showing that the LA function plays an important role in predicting SBI. The Cardiovascular Abnormalities and Brain Lesions (CABL) study showed that LAEF assessed using echocardiography was significantly associated with the presence of SBI in the general population without a history of stroke[23]. However, this study primarily focused on patients with a sinus rhythm. To date, no study has investigated the influence of LAEF on the presence of SBI in patients with paroxysmal AF.

Our study revealed that LAEF is associated with the presence of SBI in patients with paroxysmal AF. Based on our results, we hypothesized that an impaired LAEF plays an important role in the progression of thrombogenesis in the LA with the subsequent development of SBI in patients with paroxysmal AF. The mechanisms underlying our finding remain unclear. There is, however, considerable evidence to explain the role of impaired LAEF in the process of thrombogenesis. Impaired LAEF has been proven to be associated with the presence of an LA thrombus, which leads to the development of a symptomatic stroke in patients with AF[11]. Similarly, an impaired LAEF is known to be associated with spontaneous echo contrast, which is a risk factor for cerebral microembolism in patients with AF[11]. Moreover, LAEF is associated with the CHA_2DS_2-VASc score[12], which is a well-accepted tool for risk stratification with regard to thrombogenesis or symptomatic stroke in patients with AF. Although we focused only on paroxysmal AF, LAEF itself may accelerate LA thrombogenesis and cause subsequent SBI even in patients with paroxysmal AF.

A few studies have reported that LAVI was shown to be associated with the presence of SBI in patients with AF[8-10]; however, our study showed no association between LAVI and SBI in patients with paroxysmal AF. This difference might be at least partly attributable to the differences in study cohorts (studies that investigated any type of AF vs our study that investigated only paroxysmal AF). Impaired LAEF is known to be an earlier stage of abnormality than that noted in LA enlargement[24]. Paroxysmal AF may indicate a shorter history of AF; thus, LAEF may be a better predictor than LAVI to predict the presence of SBI in patients with paroxysmal AF.

Limitations

Limitations of our study: 1) Our study included a relatively small number of patients. Thus, future

studies including a larger number of patients are necessary to confirm whether LAEF is significantly associated with the presence of SBI. 2) Because cross-sectional data cannot investigate causality, a prospective study would be necessary to establish whether LAEF can conclusively predict the presence of SBI. 3) Because our study population comprised patients scheduled for transcatheter pulmonary vein isolation or electrical cardioversion, a selection bias might have influenced our study results. 4) Because it is difficult to ascertain the mechanisms of SBI (particularly in patients presenting with lacunar infarction), there exists the possibility that our study also included non-embolic causes of SBI. 5) Although a 1.5-T MRI is an acceptable modality for the assessment of SBI, the detection rate of SBI may be different between 1.5-T and 3.0-T MRI testing[25]. 6) This study did not evaluate the LA parameters using novel methods such as a 3-dimensional echocardiographic method[26] or the speckle tracking method[27].

Conclusions

Impaired LAEF is associated with the presence of SBI in patients with paroxysmal AF, and LAEF might be a useful parameter for risk stratification of thromboembolism in patients presenting with paroxysmal AF.

Sources of funding

This study was partly supported by the Grants-in-Aid for Scientific Research (No. 25461087) from the Japan Society for the Promotion of Science, Tokyo, Japan.

References

1. Petersen P, Madsen EB, Brun B, Pedersen F, Gyldensted C, Boysen G. Silent cerebral infarction in chronic atrial fibrillation. Stroke 1987;18:1098-1100.
2. Smith EE, Saposnik G, Biessels GJ, Doubal FN, Fornage M, Gorelick PB, et al. Prevention of stroke in patients with silent cerebrovascular disease: a scientific statement for healthcare professionals from the American Heart Association/American Stroke Association. Stroke 2017;48:e44-e71.
3. Lin HJ, Wolf PA, Kelly-Hayes M, Beiser AS, Kase CS, Benjamin EJ, et al. Stroke severity in atrial fibrillation. The Framingham Study. Stroke 1996;27:1760-1764.
4. Ay H, Oliveira-Filho J, Buonanno FS, Ezzeddine M, Schaefer PW, Rordorf G, et al. Diffusion-weighted imaging identifies a subset of lacunar infarction associated with embolic source. Stroke 1999;30:2644-2650.
5. Feinberg WM, Seeger JF, Carmody RF, Anderson DC, Hart RG, Pearce LA. Epidemiologic features of asymptomatic cerebral infarction in patients with nonvalvular atrial fibrillation. Arch Intern Med 1990;150: 2340-2344.
6. Gupta A, Giambrone AE, Gialdini G, Finn C, Delgado D, Gutierrez J, et al. Silent brain infarction and risk of future stroke: a systematic review and meta-analysis. Stroke 2016;47:719-725.
7. Vermeer SE, Prins ND, den Heijer T, Hofman A, Koudstaal PJ, Breteler MM. Silent brain infarcts and the risk of dementia and cognitive decline. N Engl J Med 2003;348:1215-1222.
8. Watanabe A, Suzuki S, Kano H, Matsuno S, Takai H, Kato Y, et al. Left atrial remodeling assessed by transthoracic echocardiography predicts left atrial appendage flow velocity in patients with paroxysmal atrial fibrillation. Int Heart J 2016;57:177-182.
9. Kim TH, Shim CY, Park JH, Nam CM, Uhm JS, Joung B, et al. Left ventricular diastolic dysfunction is associated with atrial remodeling and risk or presence of stroke in patients with paroxysmal atrial fibrillation. J Cardiol 2016;68:104-109.
10. Chung H, Joung B, Lee KY, Uhm JS, Pak HN, Lee MH, et al. Left atrial volume index predicts recurrence of stroke in patients with nonsustained atrial tachycardia. J Stroke Cerebrovasc Dis 2015;24:2408-2415.
11. Kim MN, Kim SA, Choi JI, Park SM, Park SW, Kim YH, et al. Improvement of predictive value for thromboembolic risk by incorporating left atrial functional parameters in the CHADS2 and CHA2DS2-VASc scores. Int Heart J 2015;56:286-292.
12. Islas F, Olmos C, Vieira C, De Agustín JA, Marcos-Alberca P, Saltijeral A, et al. Thromboembolic risk in atrial fibrillation: association between left atrium mechanics and risk scores. a study based on 3D wall-motion tracking technology. Echocardiography 2015;32:644-653.
13. Shimamoto K, Ando K, Fujita T, Hasebe N, Higaki J, Horiuchi M, et al. The Japanese Society of Hypertension

guidelines for the management of hypertension (JSH 2014). Hypertens Res 2014;37:253-390.
14. Seino Y, Nanjo K, Tajima N, Kadowaki T, Kashiwagi A, Araki E, et al. Report of the committee on the classification and diagnostic criteria of diabetes mellitus. J Diabetes Investig 2010;1:212-228.
15. Teramoto T, Sasaki J, Ueshima H, Egusa G, Kinoshita M, Shimamoto K, et al. Executive summary of Japan Atherosclerosis Society (JAS) guideline for diagnosis and prevention of atherosclerotic cardiovascular diseases for Japanese. J Atheroscler Thromb 2007;14:45-50.
16. Matsuo S, Imai E, Horio M, Yasuda Y, Tomita K, Nitta K, et al. Revised equations for estimated GFR from serum creatinine in Japan. Am J Kidney Dis 2009;53:982-992.
17. KDIGO CKD Work Group. KDIGO clinical practice guideline for the evaluation and management of chronic kidney disease. Kidney Int 2013;3(Suppl):1-150.
18. Lip GY, Nieuwlaat R, Pisters R, Lane DA, Crijns HJ. Refining clinical risk stratification for predicting stroke and thromboembolism in atrial fibrillation using a novel risk factor-based approach: the euro heart survey on atrial fibrillation. Chest 2010;137:263-272.
19. Lang RM, Badano LP, Mor-Avi V, Afilalo J, Armstrong A, Ernande L, et al. Recommendations for cardiac chamber quantification by echocardiography in adults: an update from the American Society of Echocardiography and the European Association of Cardiovascular Imaging. J Am Soc Echocardiogr 2015;28:1-39.
20. Abhayaratna WP, Seward JB, Appleton CP, Douglas PS, Oh JK, Tajik AJ, et al. Left atrial size: physiologic determinants and clinical applications. J Am Coll Cardiol 2006;47:2357-2363.
21. Nagueh SF, Appleton CP, Gillebert TC, Marino PN, Oh JK, Smiseth OA, et al. Recommendaton for the evaluation of left ventricular diastolic function by echocardiography. J Am Soc Echocardiogr 2009;22:107-133.
22. Zhu YC, Dufouil C, Tzourio C, Chabriat H. Silent brain infarcts: a review of MRI diagnostic criteria. Stroke 2011;42:1140-1145.
23. Russo C, Jin Z, Liu R, Iwata S, Tugcu A, Yoshita M, et al. LA volumes and reservoir function are associated with subclinical cerebrovascular disease: the CABL (Cardiovascular Abnormalities and Brain Lesions) study. JACC Cardiovasc Imaging 2013;6:313-323.
24. Gupta DK, Shah AM, Giugliano RP, Ruff CT, Antman EM, Grip LT, et al. Left atrial structure and function in atrial fibrillation: ENGAGE AF-TIMI 48. Euro Heart J 2014;35:1457-1465.
25. Wardlaw JM, Brindle W, Casado AM, Shuler K, Henderson M, Thomas B, et al. A systematic review of the utility of 1.5 versus 3 Tesla magnetic resonance brain imaging in clinical practice and research. Eur Radiol 2012;22:2295-2303.
26. Fukuda S, Watanabe H, Daimon M, Abe Y, Hirashiki A, Hirata K, et al. Normal values of real-time 3-dimensional echocardiographic parameters in a healthy Japanese population: the JAMP-3D Study. Circ J 2012;76:1177-1181.
27. Mori M, Kanzaki H, Amaki M, Ohara T, Hasegawa T, Takahama H, et al. Impact of reduced left atrial functions on diagnosis of paroxysmal atrial fibrillation: results from analysis of time-left atrial volume curve determined by two-dimensional speckle tracking. J Cardiol 2011;57:89-94.

Osaka City Med. J. Vol. 64, 131-142, 2018

A Non-clinical Experimental Study of the Ligation Process with Knot Pushers

Shinsuke Nishimura[1)], Masaki Nishimura[2)], Mitsuharu Hosono[1)],
Takashi Murakami[1)], Yosuke Takahashi[1)], Takahiro Kitagawa[2)],
Seiichi Yasuki[2)], Shunsuke Kita[2)], and Toshihiko Shibata[1)]

Department of Cardiovascular Surgery[1)], Osaka City University Graduate School of Medicine; and Osaka Research Institute of Industrial Science and Technology[2)]

Abstract

Background

There have been no quantitative evaluations of the ligation process with knot pushers. The purpose of this study is to evaluate the traction method of the suture, the differences between suture types, and the influence of water addition.

Methods

Three types of sutures were employed: Suture-A (braided polyester), Suture-B (braided silk), and Suture-C (monofilament polyvinylidene difluoride). The pushing force of the knot pusher was measured. The tension force was achieved with weights. The pushing force was evaluated in six weight conditions termed Group (100-100), Group (200-200), Group (300-300), Group (200-100), Group (300-100), and Group (300-200). We compared the pushing force in dry and wet conditions.

Results

The pushing force was 114±1 gf for Group (100-100), 328±5 gf for Group (200-200), 478±2 gf for Group (300-300), 109±1 gf for Group (200-100), 100±3 gf for Group (300-100), and 231±3 gf for Group (300-200). The pushing force with Suture-A, -B, and -C was 104±1, 112±2, and 97±1 gf, respectively ($p<0.0001$). There was no significant difference in the pushing force between dry and wet conditions in Suture-A and Suture-C, while the pushing force was significantly larger in the wet condition with Suture-B.

Conclusions

When surgeons perform knot pusher ligation, it is important to push down the suture beside the knot and not to pull the loop side suture too much. It was shown that addition of water did not significantly affect the pushing force for hydrophobic sutures.

Key Words: Ligation technique; Knot pusher; Pushing force

Received December 20, 2017; accepted April 17, 2018.

Correspondence to: Shinsuke Nishimura, MD.
Department of Cardiovascular Surgery, Osaka City University Graduate School of Medicine,
1-4-3 Asahimachi, Abeno-ku, Osaka 545-8585, Japan
Tel: +81-6-6645-3980; Fax: +81-6-6646-3071
E-mail: s.nishimura0710@gmail.com

Introduction

The number of minimally invasive cardiac surgeries (MICS) has been increasing in recent years[1-5]. The deep operation site in conjunction with the small skin incision make it difficult to perform manual ligation, so we have to use ligature instruments like knot pushers. However, there are technical differences between manual ligation and knot pusher ligation[6]. In knot pusher ligation, the sliding knot technique is a common method used for deep site ligation[7].

Usually, knot pusher ligation requires working with an assistant. The operator holds the knot pusher with one hand and grabs one side of the suture with the other hand while an assistant grabs the other side of the suture. The operator makes a half hitch and then pushes down the knot to the seating position. We sometimes feel that the knot is not advanced smoothly to the seating position, and we know that the resistance for pushing down the knot depends on the type of suture.

We empirically know the surgeon's actions such as changing the pushing direction of the knot pusher, adjusting the traction force, or adding water to the hands and sutures affect the ligation process. While several studies have reported the knot strength and knot security, there have been no quantitative evaluations of the ligation process with a knot pusher[8-18]. In this study, we made a ligation-simulating model to quantitatively reveal the ligation process with a knot pusher and carried out non-clinical engineering experiments. We evaluated the pushing force that was important to perform stressless ligation without applying useless force in actual operations.

Methods

Knot pusher and suture

There are a variety of knot pushers manufactured with different materials and shapes[19]. In our study, a Geister knot pusher (ValveGate® 34-7495, Tuttligen, Germany) was used. There are two ways to use this knot pusher in terms of contact with the suture (Fig. 1), and we used the knot pusher as shown in Figure 1A.

We employed three commercially available non-absorbable surgical sutures used in cardiovascular surgery in Japan (Table 1). Cardiac surgeons usually use 2-0 braided sutures for fixing an annuloplasty ring, and 4-0 monofilament sutures for closing the atrium. Thus we selected the size of the sutures according to the clinical usage. Two of the sutures were braided (Suture-A and -B) and the third was a monofilament suture (Suture-C). Suture-A is Teffdesser Ⅱ® (CROWNJUN, Tokyo, Japan), Suture-B

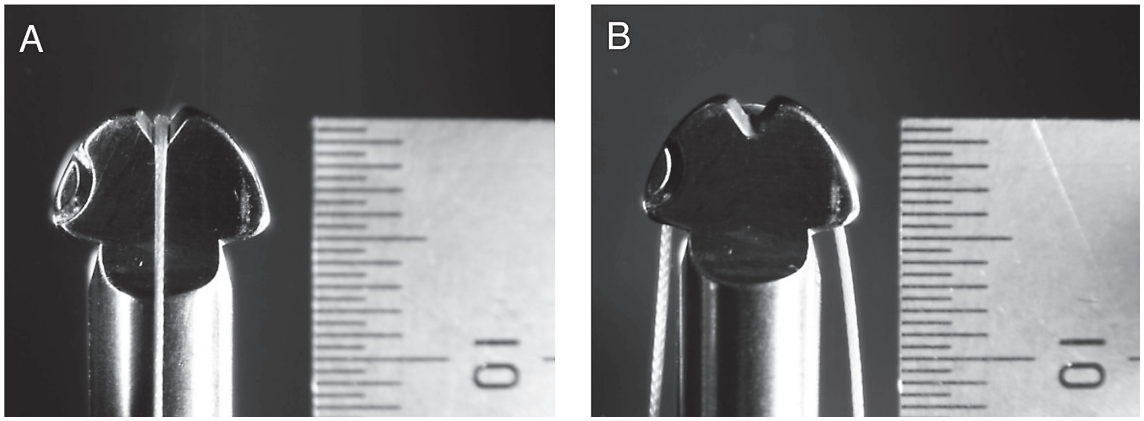

Figure 1. A and B, Tip shape of the knot pusher. There are two ways for the knot pusher to contact the suture.

Table 1. Sutures used in this experiment

	Trade name	Type	Material	USP size
A	Teffdesser Ⅱ	Braided Suture	Polyester coated with PTFE	2-0
B	Braided silk	Braided Suture	Silk	2-0
C	Asflex	Monofilament Suture	Polyvinylidene difluoride	4-0

USP, United States Pharmacopeia; and PTFE, polytetrafluoroethylene.

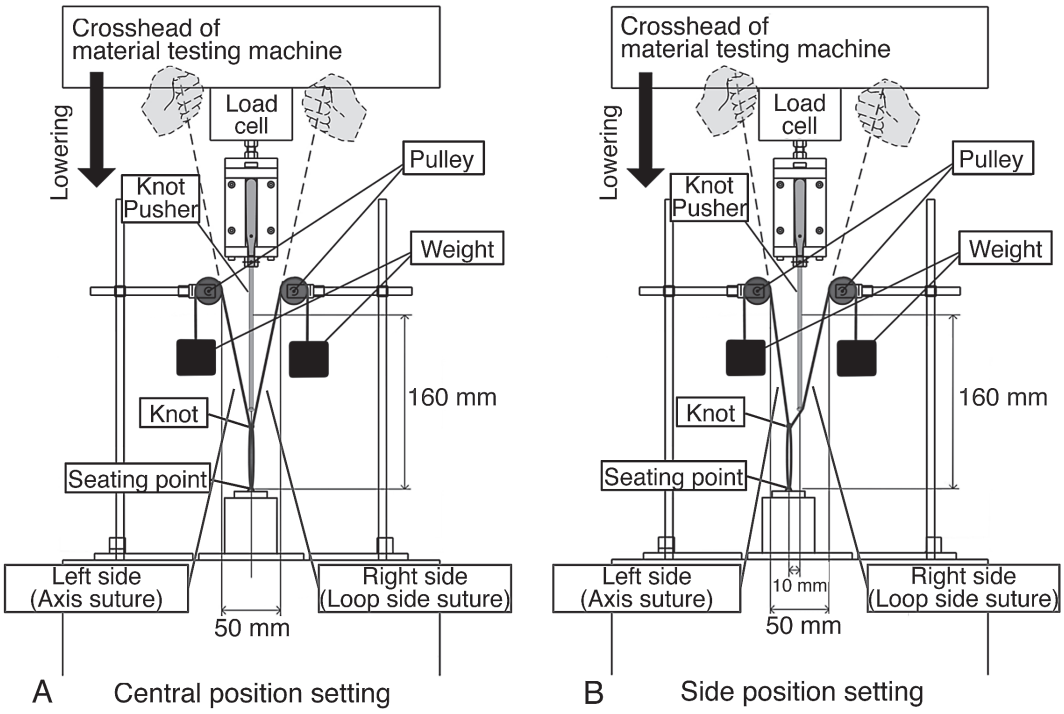

Figure 2. Schema of the experimental apparatus. The knot pusher was connected to the load cell and the suture was fixed to the seating point. Constant tension force was applied via pulleys with weights on each side. Two apparatus settings were tested: the "central position setting" (A), and the "side position setting" (B).

is Braided silk® (CROWNJUN, Tokyo, Japan), and Suture-C is Asflex® (CROWNJUN, Tokyo, Japan). The sizes of the sutures were 2-0 or 4-0 in United States Pharmacopeia (USP).

Experimental apparatus

The schematic illustration of the experimental apparatus created for this study is shown in Figure 2. The general material testing machine (AG-10kNG, SHIMADZU CORPORATION, Kyoto, Japan) was used for the ligation model apparatus. The knot pusher was connected to a jig that was fixed to the load cell, which is a sensor that detects force and converts it to an electrical signal. A pedestal was put in the basement of the apparatus, and a seating point was created on the pedestal with a hook. The suture for the test was fixed to the hook with manual ligation. A sliding knot was formed with the suture. In other words, the left side of the suture was set as the suture axis and a half hitch was made with the right side of the suture. The knot pusher tip was then put on the loop side of the suture in a neutral position. Weight was fixed to each edge of the suture via pulleys to provide constant tension force.

The distance between the two pulleys was 50 mm to simulate the small chest incision made in

MICS. The depth from the starting point of the knot pusher tip to the seating point was 160 mm. The seating point made with the hook could be moved horizontally by shifting the pedestal. We tested two apparatus settings: the "central position setting" in which the seating point was set just below the knot pusher (Fig. 2A), and the "side position setting" in which the seating point was positioned laterally 10 mm to the left of the knot pusher line (Fig. 2B). In the central position setting we assumed that the knot pusher pushed down on the knot itself, while in the side position setting we assumed the knot pusher pushed down on the loop side of the suture beside the knot.

The knot pusher was connected to the load cell and was lowered toward the seating point at a constant speed of 10 mm/s. During the ligation process the pushing force was measured every 0.05 s by the load cell. The graph indicates the pushing force on the vertical axis and the pushing depth on the horizontal axis (Fig. 3). The pushing force was slightly elevated as the knot pusher was lowered, and the force was relatively constant from 30 mm to 120 mm in depth. Therefore, we evaluated the pushing force at the middle point (75 mm in depth) in the test. Fluctuations in the pushing force are related to the smoothness of the ligation process.

Experimental conditions

Before starting the experiment, we measured the traction force applied to the axis of the suture by five cardiovascular surgeons using the manual sliding knot technique. The traction force was measured using a digital force gauge (ZP-20N, IMADA, Toyohashi, Japan). The traction force applied to the axis of the suture ranged from100-250 gf. Therefore, we used weights of 100, 200, and 300 gf in our experiments.

The group was named according to the weights applied on the axis and loop sides of the suture. Group (200-100) indicates the axis side suture was connected to the 200 gf weight, and the loop side suture was connected to the 100 gf weight. We evaluated the pushing force in three even weight

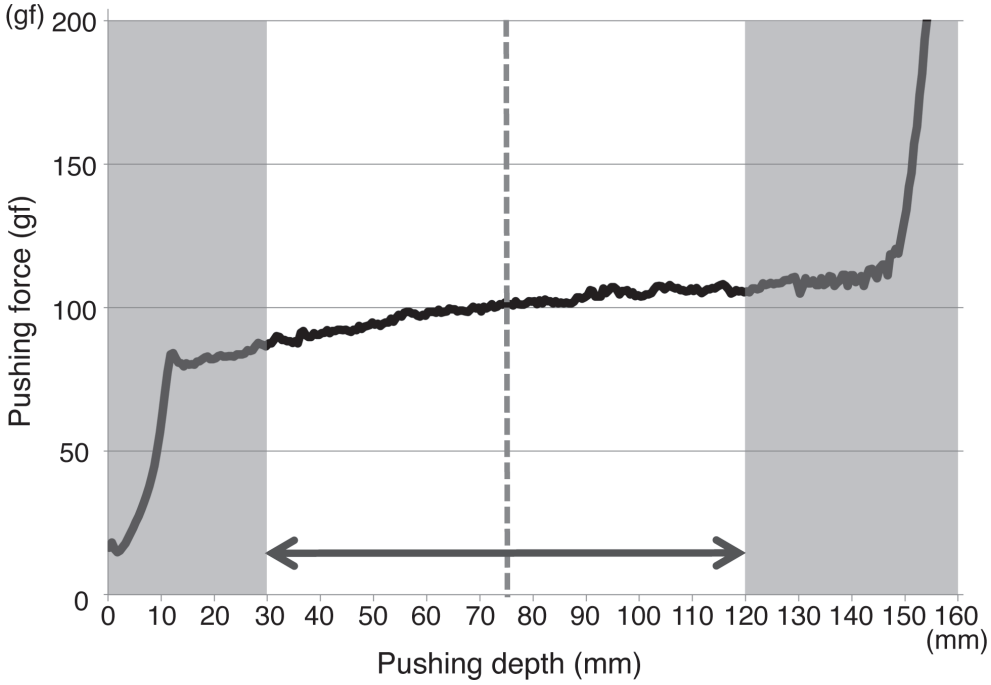

Figure 3. This graph is a typical example of the relationship between the pushing depth and the detected pushing force. We evaluated the pushing force at a pushing depth of 75 mm, and we evaluated the stability of the ligation process by the amplitude of the fluctuation of the line from a pushing depth of 30 mm to 120 mm.

conditions termed Group (100-100), Group (200-200), and Group (300-300), and in three uneven weight conditions termed Group (200-100), Group (300-100), and Group (300-200).

Experiment 1

We used Suture-A and applied various weights in the central position setting.

Experiment 2

We used Suture-A with various weight conditions to evaluate the effect of the pushing position on the pushing force. There are two ways for advancing the knot in the ligation process; the knot pusher pushes the knot itself or pushes the suture beside the knot. To simulate the former method, we adopted the central position setting (Fig. 2A), and to simulate latter method we adopted the side position setting (Fig. 2B). We compared the pushing force in both settings.

Experiment 3

We compared the pushing force using Suture-A, Suture-B, and Suture-C. Experiment 3 was performed under the side position setting using weight condition Group (200-100).

Experiment 4

We compared the pushing force in dry and wet conditions. Distilled water was supplied to the knot pusher tip with a constant flow of 5 mL/min using a syringe pump to produce the wet condition (Fig. 4). Experiment 4 was done under the side position setting using weight condition Group (200-100).

Statistical analysis

We performed the ligation tests five times with the same suture for each condition, and each time

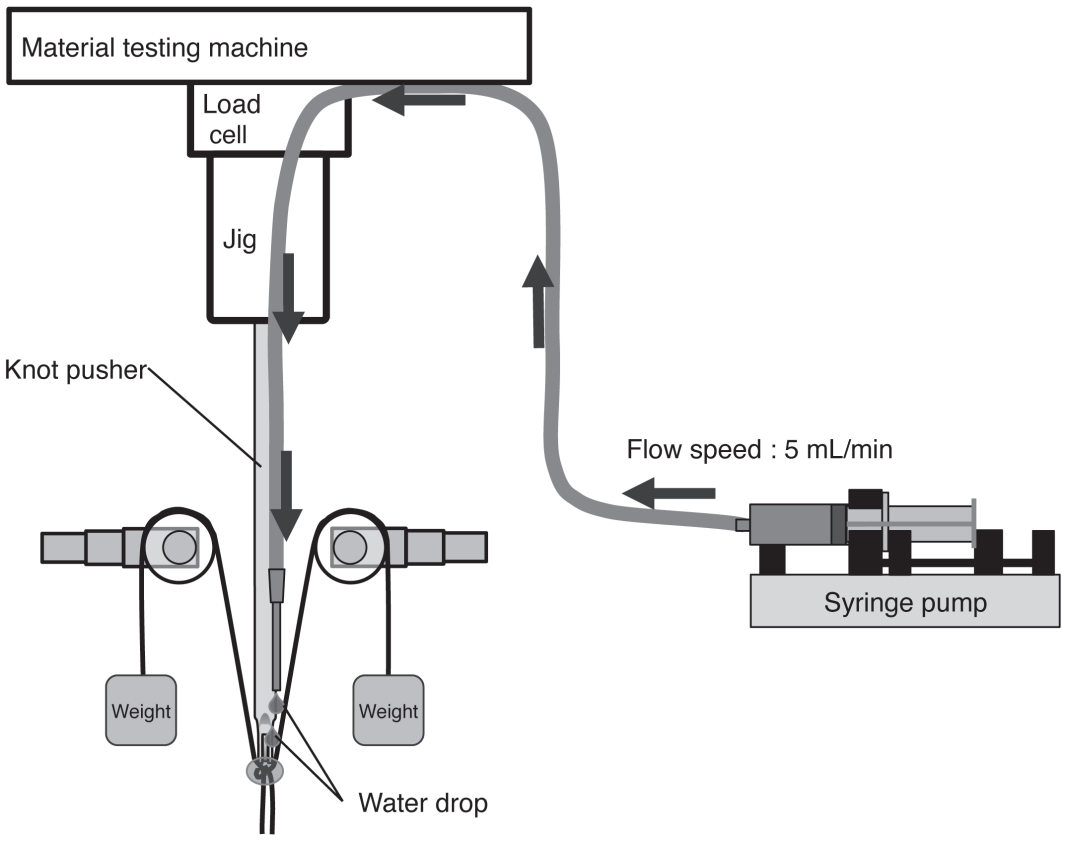

Figure 4. Experimental setup for producing wet conditions. Distilled water was dripped on the knot pusher tip at a rate of 5 mL/min to evaluate the effect of the wet condition.

we measured the pushing force as mentioned above. The pushing force was expressed as the average ±standard deviation. Statistical analysis was performed with one-way analysis of variance (ANOVA). Dunnett's test and Tukey's multiple range tests were performed with analysis for multi groups. Dunnett's test was performed in experiments 1 and 2 to compare each weight Group. Tukey's multiple range test was used to compare each suture in experiment 3. Student's *t*-test was used to compare results of the same weight Group in different apparatus settings and the results of dry and wet conditions.

Results

Experiment 1

In even weight conditions, the knot pusher kept pushing the knot itself to the seating point (Fig. 5A). However, in the uneven weight conditions, the knot was displaced to the heavier weight side, consequently the knot pusher kept pushing beside the knot (Fig. 5A).

The average pushing force in each weight group is shown in Figure 6A. In even weight conditions, the pushing force at the middle depth (75 mm) was 114±1 gf in Group (100-100), 328±6 gf in Group (200-200), and 478±2 gf in Group (300-300). In uneven weight conditions, the pushing force was 109 ±1 gf in Group (200-100), 100±3 gf in Group (300-100), and 231±3 gf in Group (300-200). There were significant differences between Group (200-100) and the other groups ($p<0.0001$) (Fig. 6A).

Experiment 2

In the side position setting, we assumed that the knot pusher would continue to push beside the knot. However, in the even weight conditions, the knot pusher kept pushing the knot itself because the point of intersection was shifted to the center to balance both side weights. In the uneven weight conditions, the knot pusher kept pushing down beside the knot like in the central position (Fig. 5B).

The pushing force resulted from the side position setting is shown in Figure 6B. In even weight conditions, the pushing force was 109±1 gf in Group (100-100), 257±8 gf in Group (200-200), and 482

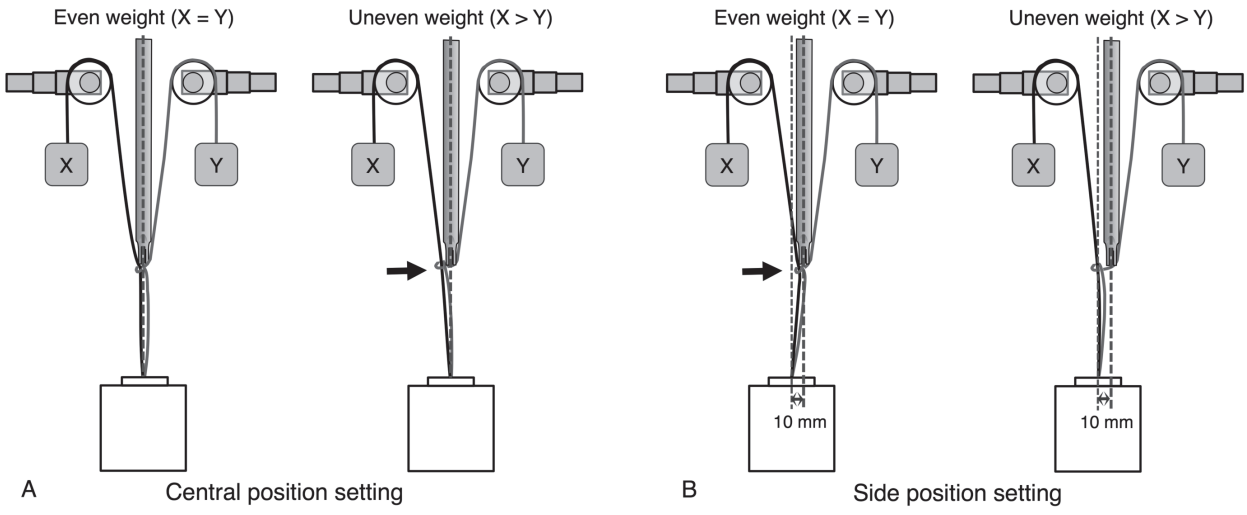

Figure 5. A, Central position setting. In the even weight setting (X=Y), the knot was located just beneath the knot pusher tip. In the uneven weight setting (X>Y), the knot was displaced to the heavier left side (arrow). B, Side position setting. In the even weight setting (X=Y), the knot was located just under the knot pusher tip (arrow). In the uneven weight setting (X>Y), the knot pusher pushed down the side of the knot the same way as in the central position.

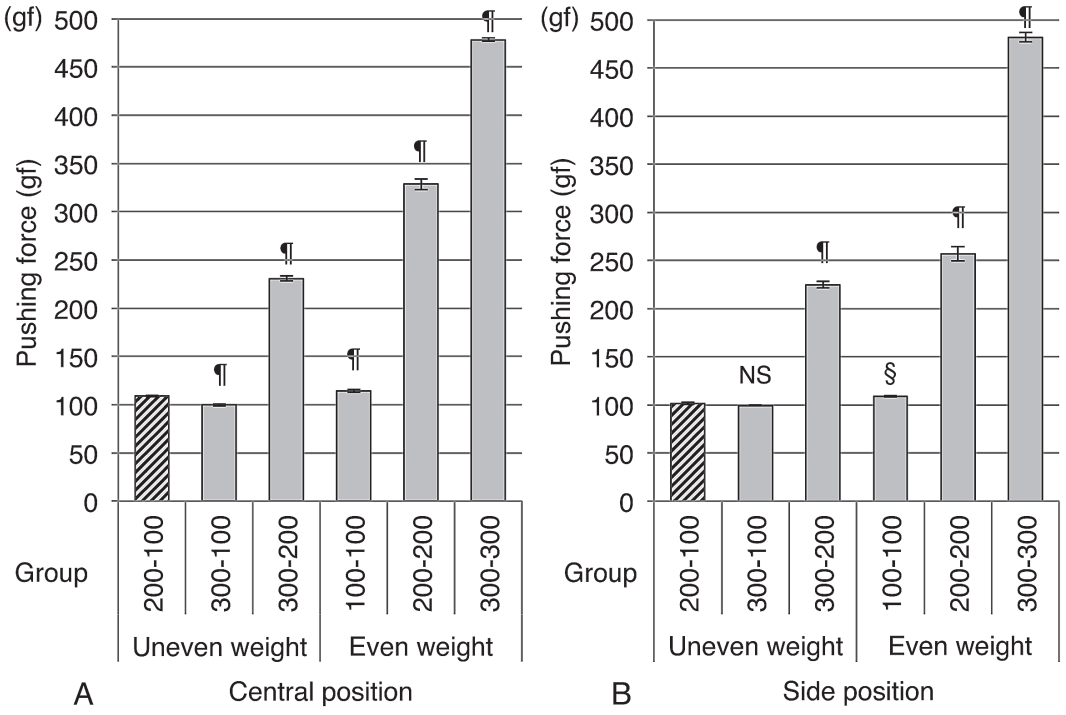

Figure 6. The bar graph shows the average pushing force at a depth of 75 mm for each weight setting with Suture-A. A, Results of tests in the central position setting. There were significant differences between Group (200-100) and the other groups ($p<0.0001$). B, Results of tests in the side position setting. There were significant differences between Group (200-100) and all other groups except Group (300-100). NS, not significant; § $p<0.001$ vs Group(200-100), ¶ $p<0.0001$ vs Group (200-100).

Table 2. Pushing force of central position and side position with Suture A

Weight condition		Pushing force (gf)		p value
		Central position	Side position	
Equal weight	Group (100-100)	114±1	109±1	<0.0001
	Group (200-200)	328±6	257±7	<0.0001
	Group (300-300)	478±2	482±5	0.0692
Unequal weight	Group (200-100)	109±1	101±1	0.0003
	Group (300-100)	100±1	99±1	0.795
	Group (300-200)	231±3	225±4	0.0045

(mean±standard deviation)

±5 gf in Group (300-300). In uneven weight settings, the pushing force was 101±1 gf in Group (200-100), 99±1 gf in Group (300-100), and 225±4 gf in Group (300-200). In the side position setting, there were significant differences between Group (200-100) and the other groups except Group (300-100), Group (200-100) vs Group (300-100): $p=0.99$, Group (200-100) vs Group (100-100): $p=0.0086$, Group (200-100) vs the other groups: $p<0.0001$.

Comparing the pushing forces measured in the central position setting and side position setting in the same weight group, they were not significantly different for Group (300-300) and Group (300-100), and in the other groups, the pushing forces of the side position setting were significantly smaller (Table 2).

Experiment 3

The pushing force was 104±1 gf with Suture-A, 112±2 gf with Suture-B, and 97±1 gf with Suture-C (Figs. 7A and 7B). There were significant differences in pushing force among all the sutures (Suture-A vs Suture-B: $p<0.0001$, Suture-A vs Suture-C: $p<0.0001$, Suture-B vs Suture-C: $p<0.0001$) (Fig. 7B). The fluctuation of the line graph seemed to be larger with Suture-B than the other two sutures (Fig. 7A).

Experiment 4

The pushing force of Suture-A was 104±1 gf in the dry condition and 104±1 gf in the wet condition (Fig. 8A). The pushing force of Suture-B was 112±2 gf in the dry condition and 122±1 gf in the wet condition (Fig. 8B). The pushing force of Suture-C was 97±1 gf in the dry condition and 96±2 gf in the wet condition (Fig. 8C). There were no significant differences between the dry and wet conditions with Suture-A and Suture-C. The pushing force was significantly larger in the wet condition with Suture-B ($p<0.0001$) (Fig. 8D). Judging from the waveform of the graph, the fluctuation of the pushing force with Suture-B was much larger than those of the other sutures (Fig. 8B).

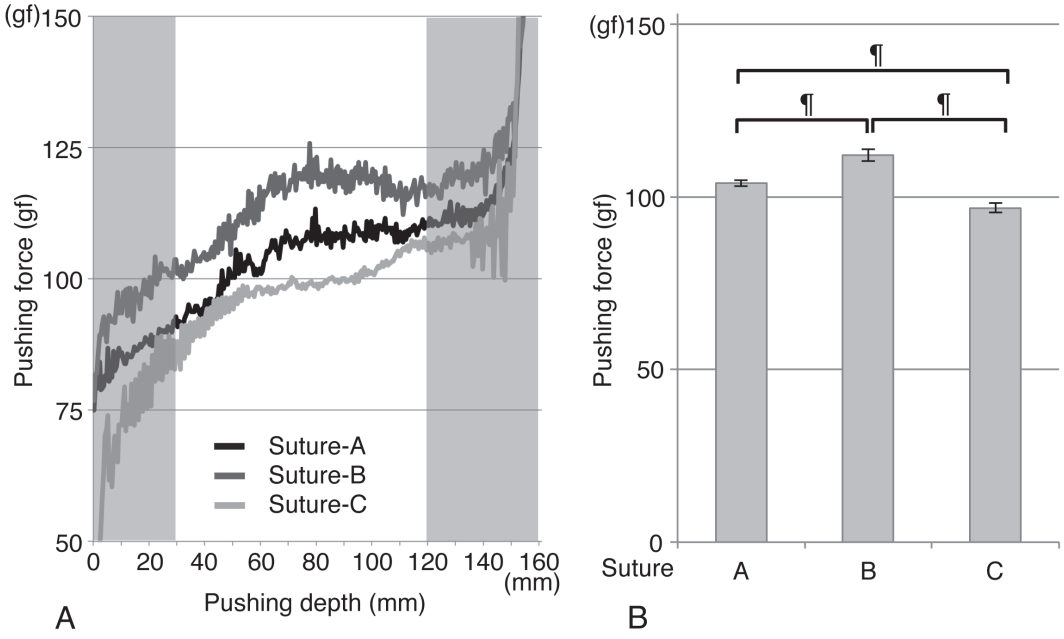

Figure 7. A, Typical line graphs of the relationship between the pushing force and pushing depth for Suture-A, -B, and -C. The amplitude of the fluctuation of the line in Suture-B was larger than those of the other sutures. B, Average pushing force for Suture-A, -B, and -C. There were significant differences between all sutures. ¶ $p<0.0001$.

Discussion

In this study, we examined the ligation processes using a knot pusher with a ligation model. We assessed the ligation process experimentally because surgeons frequently perform ligations sensuously or empirically during operations.

It was quantitatively shown that a smaller traction force on the loop side of the suture decreased the pushing force of the knot pusher. Pushing the suture beside the knot with a knot pusher led to a smaller pushing force than when the knot pusher pushed the knot itself. Finally, the addition of

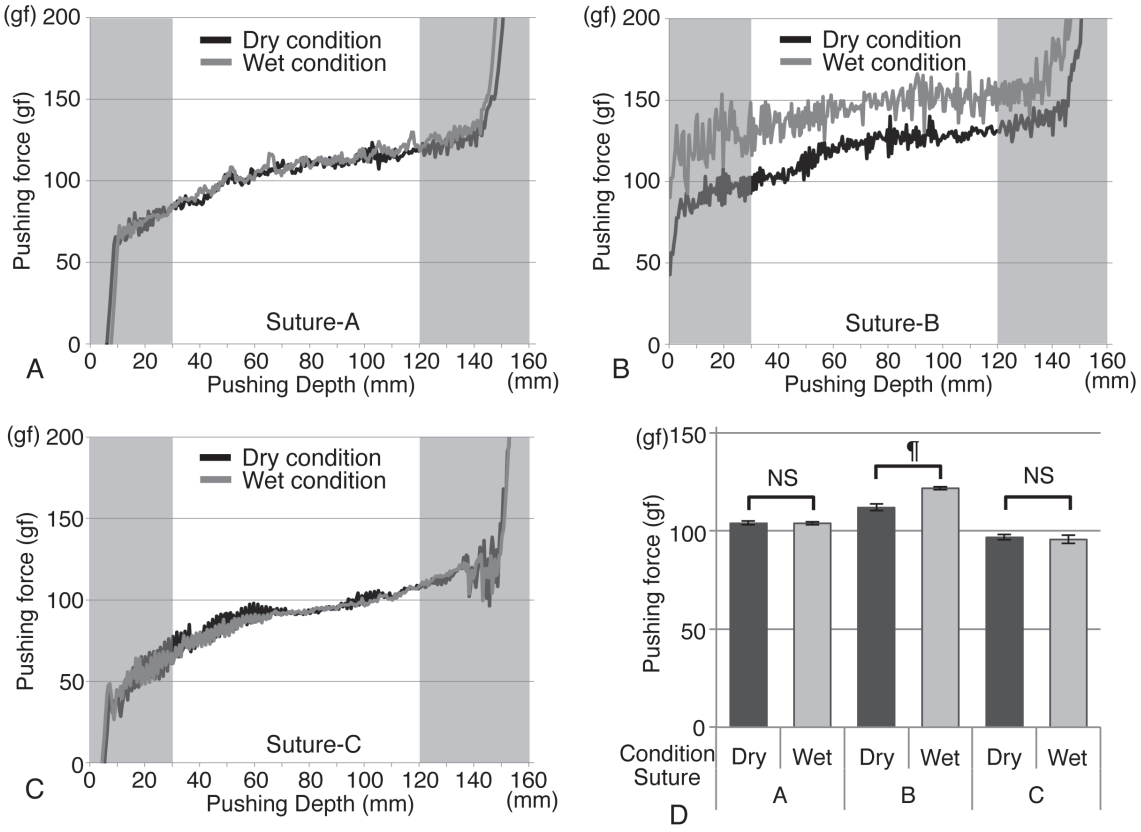

Figure 8. The typical relationship between the pushing force and pushing depth when water was added to each suture. A, Suture-A; B, Suture-B; and C, Suture-C. D, Average pushing force for each suture in dry and wet conditions. In Suture-A and -C, the lines were similar between dry and wet conditions. In Suture-B, the fluctuation of the line in the wet condition was larger than in the dry condition. The pushing force of Suture-B in the wet condition was significantly larger than in the dry condition. NS, not significant; ¶ $p<0.0001$.

water, which is conventionally performed in the ligation process, had no significant effect on the pushing force when we used hydrophobic sutures with knot pushers.

Experimental apparatus

Because the endoscopic surgery and robotic surgery have been developed, there are some reports about the mechanical strength of some knots, like Roeder Knot and Weston Knot[13-16]. However, there have been no reports about the assessment of ligation processes with a knot pusher. Although we needed to simulate the ligation process, no ready-made apparatus existed. Therefore we established an original examination apparatus to investigate the pushing force with a knot pusher. In the clinical setting, surgeons can control the direction in which the knot pusher is advanced. Our experimental apparatus simulated only vertical movement of the knot pusher, thus this apparatus was not able to fully simulate the ligation procedure as performed by a surgeon. However, we thought this model would be appropriate for simulating the knot pusher ligation in cardiovascular surgery because the knot pushers can only be pushed in limited directions during deep site surgeries such as mitral valve surgery.

Experiment 1

We first evaluated the pushing force and checked the movement of the sutures with all weight settings in the central position setting. We assumed that the knot pusher would continue pushing the knot to the seating point, and this was true in the even weight conditions. However, in the

uneven weight conditions, the knot was displaced to the side of the axis suture with the heavier weight to remain balanced. This caused the knot pusher to continue pushing the suture beside the knot, and not the knot itself (Fig. 5A).

The pushing force of Group (200-100) was significantly smaller than that of Group (100-100) ($p < 0.0001$), and the pushing force of Group (300-200) was much smaller than that of Group (200-200). Therefore it was suggested that the total amount of weight was not the only condition that affected the pushing force. The pushing force of Group (300-100) was significantly smaller than that of Group (200-100) ($p < 0.0001$), which indicated that as the left side weight increased, the pushing force decreased to keep the axis suture tight. The pushing force of Group (300-100) was much smaller than that of Group (300-200), as shown in Figure 6A. This suggests that as the weight of the loop side suture increased, the pushing force of the knot pusher increased as well.

From the findings of the experiment 1, it was shown that the pushing force in the uneven weight condition was smaller than that in the even weight condition, and the traction force on both sides of the suture affected the pushing force. Increasing the weight on the axis suture made the pushing force smaller and increasing the weight on the loop side of the suture made the pushing force larger.

Experiment 2

Comparing the pushing forces of the central position setting and side position setting using the same weight groups, the pushing forces of the side position setting were smaller than those of the central position setting except for Group (300-100) (Table 2). From the findings of experiment 2, it was found that pushing beside the knot decreased the pushing force.

There was no significant difference between the pushing force of Group (200-100) and Group (300-100) in the side position setting ($p = 0.99$), though there was a significant difference in the central position setting. It was shown that pushing beside the knot reduced the influence of the axis side weight. Since the traction force of the axis suture has a deep relation to the traction force of the tissue at the seating point in the surgery, a smaller traction force of the axis suture helps prevent injuries to the tissue.

To perform a safer ligation with the knot pusher, it is important to keep in mind which suture is the axis suture and not to tug the loop side suture too much.

Based on the results of experiments 1 and 2, we performed experiments 3 and 4 in the side position setting with the weight condition Group (200-100), because this setting provided a stable condition for pushing down the knot.

Experiment 3

Each suture applied in the experiment 3 has different characteristics (Table 1). The pushing force of Suture-C was the smallest and that of Suture-B was largest. There were significant differences among each suture (Fig. 7B). Suture-C is size 4-0 in USP, so the diameter is different from the other two. The diameter of Suture-C possibly affected the pushing force. The amplitude of the pushing force fluctuation from 30-120 mm pushing depth with Suture-B seemed to be larger, as shown in Figure 7A.

Experiment 4

In clinical situations, we often add water to the hands when we perform manual ligation to reduce the friction force between the suture and the rubber gloves. We made a system using a syringe pump to ensure that the tip of the knot pusher was always kept wet with distilled water (Fig. 4).

There was no significant difference in the pushing force between the dry and wet conditions with

Suture-A and Suture-C (Fig. 8D). The water addition may have had no effect on the pushing force of these sutures because they are made of hydrophobic materials.

In Suture-B, which is hydrophilic, the pushing force in the wet condition was significantly larger and the amplitude of the pushing force fluctuation was also noticeably larger than that in the dry condition (Fig. 8B). Although we could not detect the friction force directly with our experimental apparatus, it was inferred that the friction force increased when water was added to the hydrophilic suture.

Addition of water had no effect on the pushing force when we used a smooth head knot pusher and hydrophobic sutures like Suture-A and Suture-C. The purpose of this experiment was to reveal the effect of water addition on the relationship between the knot pusher and sutures. Therefore, we do not mention the effect of water addition on the relationship between the surgeon's hands with rubber gloves and the sutures during the manual ligation.

Limitations of this study

In this study, the knot pusher pushed down the loop side suture toward the seating point. The usage of the knot pusher depends on the operator, and some knot pushers are used differently, like the knot pusher shown in Figure 1B. Other settings are available with this experimental apparatus; for example, the knot pusher can be pushed down to the seating point along the axis suture by changing the settings. However, this effect was not studied in the current work. Additionally, it was difficult to evaluate the amplitude of the fluctuations numerically, so we evaluated them visually on the figures. This calculation can be made more precisely in future studies.

References

1. Goldstone AB, Atluri P, Szeto WY, Trubelja A, Howard JL, MacArthur JW Jr, et al. Minimally invasive approach provides at least equivalent results for surgical correction of mitral regurgitation: a propensity-matched comparison. J Thorac Cardiovasc Surg 2013;145:748-756.
2. Cosgrove DM 3rd, Sabik JF. Minimally invasive approach for aortic valve operations. Ann Thorac Surg 1996;62:596-597.
3. Gillinov AM, Banbury MK, Cosgrove DM. Hemisternotomy approach for aortic and mitral valve surgery. J Card Surg 2000;15:15-20.
4. Kim BS, Soltesz EG, Cohn LH. Minimally invasive approaches to aortic valve surgery: Brigham experience. Semin Thorac Cardiovasc Surg 2006;18:148-153.
5. Shibata T. Loop technique for mitral valve repair. Gen Thorac Cardiovasc Surg 2014;62:71-77.
6. Taylor FW. Surgical knots. Ann Surg 1938;107:458-468.
7. Bo W, Fusheng J, Tianyou W. A novel ligation technique facilitating minithoracotomy. Ann Thorac Surg 2009;88:1989-1992.
8. Haxton H. The influence of suture materials and methods on the healing of abdominal wounds. BR J Surg 1965;52:372-375.
9. Trimbos JB. Security of various knots commonly used in surgical practice. Obstet Gynecol 1984;64:274-280.
10. Batra EK, Taylor PT, Franz DA, Towler MA, Edlich RF. A portable tensiometer for assessing surgeon's knot tying technique. Gynecol Oncol 1993;48:114-118.
11. Dinsmore RC. Understanding surgical knot security: a proposal to standardize the literature. J Am Coll Surg 1995;180:689-699.
12. Gunderson PE. The half-hitch knot: a rational alternative to the square knot. Am J Surg 1987;154:538-540.
13. Moreno M, Magos FJ, Arcovedo R, Olachea P, Palacios JA, Salazar A, et al. Comparison of the performance of the Gea extracorporeal knot with the Roeder extracorporeal knot and the classical knot. Surg Endosc 2004;18: 157-160.
14. Milla MJ, Peindl RD, Connor PM. Arthroscopic knot tying: the role of instrumentation in achieving knot security. Arthroscopy 2005;21:69-76.
15. Baums MH, Sachs C, Kostuj T, Schmidt-Horlohé K, Schultz W, Klinger HM. Mechanical testing of different knot types using high-performance suture material. Knee Surgery Sports Traumatology Arthroscopy 2015;23:

1351-1358.
16. Dorsey JH, Sharp HT, Chovan JD, Holtz PM. Laparoscopic knot strength: a comparison with conventional knots. Obstet Gynecol 1995;86:536-540.
17. Sharp HT, Dorsey JH, Chovan JD, Holtz PM. The effect of knot geometry on the strength of laparoscopic slip knots. Obstet Gynecol 1996;88:408-411.
18. Grapow MT, Mytsyk M, Fassl J, Etter P, Matt P, Eckstein FS, et al. Automated fastener versus manually tied knots in minimally invasive mitral valve repair: impact on operation time and short- term results. J Cardiothorac Surg 2015;10:146.
19. Shibata T, Hattori K, Kato Y, Bito Y. Thimble type knot pusher: bioprosthesis stents no longer interfere with tying. Interact Cardiovasc Thorac Surg 2010;11:131-132.

Osaka City Med. J. Vol. 64, 143-151, 2018

Experimental Methanol Poisoning: Electron Microscopic Findings Obtained between 2 and 14 Days after Administration

Nobuhiko Ueda, and Kunihiko Shiraki

Department of Ophthalmology and Visual Science,
Osaka City University Graduate School of Medicine

Abstract

Background

We observed changes in retinal ganglion cells and the optic nerve using electron microscopy between 2 and 14 days after experimental methanol poisoning.

Methods

Rats in the poisoning group received an intraperitoneal injection of methanol (3.5 g/kg) after 5 weeks on a folate-deficient diet. Rats in the control group received an intraperitoneal injection of saline after 5 weeks on a normal diet. In both groups, electron microscopic analysis was performed on eyeballs enucleated at 2, 7, and 14 days post-injection.

Results

In the poisoning group, retinal ganglion cells showed swelling and a decrease in organelle number at 2 days post-injection, and aggregation of organelles at 7 and 14 days post-injection. Axons in the optic nerve head exhibited swelling and a marked decrease in organelle number at 2 days post-injection. These findings were less marked at 7 and 14 days post-injection. Degeneration of axons and myelin in the intraorbital optic nerve was observed at 2 days post-injection. These findings were less marked at 7 and 14 days post-injection.

Conclusions

These findings suggest that significant retinal ganglion cell degeneration occurs between 2 and 14 days post-injection, while degeneration of the optic nerve head is most marked at 2 days post-injection.

Key Words: Methanol; Poisoning; Retina; Optic nerve; Electron microscopy

Introduction

Acute methanol poisoning can lead to severe visual impairment. Onset of symptoms occurs 18 to 48 hours following methanol ingestion. Systemic metabolic acidosis from acute methanol poisoning can cause headaches, abdominal pain, coma, and in some cases even death. With respect to the

Received April 2, 2018; accepted November 27, 2018.
Correspondence to: Nobuhiko Ueda, MD.
Department of Ophthalmology and Visual Sciences, Osaka City University Graduate School of Medicine, 1-4-3 Asahimachi, Abeno-ku, Osaka 545-8585, Japan
Tel: +81-6-6645-3867; Fax: +81-6-6634-3867
E-mail: bwz12269@nifty.com

eye, symptoms include decreased visual acuity, mydriasis, attenuation of the pupillary light reflex, hyperemia and swelling of the optic nerve head, and peripapillary retinal edema. Visual acuity usually recovers within six days of onset of symptoms. However, unless full recovery occurs, further declines in visual acuity are expected, resulting in optic nerve atrophy and a poor prognosis[1].

Methanol is metabolized in the liver into formaldehyde and then formic acid[2]. Formic acid inhibits cytochrome c oxidase, an enzyme of the mitochondrial electron transport chain[3]. It is thought that this inhibition reduces adenosine triphosphate (ATP) production and increases reactive oxygen species in the mitochondria[4,5], thereby resulting in damage to retinal ganglion cells (RGC).

It has been thought that animal models of acute methanol poisoning can be useful for developing therapies. Past research has employed the rhesus monkey[6] and the rat[7-9] as animal models. Both models have been examined in detail within a span of three days following methanol administration. However, to the best of our knowledge, no studies using animal models have explored the subacute phase of poisoning, extending to 14 days after administration, and such research would be of significant value for analyzing the pathology of acute methanol poisoning in the acute phase and beyond. Thus, we performed a qualitative analysis of acute methanol poisoning in the rat model by using light microscopy (LM) and electron microscopy (EM) to observe changes in the optic nerve and RGC between 2 and 14 days after methanol administration.

Methods (Fig. 1)

The present study was carried out under the control guidance of a committee in accordance with The Guidelines on Animal Experiments at Osaka City University.

The experiment used 24 four-week-old male Wistar rats, which were divided into two groups based on the following criteria.

1. A poisoning group of 12 rats were fed a folate-deficient diet for five weeks ad libitum and then received an intraperitoneal injection of methanol (3.5 g/kg).

2. A control group of 12 rats were fed a normal diet for five weeks and then received an intraperitoneal injection of saline (11.7 mL/kg).

The folate-deficient diet was obtained from Dyets Inc., USA (#517777). A 30% (w/v) mixture of methanol and saline was prepared for intraperitoneal injection.

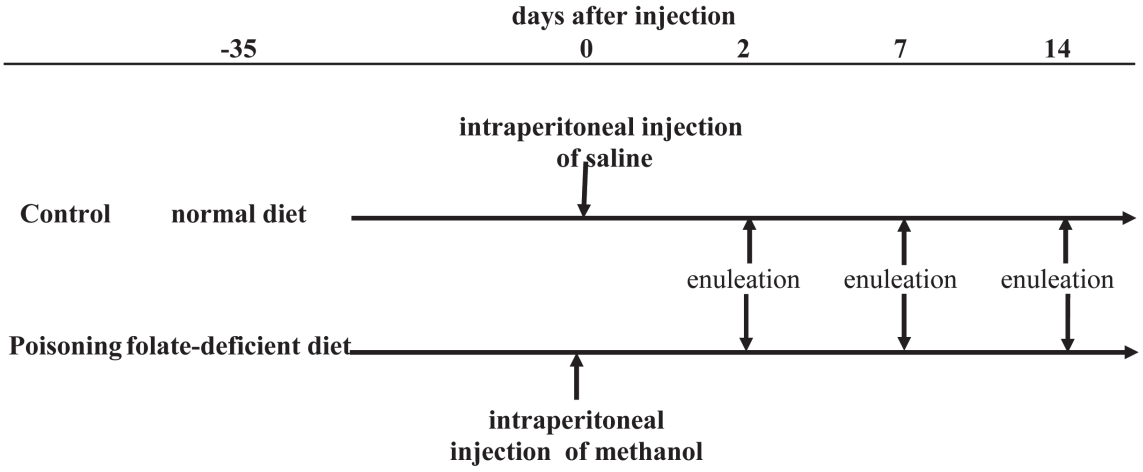

Figure 1. An overview of the experimental protocol.

At 2, 7, and 14 days post-injection (dpi), eyeballs from four rats in each group were enucleated following perfusion fixation with a solution of 2.5% glutaraldehyde and 2% paraformaldehyde in a 0.1 M phosphate buffer under inhalation anesthesia using isoflurane.

The intraorbital optic nerve as well as the optic nerve head and surrounding retina were harvested after resecting the optic nerve at a length of 1 mm from the eyeball. The harvested tissue was pre-fixed with the same fixative solution described above, post-fixed with osmium tetroxide and then embedded in resin. An ultramicrotome was used to cut samples into 1 μm slices, which were then stained with toluidine blue then examined with a light microscope. The retina, the horizontal longitudinal section of the optic nerve head and the cross-section of the intraorbital optic nerve at a position of 1 mm from the eyeball were examined. Ultra-thin sections prepared at the same time were double-stained with uranyl acetate and lead citrate and then examined with an electron microscope (Hitachi H-7500).

Results (Table 1)

LM findings of the inner retina (Fig. 2)

Compared to the control group (Fig. 2A), at 2 dpi the poisoning group exhibited vacuolar degeneration in the nerve fiber layer, ganglion cell layer and inner plexiform layers (Fig. 2B). Although this finding diminished at 7 dpi, enlargement of some RGC somas was observed (Fig. 2C).

Table 1. Summary of Results

	Inner retina	
	LM	EM
2 dpi	vacuolar degeneration	numerous vacuoles in RGC
7 dpi	enlargement of some RGC somas	vacuoles decreased, organelle aggregation in RGC
14 dpi	eccentric locations of nuclei	organelle aggregation was more pronounced in RGC

	Optic nerve head	
	LM	EM
2 dpi	No remarkable change	Swollen axons
7 dpi	No remarkable change	No remarkable change
14 dpi	No remarkable change	No remarkable change

	Intraorbital optic nerve	
	LM	EM
2 dpi	No remarkable change	Deformation and size disparity of axons Gaps between axons and myelin sheaths
7 dpi	No remarkable change	Changes in axons & myelin sheaths diminished
14 dpi	No remarkable change	No remarkable change

dpi, days post-injetion; LM, Light microscopy; EM, Electron microscopy; and RGC, retinal ganglion cells.

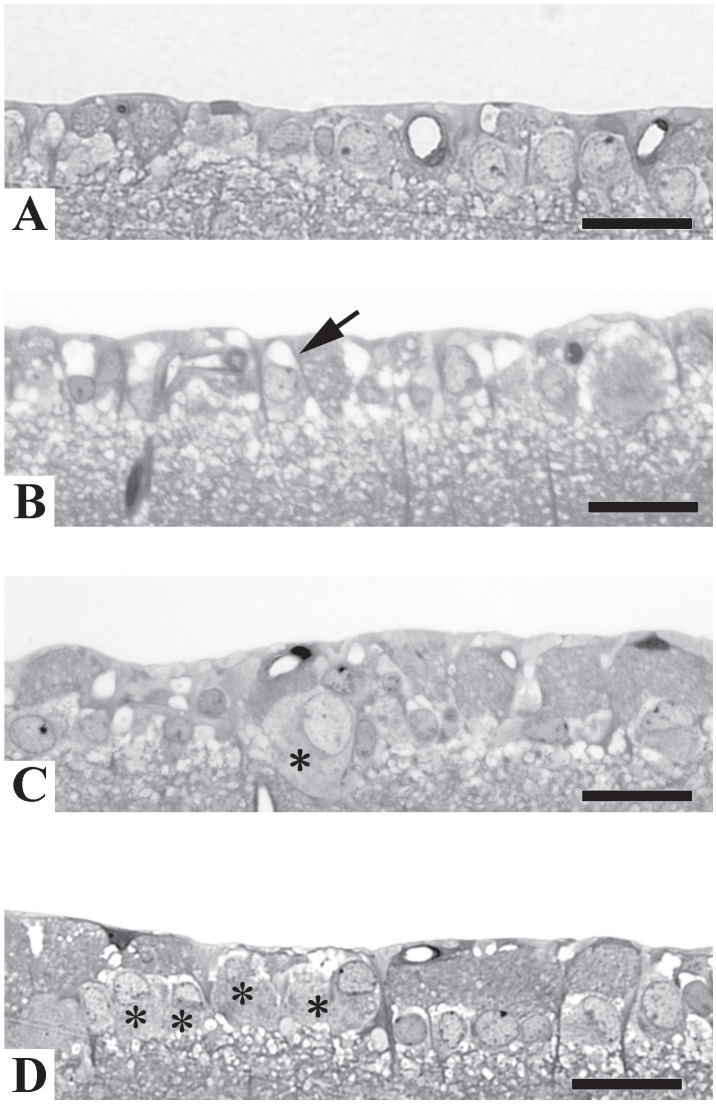

Figure 2. Light micrographs of the inner retina. A, Control group specimen at 2 days post-injection (dpi). No changes were observed in the control group at 2, 7, and 14 dpi. B, Poisoning group specimen at 2 dpi. Numerous vacuoles were observed in the nerve fiber and inner plexiform layers (arrow). C, Poisoning group specimen at 7 dpi. Retinal ganglion cell (RGC) soma enlargement was observed (*). D, Poisoning group specimen at 14 dpi. RGC soma enlargement and eccentric locations of nuclei at the periphery of the soma were observed (*). Bar=25 μm.

At 14 dpi, many of the RGC somas were swollen and a portion displayed eccentric locations of nuclei at the periphery of somas (Fig. 2D).

EM findings of the inner retina (Fig. 3)

Compared to the control group (Fig. 3A), the RGC cytoplasm in the poisoning group exhibited numerous vacuoles at 2 dpi (Fig. 3B), likely induced by the swelling of intracellular organelles. Although these vacuoles decreased in number at 7 dpi, organelle aggregation was observed in the RGC cytoplasm (Fig. 3C). At 14 dpi, RGC nuclei were eccentrically located at the periphery of somas and organelle aggregation was more pronounced in the cytoplasm (Fig. 3D).

LM findings of the optic nerve head

No remarkable change was detected between the control group and the poisoning group for all time points.

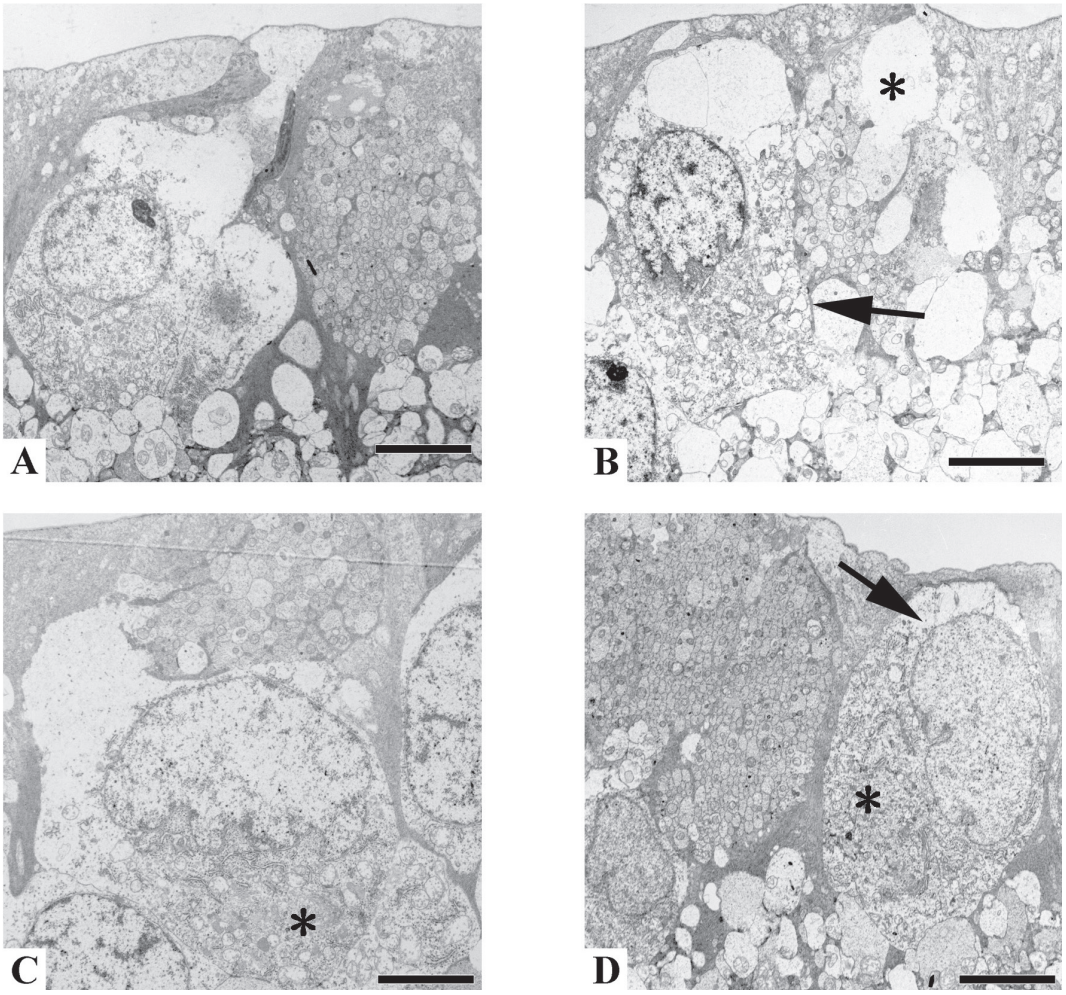

Figure 3. Electron micrographs of the inner retina. A, Control group specimen at 2 dpi. No changes were observed in the control group at 2, 7, and 14 dpi. B, Poisoning group specimen at 2 dpi. Marked vacuole formation was observed in the nerve fiber layer (＊), and numerous vacuoles appeared in the RGC cytoplasm (arrow). C, Poisoning group specimen at 7 dpi. Aggregation of intracellular organelles was observed in the RGC cytoplasm (＊). D, Poisoning group specimen at 14 dpi. RGC nuclei eccentric locations at the periphery of cell somas (arrow) and aggregation of intracellular organelles with high electron density were observed in the cytoplasm (＊). Bar=5 μm.

EM findings of the optic nerve head (Fig. 4)

Compared to the control group (Fig. 4A), the poisoning group exhibited swollen axons in the optic nerve head and a marked reduction in intracellular organelles at 2 dpi (Fig. 4B). These findings disappeared at 7 dpi (Fig. 4C) and 14 dpi (Fig. 4D).

LM findings of the intraorbital optic nerve

No remarkable change was detected between the control group and the poisoning group for all time points.

EM findings of the intraorbital optic nerve (Fig. 5)

Compared to the control group (Fig. 5A), axons in the intraorbital optic nerve of the poisoning group exhibited deformation and size disparity. Gaps were also detected between axons and myelin sheaths at 2 dpi (Fig. 5B). These findings diminished at 7 dpi (Fig. 5C) and were undetectable at 14 dpi (Fig. 5D).

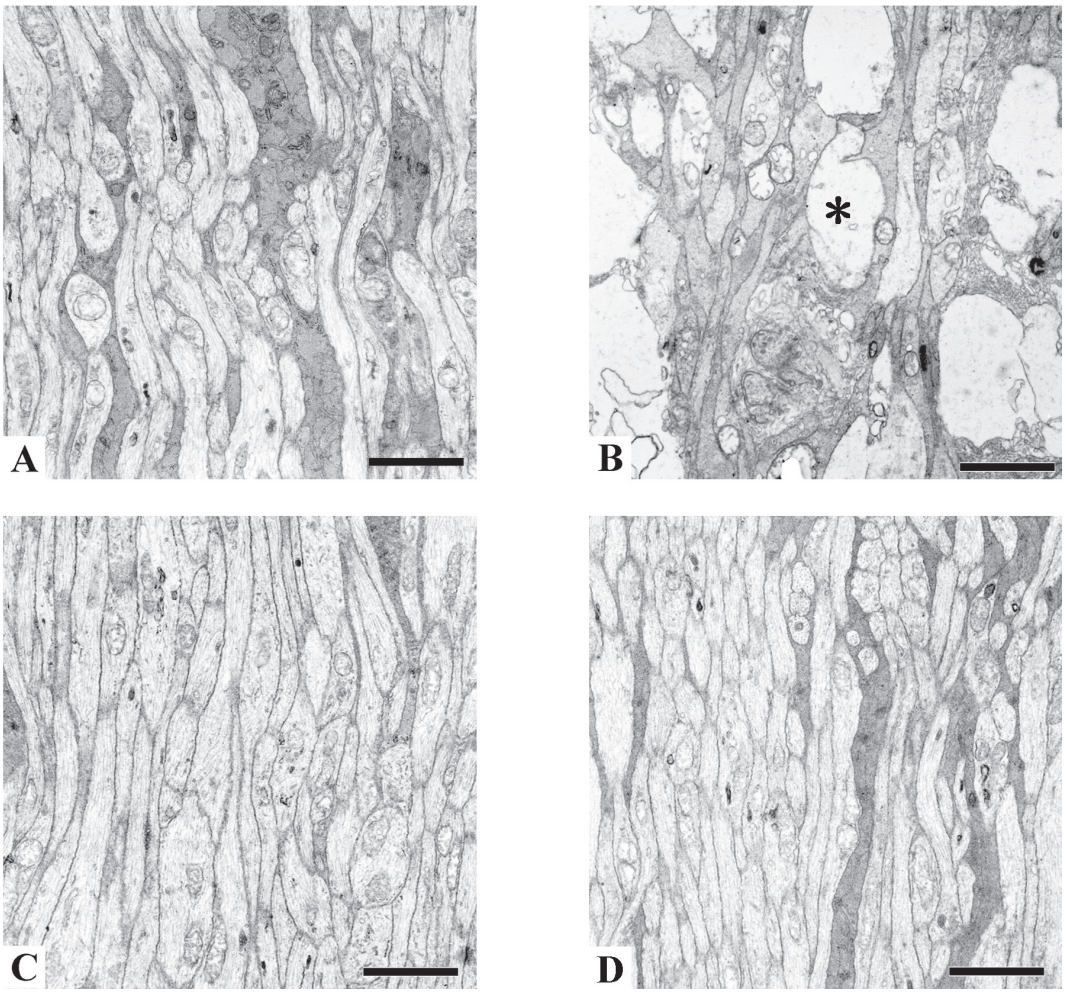

Figure 4. Electron micrographs of the optic nerve head. A, Control group specimen at 2 dpi. No changes were observed in the control group at 2, 7, and 14 dpi. B, Poisoning group specimen at 2 dpi. Swollen axons and a marked decrease in intracellular organelles were observed (*). C, Poisoning group specimen at 7 dpi. D, Poisoning group specimen at 14 dpi. Improvements were observed in axon swelling and intracellular organelle reduction. Bar=2 μm.

Discussion

The present study employed EM of the retina and optic nerve to investigate a rat model of acute methanol poisoning. As a result, at 2 dpi we identified vacuolar degeneration in the inner retina, swollen axons in the optic nerve head and axon deformation in the intraorbital optic nerve. RGC soma enlargement in the inner retina was observed at 7 dpi and beyond. In contrast, changes in the optic nerve head and intraorbital optic nerve were found to have improved at 7 dpi and 14 dpi.

Accumulation of formic acid following methanol administration is less likely in rats compared to primates[10]. As such, rat models of acute methanol poisoning have used nitrous oxide[7] and folate-deficient feed[10] to inhibit the metabolism of formic acid. In the nitrous oxide model, rats must be kept in containers infused with a gaseous mixture of nitrous oxide and oxygen. Nitrous oxide poses safety risks because it can be either combustible or readily support combustion. On the other hand, the folate-deficient model requires feeding rats an expensive folate-deficient diet from five weeks before the initial methanol administration until the conclusion of the experiment. We decided, however, to adopt this model because, unlike nitrous oxide, no safety issues needed to be addressed.

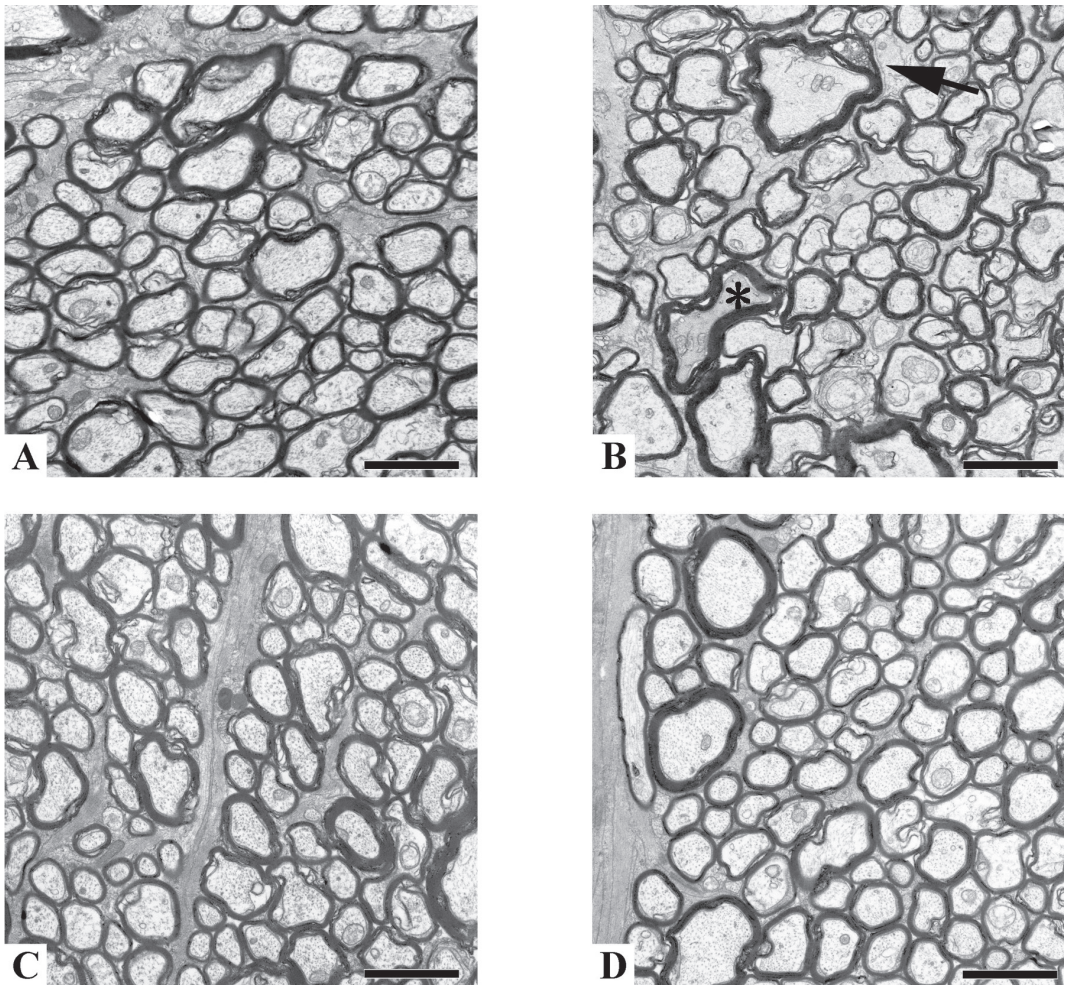

Figure 5. Electron micrographs of the intraorbital optic nerve. A, Control group specimen at 2 dpi. No changes were observed in the control group at 2, 7, and 14 dpi. B, Poisoning group specimen at 2 dpi. Axon deformation (*) and gaps between axons and myelin sheaths were observed (arrow). C, Poisoning group specimen at 7 dpi. A decrease in changes in axons and myelin sheaths was observed. D, Poisoning group specimen at 14 dpi. No obvious differences with the control group were observed. Bar=2 μm.

In a previous study, we divided rats into four groups based on the criteria noted below and measured the serum formic acid concentration of blood samples collected at 2 dpi. 1) The normal diet-saline group was fed a normal diet for 5 weeks and then given an intraperitoneal injection of saline. 2) The normal diet-methanol group on a was fed a normal diet for 5 weeks and then given an intraperitoneal injection of methanol (3.5 g/kg). 3) The folate-deficient diet-saline group was fed a folate-deficient diet for 5 weeks and then given an intraperitoneal injection of saline. 4) The folate-deficient diet-methanol group was fed a folate-deficient diet for 5 weeks and then given an intraperitoneal injection of methanol (3.5 g/kg). The results of the serum formic acid concentration were as follows: 1.00 mM in the normal diet-saline group; 1.18 mM in the normal diet-methanol group; 1.37 mM in the folate-deficient diet-saline group; and 12.54 mM in the folate-deficient diet-methanol group. The folate-deficient diet-methanol group had a significantly higher serum formic acid concentration than the other groups[11]. This result is relatively consistent with past research employing the primate model (11.2-12.9 mM)[6], and rat models using nitrous oxide (14.8 mM)[7] or a folate-deficient diet (16.1 mM)[10]. To investigate the effects of increased serum formic acid

concentrations on the retina and optic nerves of rats in methanol poisoning, the normal diet-saline group and the folate-deficient diet-methanol group were used as the control group and the poisoning group, respectively.

We identified vacuolar degeneration in RGC somas at 2 dpi, a finding that is consistent with previous studies in rats[7,9]. As with past research, we also observed swollen axons in the optic nerve head[2]. These findings could be considered equivalent to retinal edema and papillary swelling in human cases of acute methanol poisoning[1]. However, our observations differed from those of a previous study using the rhesus monkey model, in which retinal changes were not detected, but the aggregation of intracellular organelles within the axons of the intraorbital optic nerve was observed[6]. This study in rhesus monkeys noted a blood formic acid concentration between 11.2 and 13.1 mEq/L[6], which is comparable to a report of 12.54 mM in the rat model[11] that we employed. Therefore, these differences can be considered to be specific to the animal model, but require further investigation.

Vacuolar degeneration is generally thought to be caused by an increase in the water permeability of the cell membrane. The liver metabolizes methanol into formic acid[2]. Formic acid inhibits cytochrome c oxidase[3], an enzyme in the mitochondrial electron transport chain, which in turn leads to reduced ATP production in the retina[12]. Therefore, it can be inferred that the vacuolar degeneration of RGC somas and swelling of optic nerve head axons observed in this study are the consequences of enhanced membrane permeability, caused by ion pump impairment that occurs when the formic acid metabolized from methanol suppresses ATP production and triggers a shortage of intracellular energy.

In the present study, vacuolar degeneration in RGC somas and swelling of optic nerve head axons subsided from days 7 to 14 after methanol administration. We propose that this finding is comparable to improvements in retinal edema and papillary swelling seen in clinical cases[1]. To the best of our knowledge, such observations have not been made in animal models of acute methanol poisoning. We propose the following mechanism to explain this result. Sadun et al report that blood formic acid concentration returns to normal 72 hours after methanol administration in their study of an animal model of chronic methanol poisoning[13]. Considering that formic acid inhibition of cytochrome c oxidase due to formic acid and the ensuing decrease in ATP production are transient, it can be inferred that vacuolar degeneration in RGC somas as well as swelling of optic nerve head axons are also temporary.

The present study identified RGC soma enlargement and intracellular organelle aggregation between days 7 and 14 after methanol administration. To the best of our knowledge, such observations have not been made in past studies using animal models of acute methanol poisoning. We submit that our findings are related to the progressive reduction in visual acuity that occurs after temporary vision improvement in clinical cases[1].

We believe that the results of the present study may be useful for understanding the pathology of the acute to subacute phases of acute methanol poisoning and developing appropriate therapies. However, the development and evaluation of therapies will require quantitative assessment of damage to RGC somas and axons.

Using the rat model of acute methanol poisoning, we qualitatively established that although RGC soma impairment persists two to 14 days after methanol administration, damage to the optic nerve axons is temporary. Our findings suggest that the present model is useful for analyzing the pathology of and developing therapies for acute methanol poisoning in the acute and subacute phases.

References

1. Benton CD Jr, Calhoun EP Jr. The ocular effects of methyl alcohol poisoning; report of a catastrophe involving 320 persons. Am J Ophthalmol 1953;36:1677-1685.
2. Eells JT, Henry MM, Lewandowski MF, Seme MT, Murray TG. Development and characterization of a rodent model of methanol-induced retinal and optic nerve toxicity. Neurotoxicology 2000;21:321-330.
3. Nicholls P. Formate as an inhibitor of cytochrome c oxidase. Biochem Biophys Res Commun 1975;67:610-616.
4. Rajamani R, Muthuvel A, Manikandan S, Srikumar R, Sheeladevi R. Efficacy of DL-alpha-lipoic acid on methanol induced free radical changes, protein oxidative damages and hsp70 expression in folate deficient rat nervous tissue. Chem Biol Interact 2007;167:161-167.
5. Rajamani R, Muthuvel A, Senthilvelan M, Sheeladevi R. Oxidative stress induced by methotrexate alone and in the presence of methanol in discrete regions of the rodent brain, retina and optic nerve. Toxicol Lett 2006; 165:265-273.
6. Baumbach GL, Cancilla PA, Martin-Amat G, Tephly TR, McMartin KE, Makar AB, et al. Methyl alcohol poisoning. IV. Alterations of the morphological findings of the retina and optic nerve. Arch Ophthalmol 1977; 95:1859-1865.
7. Murray TG, Burton TC, Rajani C, Lewandowski MF, Burke JM, Eells JT. Methanol poisoning. A rodent model with structural and functional evidence for retinal involvement. Arch Ophthalmol 1991;109:1012-1016.
8. Sahin A, Kaya S, Türkcü G, Cingü AK, Yüksel H, Türkcü FM, et al. The effects of caffeic acid phenethyl ester in acute methanol toxicity on rat retina and optic nerve. Cutan Ocul Toxicol 2013;32:263-267.
9. El-Bakary AA, El-Dakrory SA, Attalla SM, Hasanein NA, Malek HA. Ranitidine as an alcohol dehydrogenase inhibitor in acute methanol toxicity in rats. Hum Exp Toxicol 2010;29:93-101.
10. Lee EW, Garner CD, Terzo TS. Animal model for the study of methanol toxicity: comparison of folate-reduced rat responses with published monkey data. J Toxicol Environ Health 1994;41:71-82.
11. Ueda N, Shiraki K. Electron Microscopy Findings for Experimental Methanol Poisoning. Journal of the Eye 2014;31:1555-1561. (in japanese)
12. Seme MT, Summerfelt P, Neitz J, Eells JT, Henry MM. Differential recovery of retinal function after mitochondrial inhibition by methanol intoxication. Invest Ophthalmol Vis Sci 2001;42:834-841.
13. Sadun A. Acquired mitochondrial impairment as a cause of optic nerve disease. Trans Am Ophthalmol Soc 1998;96:881-923.

Instructions for Authors

The Osaka City Medical Journal will consider the publication of any original manuscript, review, case report, or short communication. Articles should be in English.

Manuscript submission. Manuscripts should be sent to the Editor, Osaka City Medical Journal, Osaka City Medical Association, Osaka City University Medical School, 1-4-3 Asahimachi, Abeno-ku, Osaka 545-8585, Japan; phone and fax 06-6645-3782; e-mail shiigakukai@med.osaka-cu.ac.jp

The Journal accepts only manuscripts that contain material that has not been and will not be published elsewhere. Duplicate publication of scientific data is not permitted. If closely related papers might be considered to be duplicate publications, the possible duplicate should be submitted with the manuscript and the authors should explain in their covering letter what is original in the submitted paper. Submit three copies of the manuscript (two of which may be photocopies) together with CD-R or DVD-R containing the body text, tables and figures. The manuscript should be prepared by Microsoft Word or its compatible software (doc or docx). Acceptable formats for figures are JPG or TIF. Use only 12-point font size and a standard serif font. Double-space throughout the manuscript and use standard-sized (ISO A4, 212×297 mm) white bond paper. Make margins at least 25 mm wide on all sides. Number pages consecutively starting with the title page and ending with the reference list. Begin each of these sections on a separate page: title page, abstract, text, acknowledgements, references, tables (each one separate), and figure legends. Do not use abbreviations in the title or abstract and limit their use in the text, defining each when it first appears. Manuscripts should meet the requirements outlined below to avoid delay in review and publication. Society membership for all the authors is required before the submission. Authors whose native language is not English must seek the assistance of a native English speaker who is familiar with medical sciences. Please attach the certificate from the person(s) who edit the manuscript. Some minor editorial revision of the manuscript will be made when the editorial committee considers it necessary.

Title page. All submissions must include a title page. The full title of the paper, should be concise, specific, and informative, and should contain the message of the paper without being in sentence form. Next, include the full names and academic affiliations of all authors, and indicate the corresponding author, address, phone, fax, and e-mail address. Give a running title (not to exceed 50 characters including spaces), and three to five key words. Last, give the word count for text only, exclusive of title, abstract, references, tables, and figure legends.

Structured abstract. The abstract of 250 words or less should consist of four paragraphs headed **Background, Methods, Results,** and **Conclusions.**

Text. Full papers about experiments or observations may be divided into sections headed **Introduction, Methods, Results,** and **Discussion.**

Tables. Each table should be typed on a separate sheet in characters of ordinary size, double-spaced (with at least 6 mm of white space between lines). Each table must have a title and should be assigned an Arabic numeral ('Table 3'). Vertical rules should not be used.

Figures. For black-and-white figures, submit three original glossy prints or laser-quality proofs and three photocopies of each. One transparency and three color prints should be submitted of each color figure. Label the front of figures with the figure number. Indicate on the back of each figure the first author, the first few words of the manuscript title, and the direction of the top of the figure (if needed). Photomicrographs should have scale markers that indicate the magnification. Provide figure legends on a separate page, double-spaced, immediately after the tables. All illustrations and graphs, to be referred to as figures, should be numbered in Arabic numerals ('Fig. 2' etc.). The approximate position of each figure in the text should be indicated in the right margin of the manuscript. Illustrations in full color are accepted for publication if the editors judge that color is necessary, with the cost paid by the author.

References. Reference must be double-spaced and numbered consecutively in the order cited in the text. When listing references, follow the style of the Uniform Requirements (http://www.icmje.org/) and abbreviate names of journals according to PubMed (http://www.ncbi.nlm.nih.gov/sites/netrez). List all authors up to three; when there are four or more, list the first three and use et al.

Examples of reference style

1. Priori SG, Schwartz PJ, Napolitano C, et al. Risk stratification in the long-QT syndrome. N Engl J Med 2003;348:1866-1874.
2. Schwartz PJ, Priori SG, Napolitano C. The long-QT syndrome. In: Zipes DP, Jalife J, editors. Cardiac electrophysiology: from cell to bedside. 3rd ed. Philadelphia: W.B. Saunders; 2000. pp. 597-615.

Proofs. One set of proofs together with the original manuscript will be sent to the author, to be carefully checked for any essential changes or printer's errors. The author is requested to return the corrected proofs within 48 h of their receipt.

Short communications and case reports.

1. A short communication should have between 1500 and 2000 words, including the abstract. This word count is equivalent to about four double-spaced manuscript pages.
2. The original and two copies including three sets of figures and tables should be sent to the Editorial Office.

Manuscript submission fee. A nonrefundable fee of 10,000 JPY is due on submission of original manuscripts, case reports, and short communications. A manuscript returned beyond six months of the date of the initial decision will be considered a new submission.

Page charges and reprints. Authors are required to pay page charges of 10,000 JPY per printed page to share in the high costs of publication. Authors receive with the proofs a reprint order form that must be filled out and returned with the proofs to the Editorial Office. Later orders cannot be filled because reprints are made at the time the journal is printed.

Studies of human subjects. It is the responsibility of the authors to ensure that any clinical investigation they did and report in manuscripts submitted to the Osaka City Medical Journal are in accordance with the Declaration of Helsinki (http://www.wma.net).

Animal studies. It is the responsibility of the authors to ensure that their experimental procedures are in compliance with the "Guiding Principles in the Care and Use of Animals" (http://www.the-aps.org/pub_affairs/humane/pa_aps_guiding.htm) published each month in the information for authors of the American Journal of Physiology.

Conflict of Interest disclosure. It is the responsibility of the authors to disclose any Conflict of Interests by signing the form.

[Reviced: January 2018]

COPYRIGHT TRANSFER AND STATEMENT OF ORIGINALITY

We approve the submission of this paper to the Osaka City Medical Association for publication and have taken to ensure the integrity of this work. We confirm that the manuscript is original and does not in whole or part infringe any copyright, violate any right of privacy or other personal or priority right whatever, or falsely designate the source of authorship, and that it has not been published in whole or in part and is not being submitted or considered for publication in whole or in part elsewhere (abstracts excluded).
We agree to transfer copyright the manuscript entitled

_____

_____

to the Osaka City Medical Association upon its acceptance for publication.

Write clearly and signature

(Author: print or type)	(Signature)	(Date)
(Author: print or type)	(Signature)	(Date)
(Author: print or type)	(Signature)	(Date)
(Author: print or type)	(Signature)	(Date)
(Author: print or type)	(Signature)	(Date)
(Author: print or type)	(Signature)	(Date)
(Author: print or type)	(Signature)	(Date)
(Author: print or type)	(Signature)	(Date)
(Author: print or type)	(Signature)	(Date)
(Author: print or type)	(Signature)	(Date)

OCMJ for Conflict of Interest Disclosure Statement

The purpose of this form is to provide readers of your manuscript with information about your other interests that could influence how they receive and understand your work. The form is designed to be completed electronically and stored electronically. Each author should submit a separate form and is responsible for the accuracy and completeness of the submitted information.

☐ **No,** Conflict of interest

The authors declare no conflicts of interest associated with this manuscript.

☐ **Yes,** Conflict of interest

(Generate disclosure statement. More than 1,000,000 JPY should be disclosed for 1-5.),

1) Research funding, 2) Patent royalties/licensing fees, 3) Employment/Leadership position/ Advisory role, 4) Consulting fee/honorarium, 5) Others (travel fees, gifts etc) etc.

Based on the above disclosures, this form will automatically generate a disclosure statement, which will appear in the box below.

Date:

Manuscript Title:

First Author of Name: (Print of type) and (Signature)

Corresponding author:

Manuscript Identifying Number (if you know it):

Editorial Committee

The volumes and issues published in 1954-2018 were as follows: Vol 1 (one issue), Vols 2-5 (2 issues, each), Vols 6-7 (one issue, each), Vols 8-9 (2 issues, each), Vol 10 (one issue), Vol 11 (2 issues), Vol 12 (one issue), Vol 13 (2 issues), Vols 14-20 (one issue, each), Vol 21 (2 issues), Vol 22 (one issue), Vols 23-64 (2 issues, each)

Publisher : Osaka City Medical Association,
Osaka City University Medical School,
1-4-3 Asahimachi, Abeno-ku, Osaka 545-8585, Japan